Communications of the LUNAR AND PLANETARY LABORATORY

Numbers 79–91

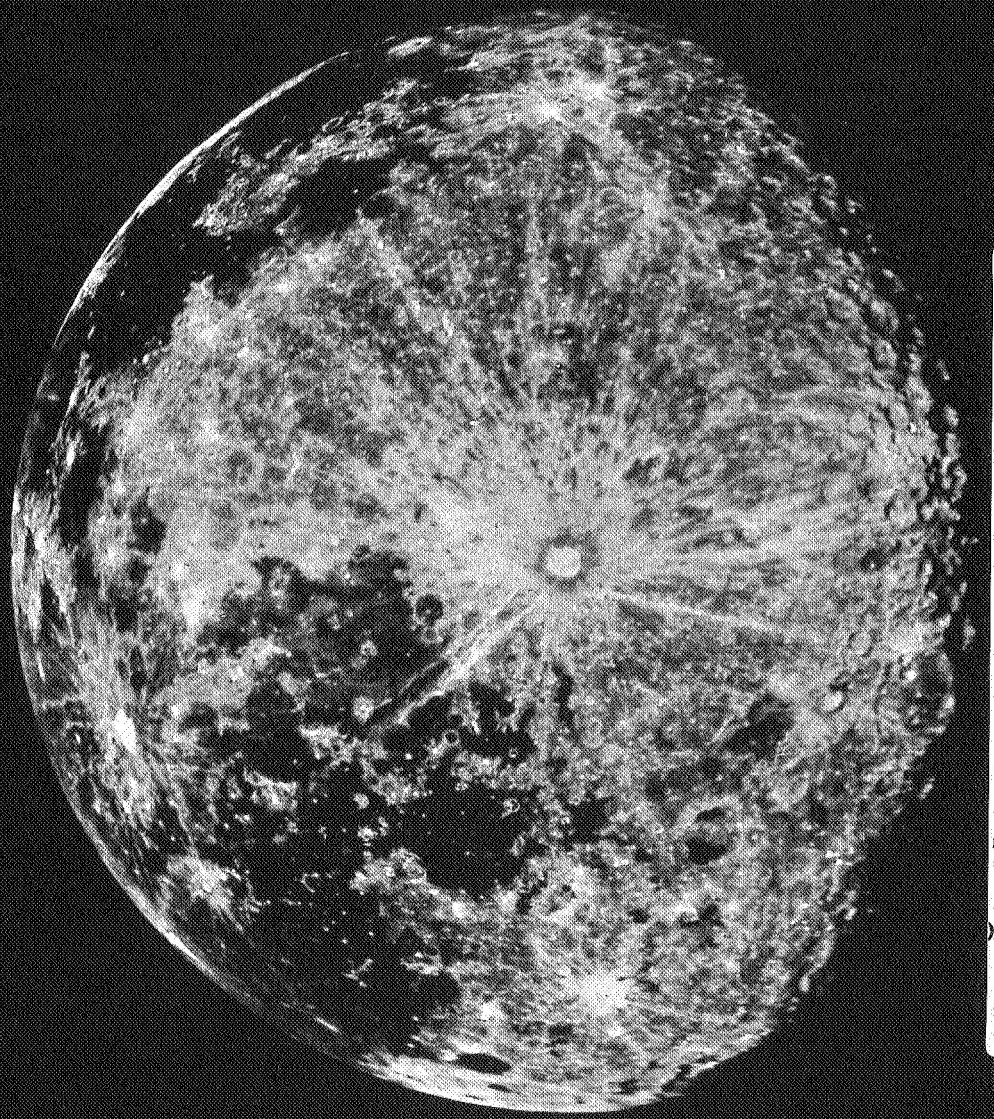

Volume 6 Part 1

THE UNIVERSITY OF ARIZONA

Communications of the LUNAR AND PLANETARY LABORATORY

Numbers 79–91

Volume 6 Part 1

THE UNIVERSITY OF ARIZONA

1967

Communications of the Lunar and Planetary Laboratory

These *Communications* contain the shorter publications and reports by the staff of the Lunar and Planetary Laboratory. They may be either original contributions, reprints of articles published in professional journals, preliminary reports, or announcements. Tabular material too bulky or specialized for regular journals is included if future use of such material appears to warrant it. The *Communications* are issued as separate numbers, but they are paged and indexed by volumes.

The *Communications* are mailed to observatories and to laboratories known to be engaged in planetary, interplanetary or geophysical research in exchange for their reports and publications. The University of Arizona Press can supply at cost copies to other libraries and interested persons.

The University of Arizona
Tucson, Arizona

GERARD P. KUIPER, *Director*
Lunar and Planetary Laboratory

Published with the support of the National Aeronautics and Space Administration and the National Science Foundation

Library of Congress Catalog Number 62-63619

No. 79 LABORATORY SPECTRA FOR TESTING THE PRESENCE OF MINOR CONSTITUENTS IN PLANETARY ATMOSPHERES, II: C_2H_2, C_2H_4, C_2H_6, CH_3SH, CH_3NH_2, H_2S

by DALE P. CRUIKSHANK

April 10, 1967

This is the second of two papers presenting laboratory observations of small amounts of various gases that may occur in the atmospheres of the planets. In this paper are spectra of several hydrocarbons and H_2S in the spectral region of the lead sulfide detector (1.0–2.6 microns). The observations were made with the same scanning spectrometer (described by Kuiper, *et al.* 1962) that was used for the spectra in Paper I of this series (Kuiper and Cruikshank 1964). The information on the laboratory apparatus given here also applies to Paper I.

The absorption cells used in the laboratory were all single-pass tubes made of glass or, for non-corrosive gases, galvanized iron. Windows of glass or Suprasil (Englehard Industries, Inc.) were used, as well as glass lenses. An incandescent laboratory lamp was used for illumination. The spectrum was scanned at three different rates. For an initial reconnaissance, a scan was made in two increments (1.0–1.9 microns and 1.9–2.6 microns) at a rate of 5/1, which corresponds to 7.5 Å per sec and 495 Å per in. on the original records. The two spectral regions were then traced at a scan rate of 12.5/1 corresponding to 3 Å per sec and 198 Å per in. on the original records. For spectral regions containing bands of particular interest, higher resolution tracings were made with a scan rate of 25/1, corresponding to 1.5 Å per sec and 99 Å per in. on the original records. The time constant was one second in all cases. The lead sulfide detector was 0.1 × 2.5 mm in dimension. The spectrometer slit was 0.18 mm wide. A grating with 600 lines per millimeter and blazed for 1.6 microns first order was used. In the spectral range 1.0–1.9 microns a Corning 2540 filter was used, and in the range 1.9–2.6 microns, a Bausch and Lomb interference filter.

Assignments were recorded only for C_2H_2 (Herzberg 1945, p. 290). Extensive references listed by Herzberg give additional information on band assignments.

This work is part of the spectroscopic studies at LPL and is sponsored by NASA under grant NsG [illegible]-161.

REFERENCES

Kuiper, G. P., and Cruikshank, D. P. 1964, "Laboratory Spectra for Testing the Presence of Minor Constituents in Planetary Atmospheres, I: CH_4, NH_3, N_2O, CO, COS, Region 1–2.5 μ," *Comm. LPL,* **2**, 141–165.

Kuiper, G. P., Goranson, R., Binder, A., and Johnson, H. L. 1962, "An Infrared Stellar Spectrometer," *Comm. LPL,* **1**, 119–127.

Herzberg, G. 1945, *Molecular Spectra and Molecular Structure, II, Infrared and Raman Spectra of Polyatomic Molecules* (Princeton: D. Van Nostrand Co.).

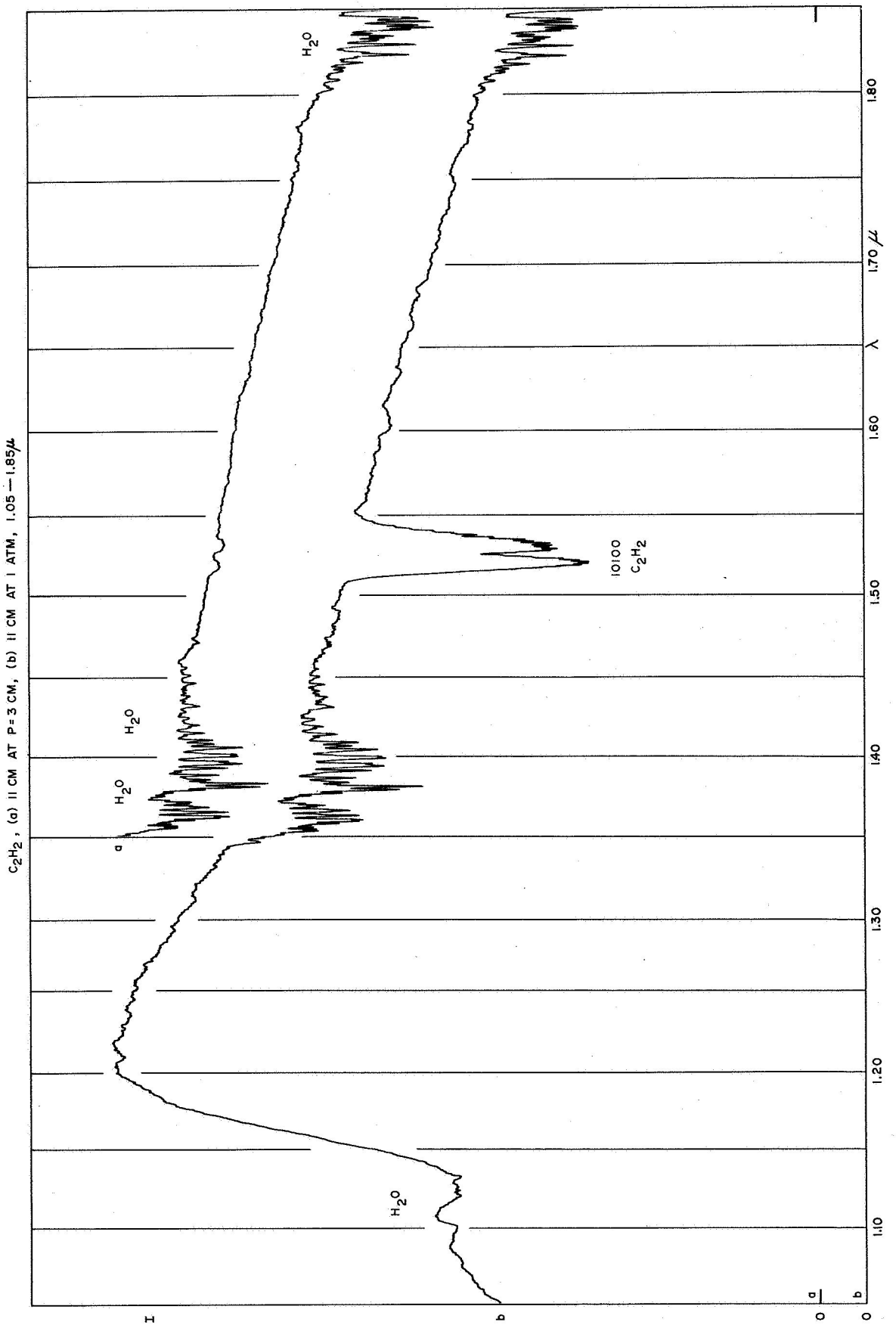
C2H2 , (a) 11 CM AT P=3 CM, (b) 11 CM AT 1 ATM, 1.05—1.85μ
H2O
H2O
H2O
H2O
10100
C2H2
1.10
1.20
1.30
1.40
1.50
1.60
1.70 μ
1.80
λ
a
b
I
0
0

Fig. 1

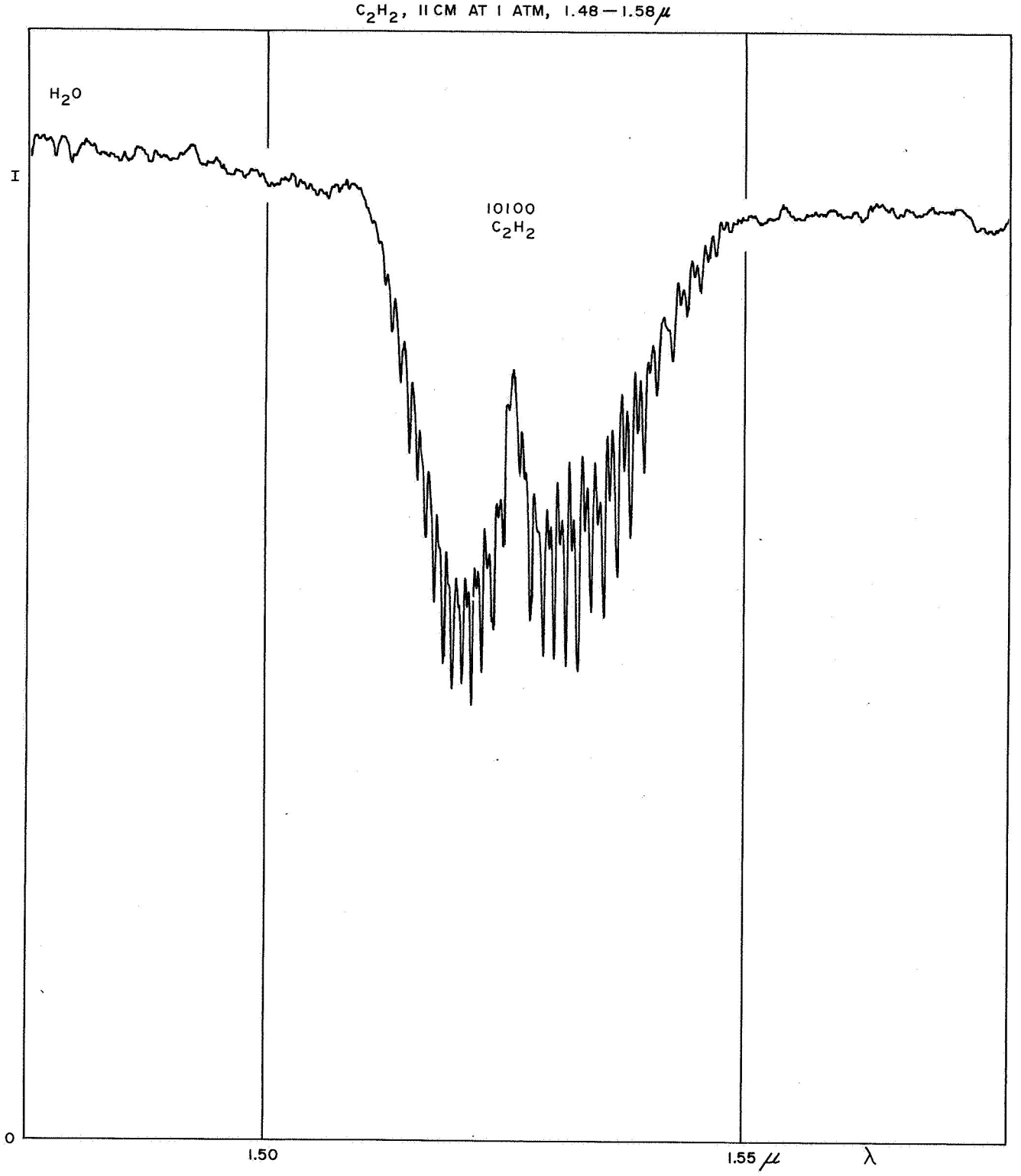

Fig. 2

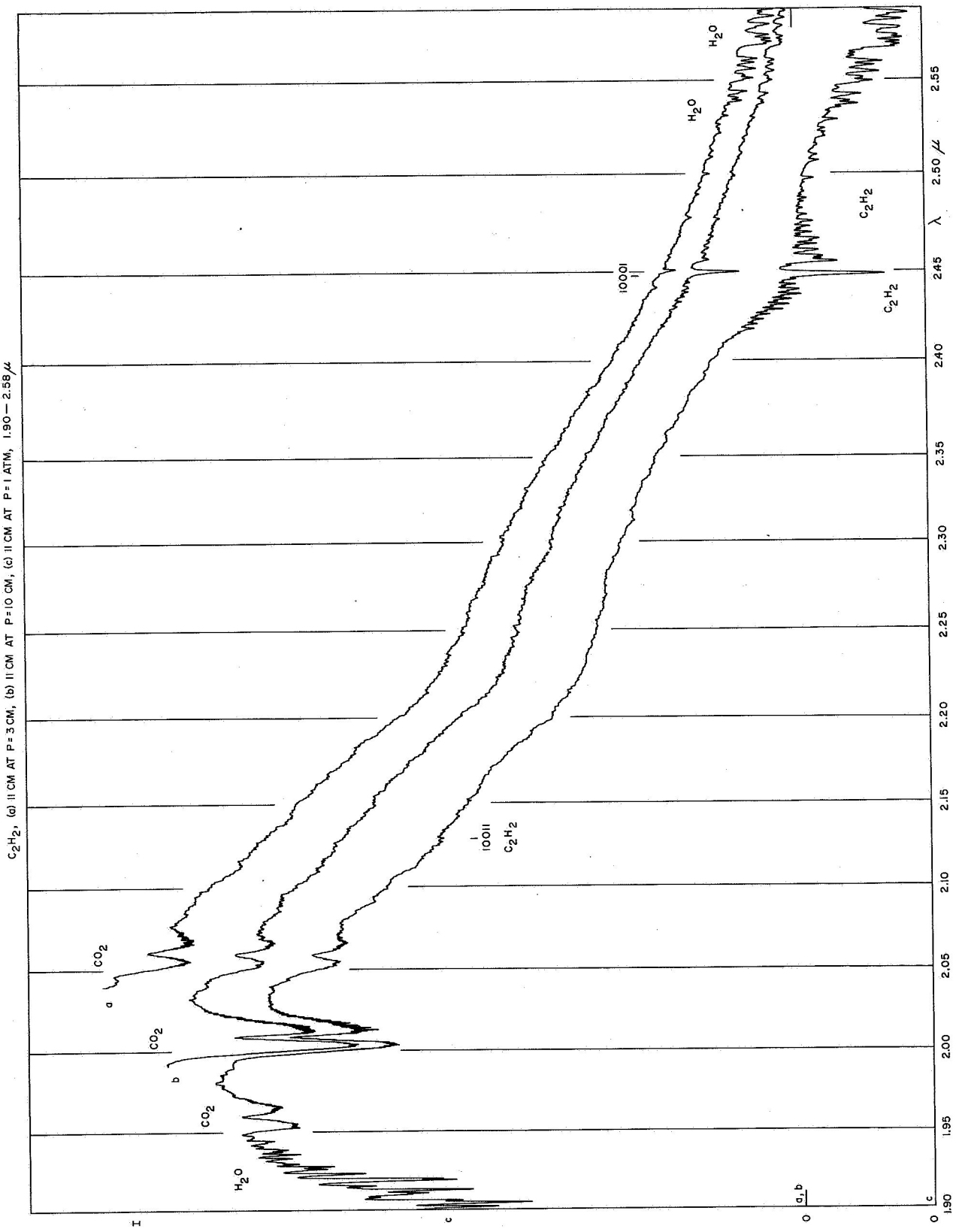
C2H2, (a) 11 CM AT P = 3 CM, (b) 11 CM AT P = 10 CM, (c) 11 CM AT P = 1 ATM, 1.90 — 2.58 μ
CO2
CO2
CO2
H2O
H2O
H2O
C2H2
C2H2
C2H2
10001
10011
a
b
c
a, b
c
H
O
O
λ
1.90
1.95
2.00
2.05
2.10
2.15
2.20
2.25
2.30
2.35
2.40
2.45
2.50 μ
2.55

Fig. 3

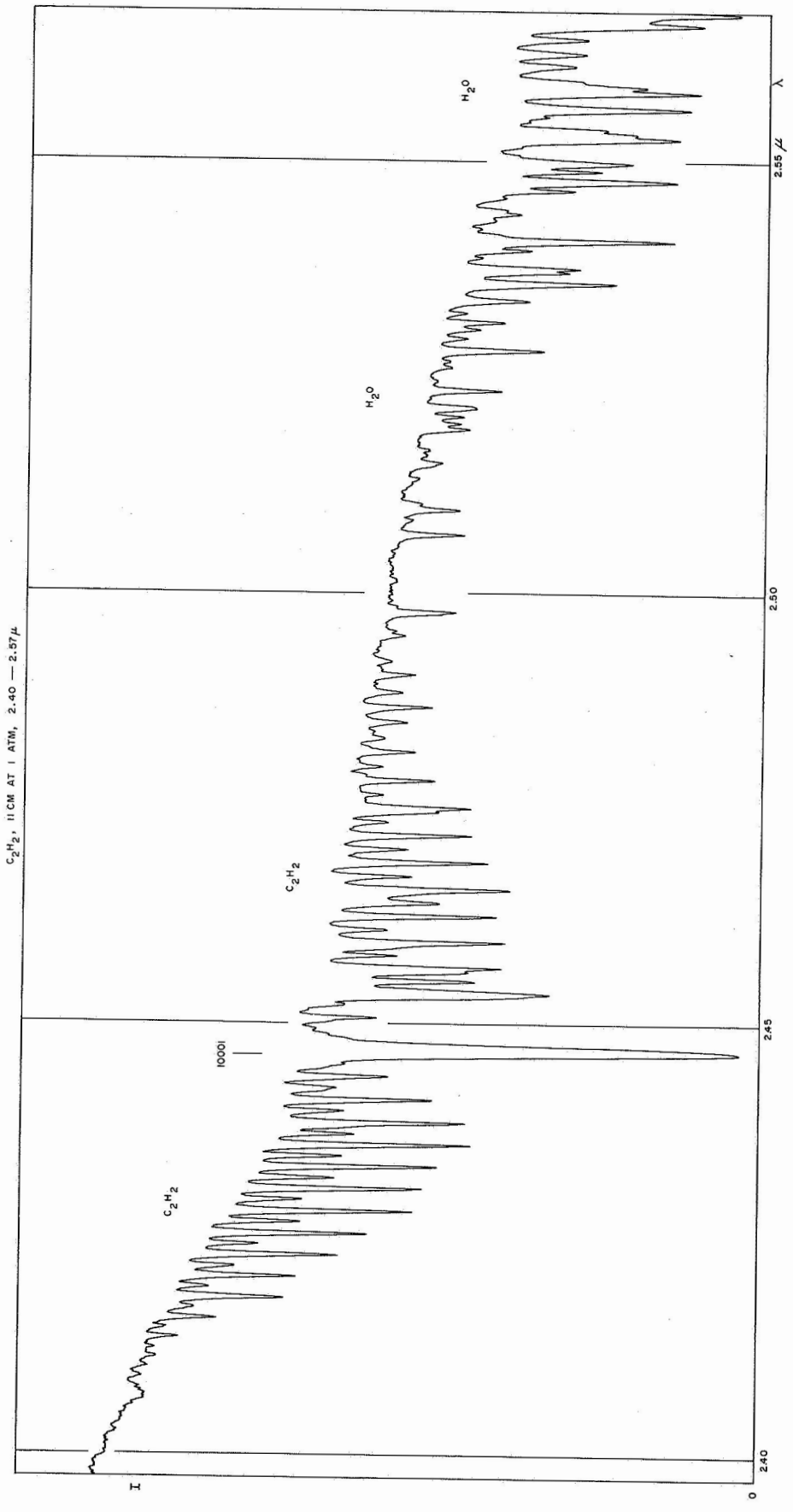
C_2H_2, 11 CM AT 1 ATM, 2.40 — 2.57 μ
C_2H_2
1000 I
C_2H_2
H_2O
H_2O
I
0
2.40
2.45
2.50
2.55 μ
λ

Fig. 4

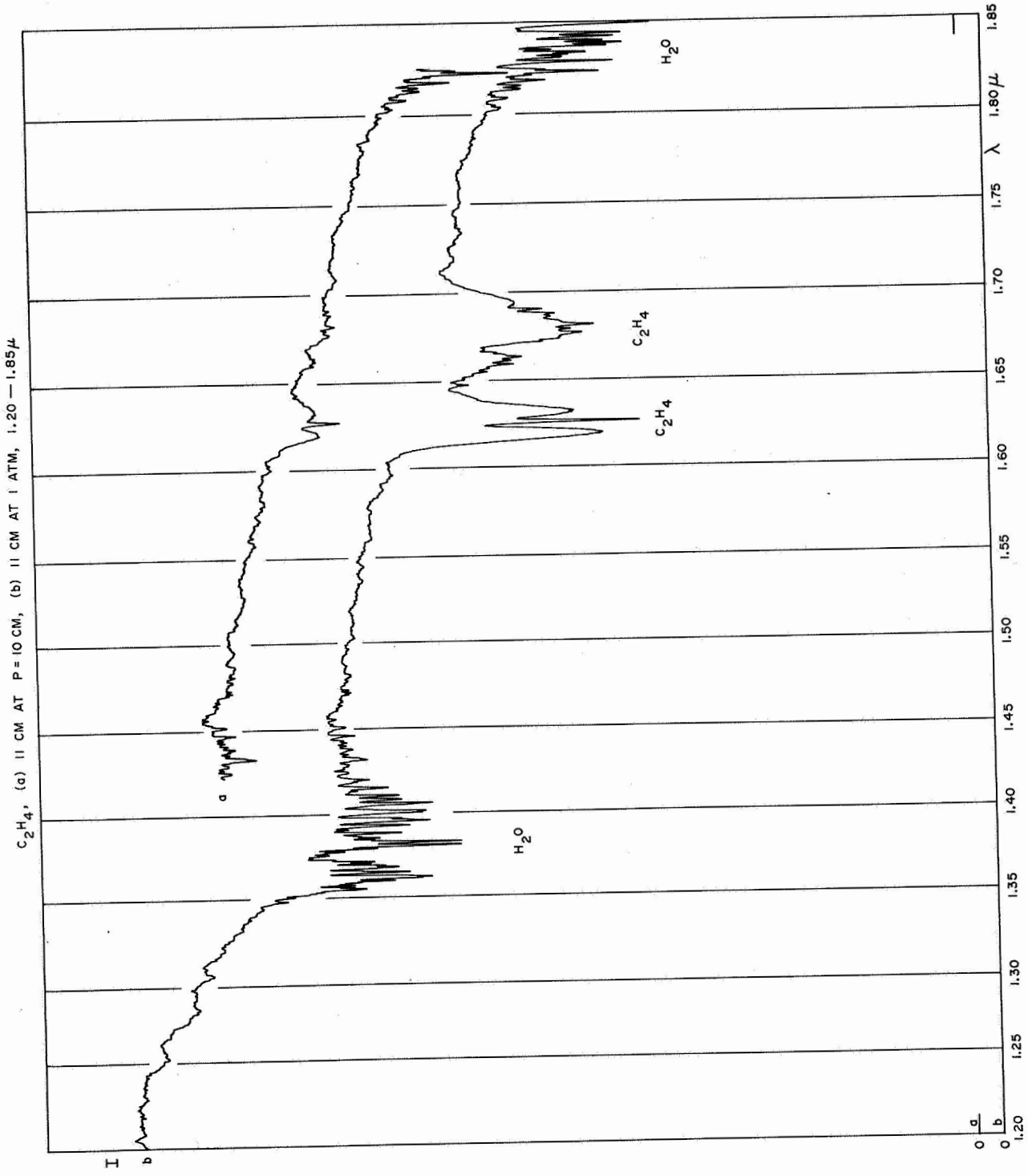
C_2H_4, (a) 11 CM AT P = 10 CM, (b) 11 CM AT 1 ATM, 1.20 — 1.85μ
I
a
b
H_2O
C_2H_4
C_2H_4
H_2O
0
a
0
b
1.20
1.25
1.30
1.35
1.40
1.45
1.50
1.55
1.60
1.65
1.70
1.75
λ
1.80μ
1.85

Fig. 5

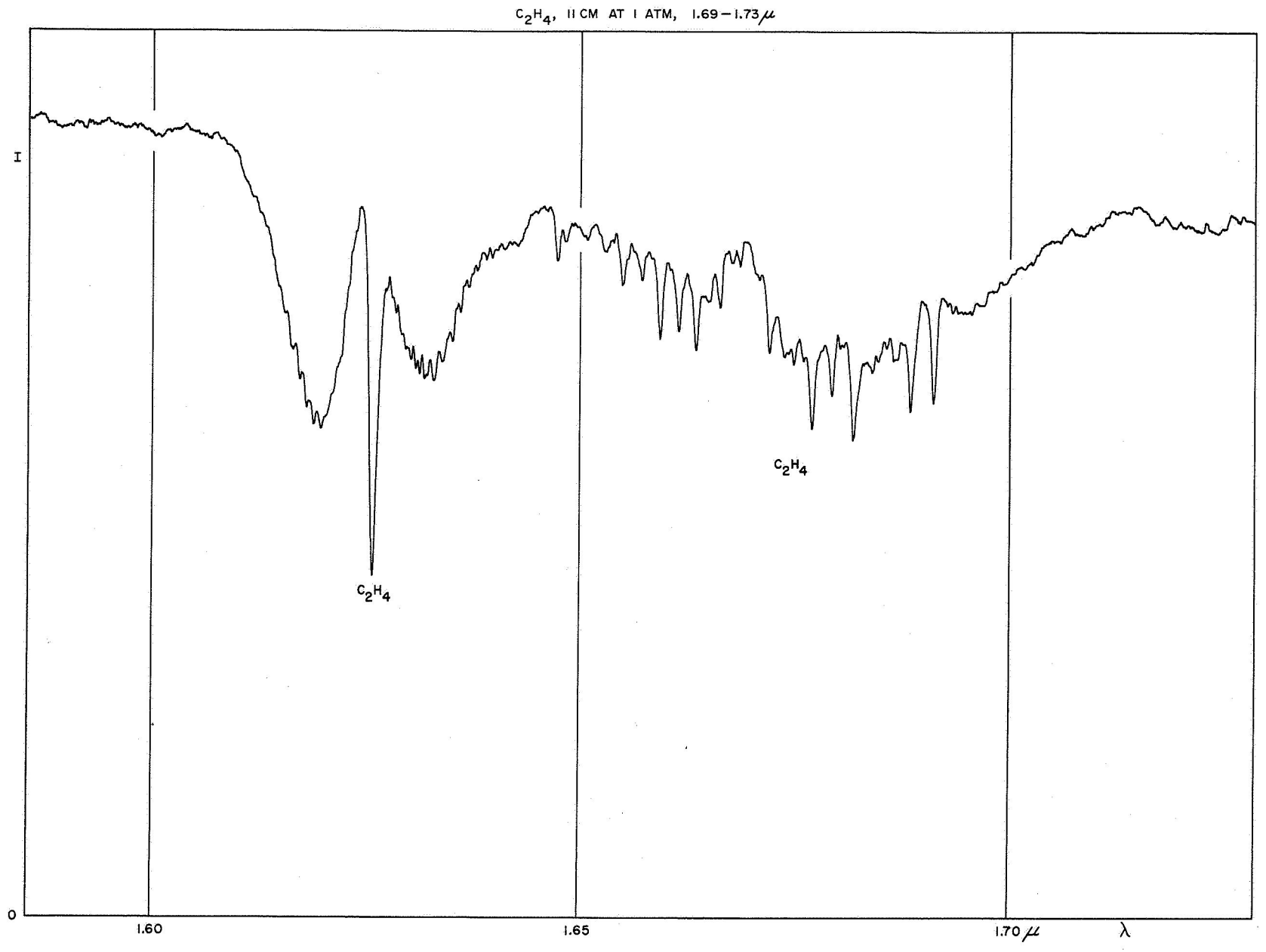

Fig. 6

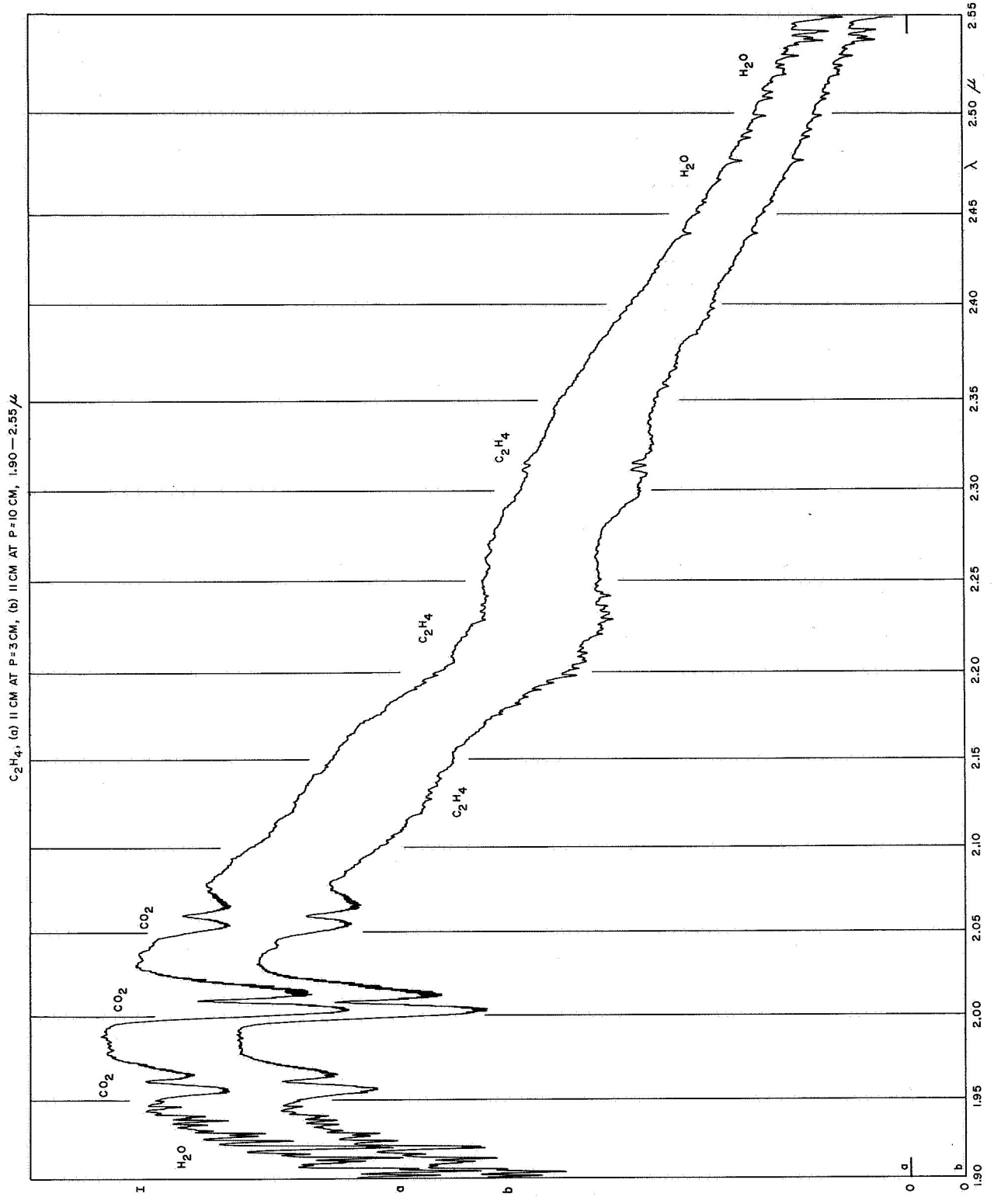
C_2H_4, (a) 11 CM AT P=3 CM, (b) 11 CM AT P=10 CM, 1.90 — 2.55 μ
H_2O
CO_2
CO_2
CO_2
C_2H_4
C_2H_4
C_2H_4
H_2O
H_2O
I
a
b
0
a
0
b
1.90
1.95
2.00
2.05
2.10
2.15
2.20
2.25
2.30
2.35
2.40
2.45
λ
2.50 μ
2.55

Fig. 7

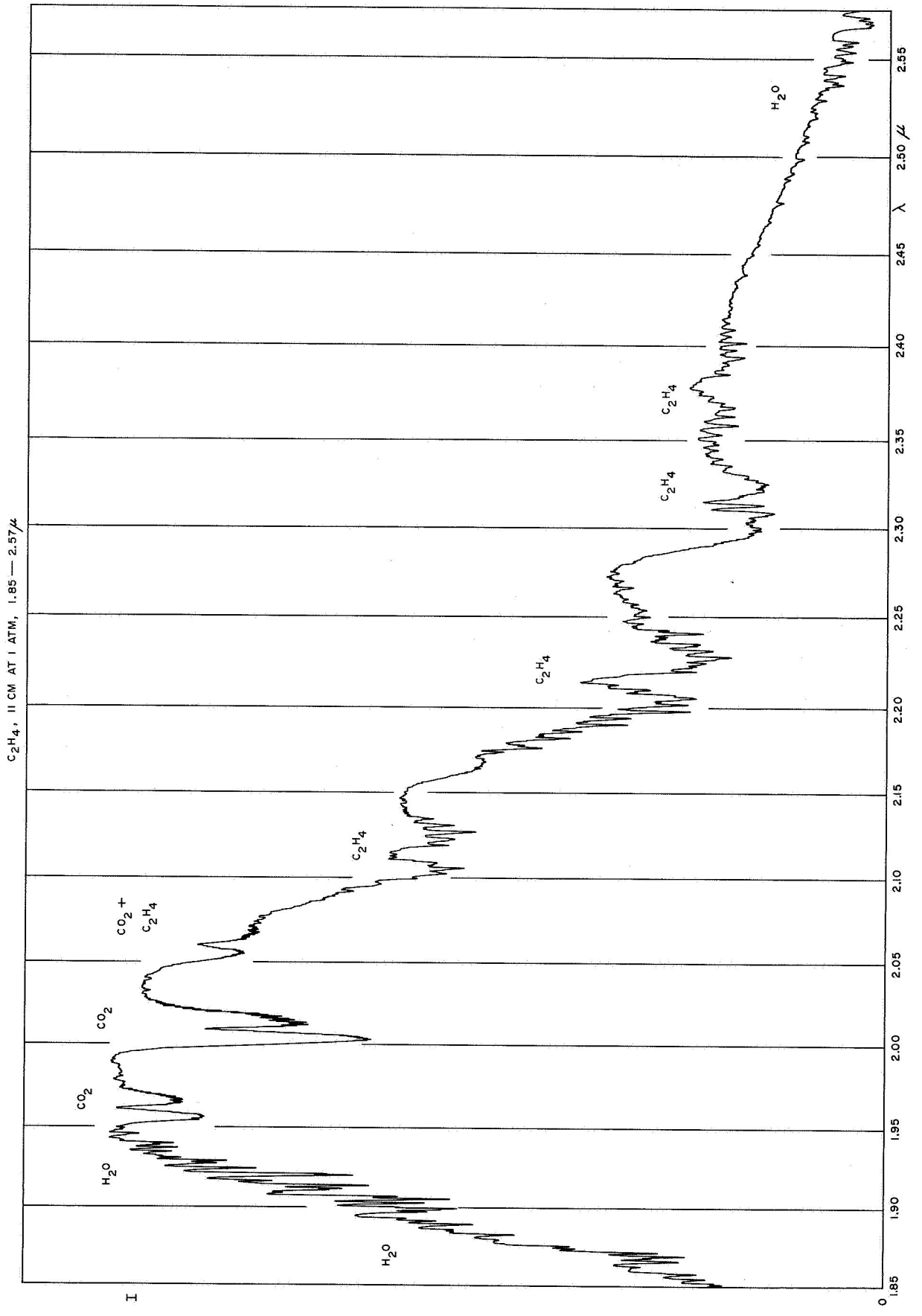
C2H4, 11 CM AT 1 ATM, 1.85 — 2.57μ
I
0
1.85
1.90
1.95
2.00
2.05
2.10
2.15
2.20
2.25
2.30
2.35
2.40
2.45
2.50 μ
λ
2.55
H2O
CO2
CO2
H2O
CO2 + C2H4
C2H4
C2H4
C2H4
C2H4
C2H4
H2O

Fig. 8

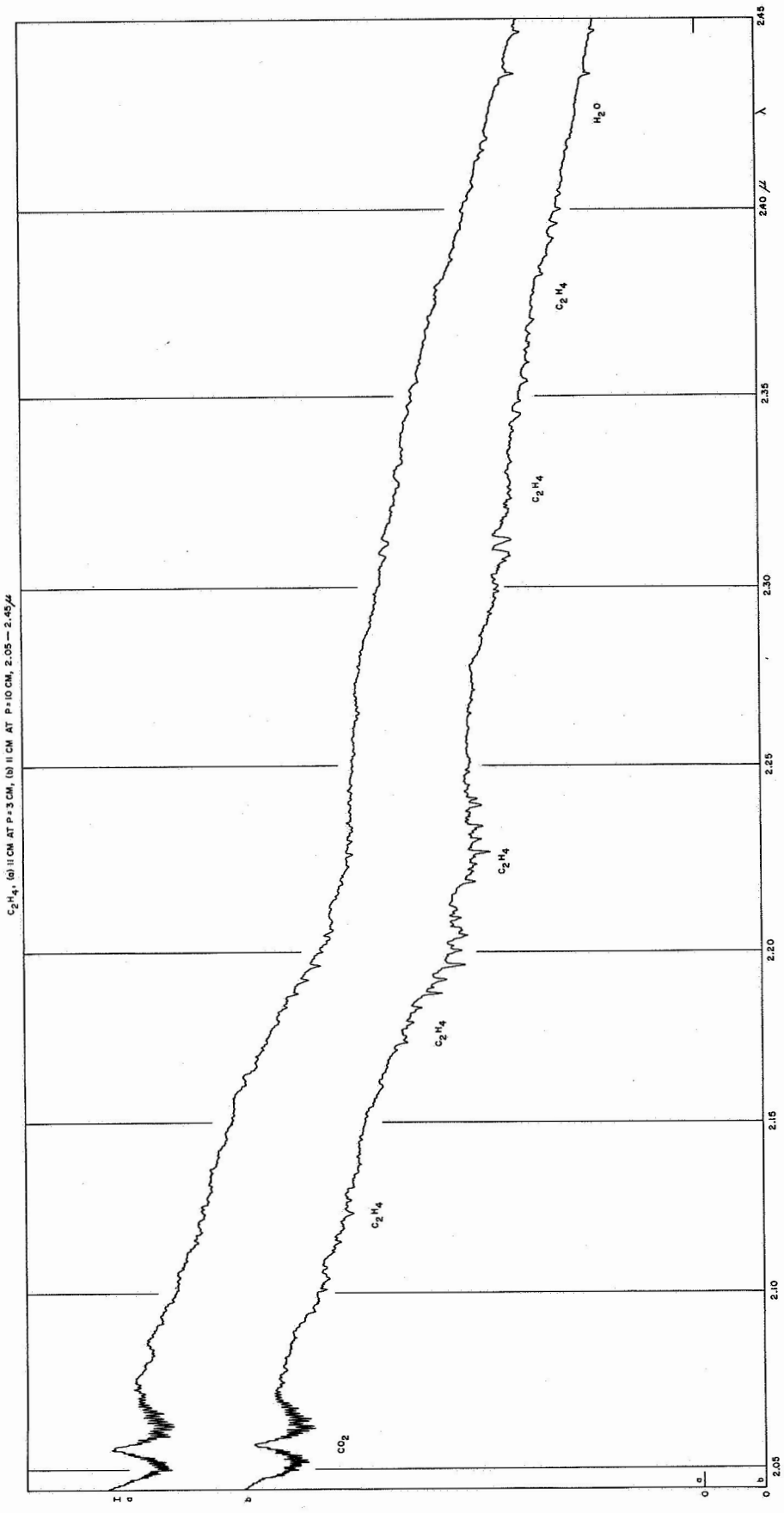
C_2H_4, (a) 11 CM AT P=3 CM, (b) 11 CM AT P=10 CM, 2.05 — 2.45μ
CO_2
C_2H_4
C_2H_4
C_2H_4
C_2H_4
C_2H_4
C_2H_4
H_2O
2.05
2.10
2.15
2.20
2.25
2.30
2.35
2.40 μ
2.45
λ

Fig. 9

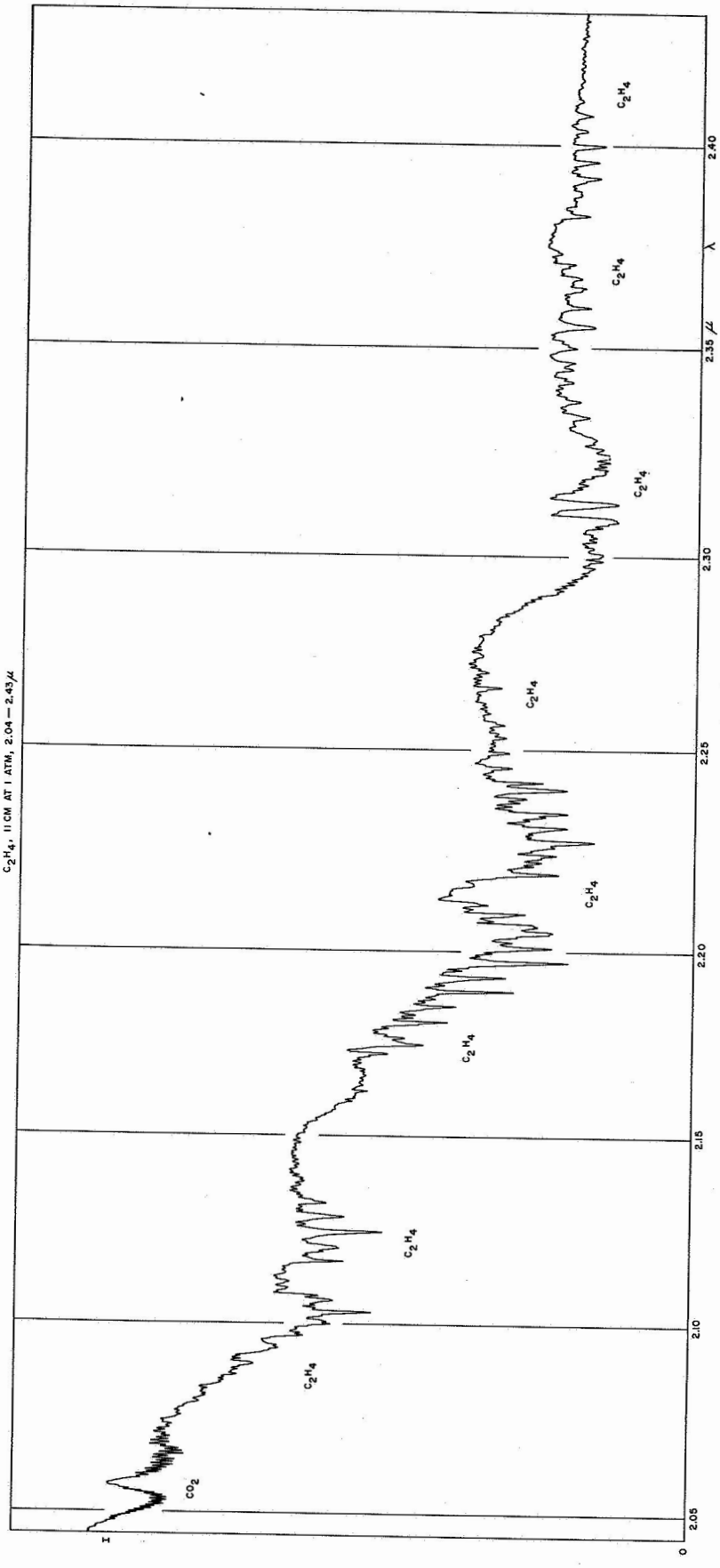
C_2H_4, 11 CM AT 1 ATM, 2.04 — 2.43 μ
CO_2
C_2H_4
2.05
2.10
2.15
2.20
2.25
2.30
2.35 μ
2.40
λ
I
0

Fig. 10

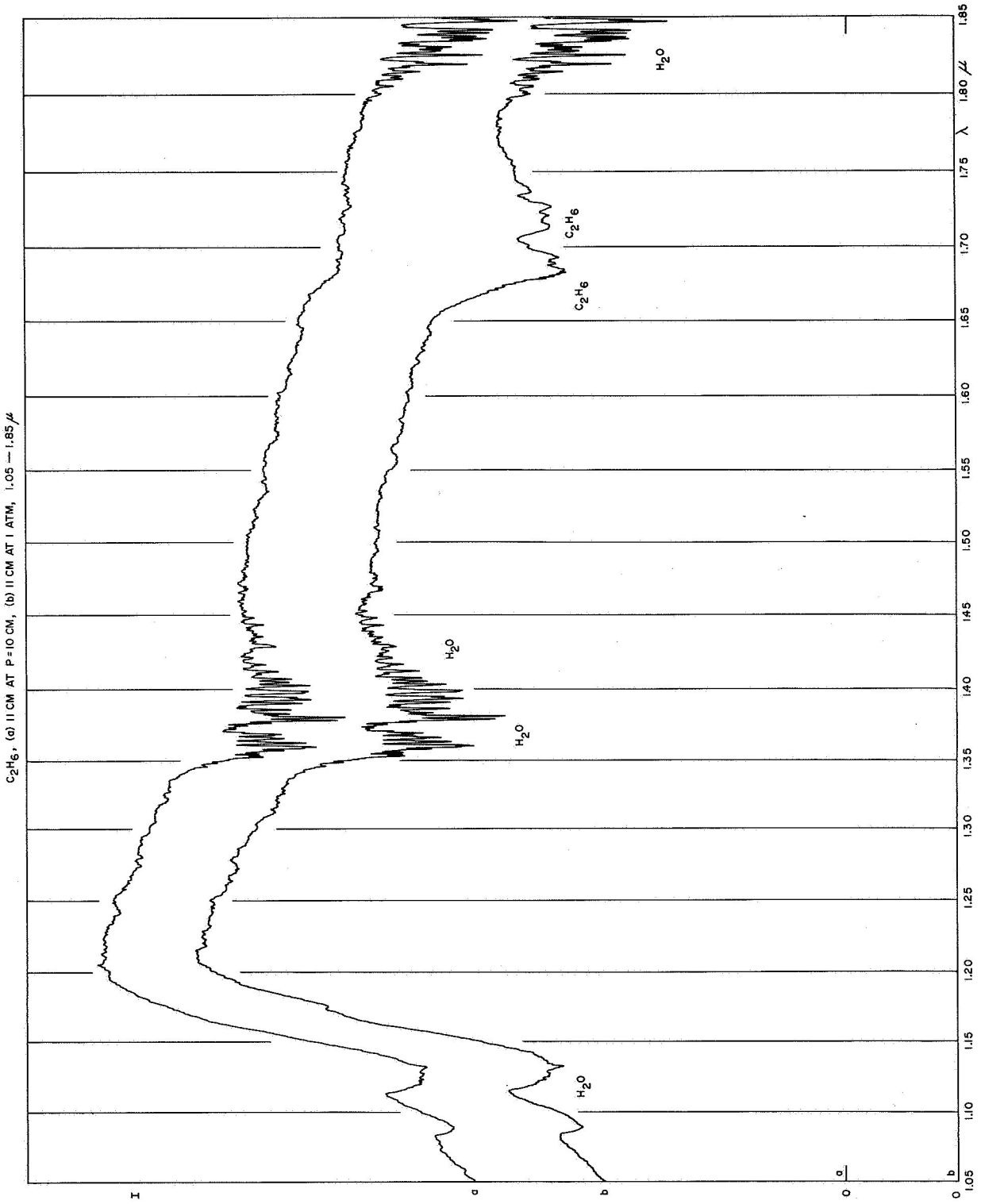
C_2H_6, (a) 11 CM AT P = 10 CM, (b) 11 CM AT 1 ATM, 1.05 — 1.85 μ
H_2O
H_2O
H_2O
C_2H_6
C_2H_6
H_2O
I
a
b
0
a
0
b
0
1.05
1.10
1.15
1.20
1.25
1.30
1.35
1.40
1.45
1.50
1.55
1.60
1.65
1.70
1.75
1.80 μ
λ
1.85

Fig. 11

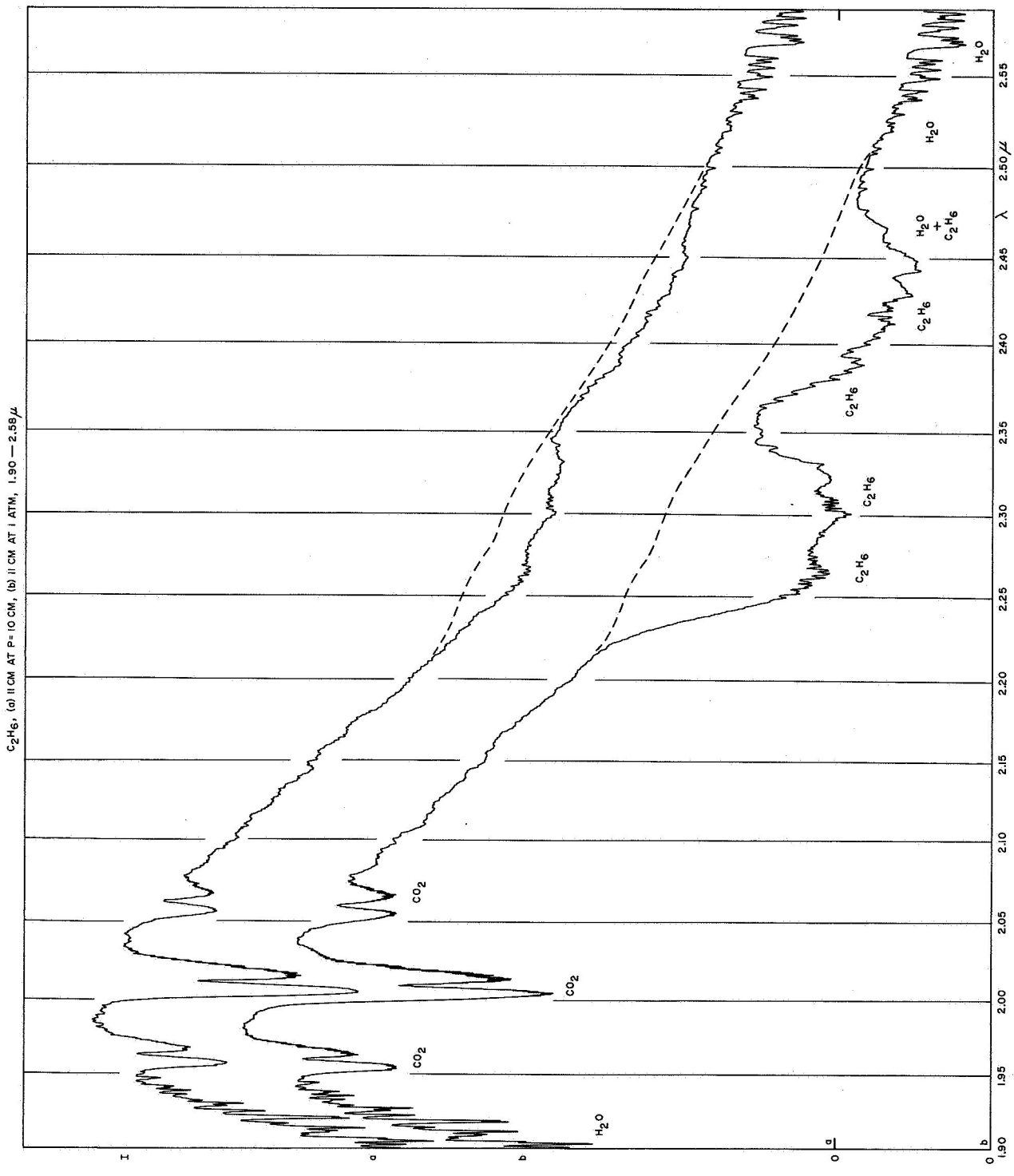
C_2H_6, (a) 11 CM AT P= 10 CM, (b) 11 CM AT 1 ATM, 1.90 — 2.58 μ
I
a
b
CO_2
CO_2
CO_2
H_2O
C_2H_6
C_2H_6
C_2H_6
C_2H_6
H_2O + C_2H_6
H_2O
H_2O
a
b
0
1.90
1.95
2.00
2.05
2.10
2.15
2.20
2.25
2.30
2.35
2.40
2.45
2.50 μ
λ
2.55

Fig. 12

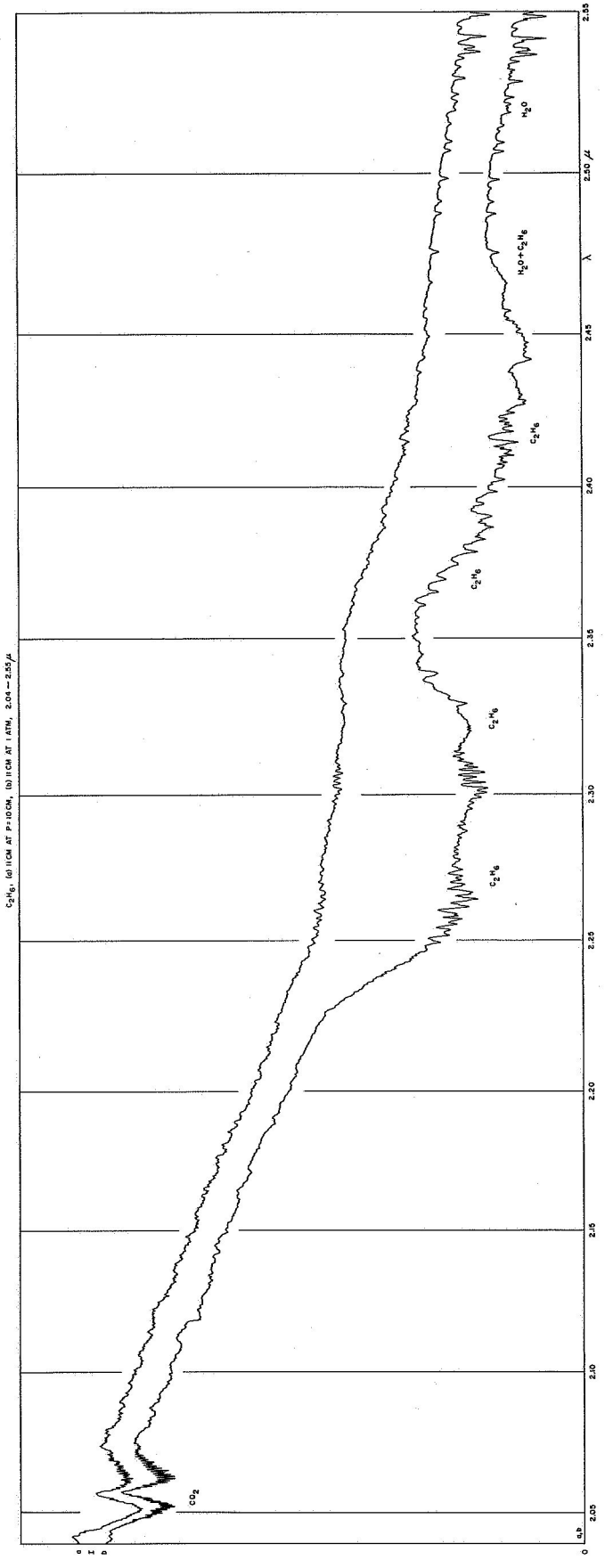
C_2H_6, (a) 11 CM AT P = 10 CM, (b) 11 CM AT 1 ATM, 2.04 – 2.55 μ
CO_2
C_2H_6
C_2H_6
C_2H_6
C_2H_6
$H_2O+C_2H_6$
H_2O
2.05
2.10
2.15
2.20
2.25
2.30
2.35
2.40
2.45
2.50 μ
λ
2.55

Fig. 13

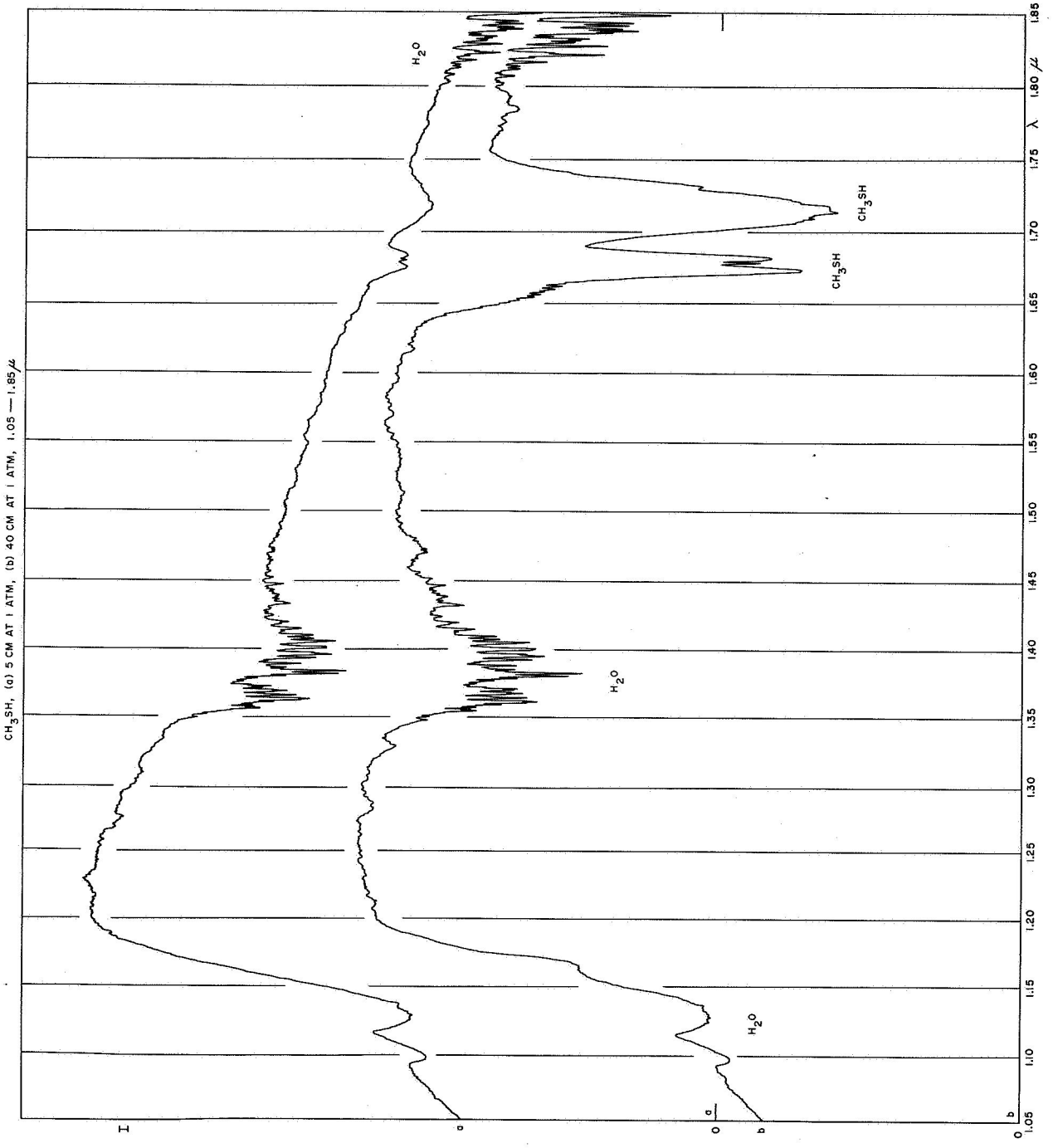
CH3SH, (a) 5 CM AT 1 ATM, (b) 40 CM AT 1 ATM, 1.05 — 1.85μ
H2O
H2O
H2O
H2O
CH3SH
CH3SH
I
a
b
λ
1.05
1.10
1.15
1.20
1.25
1.30
1.35
1.40
1.45
1.50
1.55
1.60
1.65
1.70
1.75
1.80 μ
1.85

Fig. 14

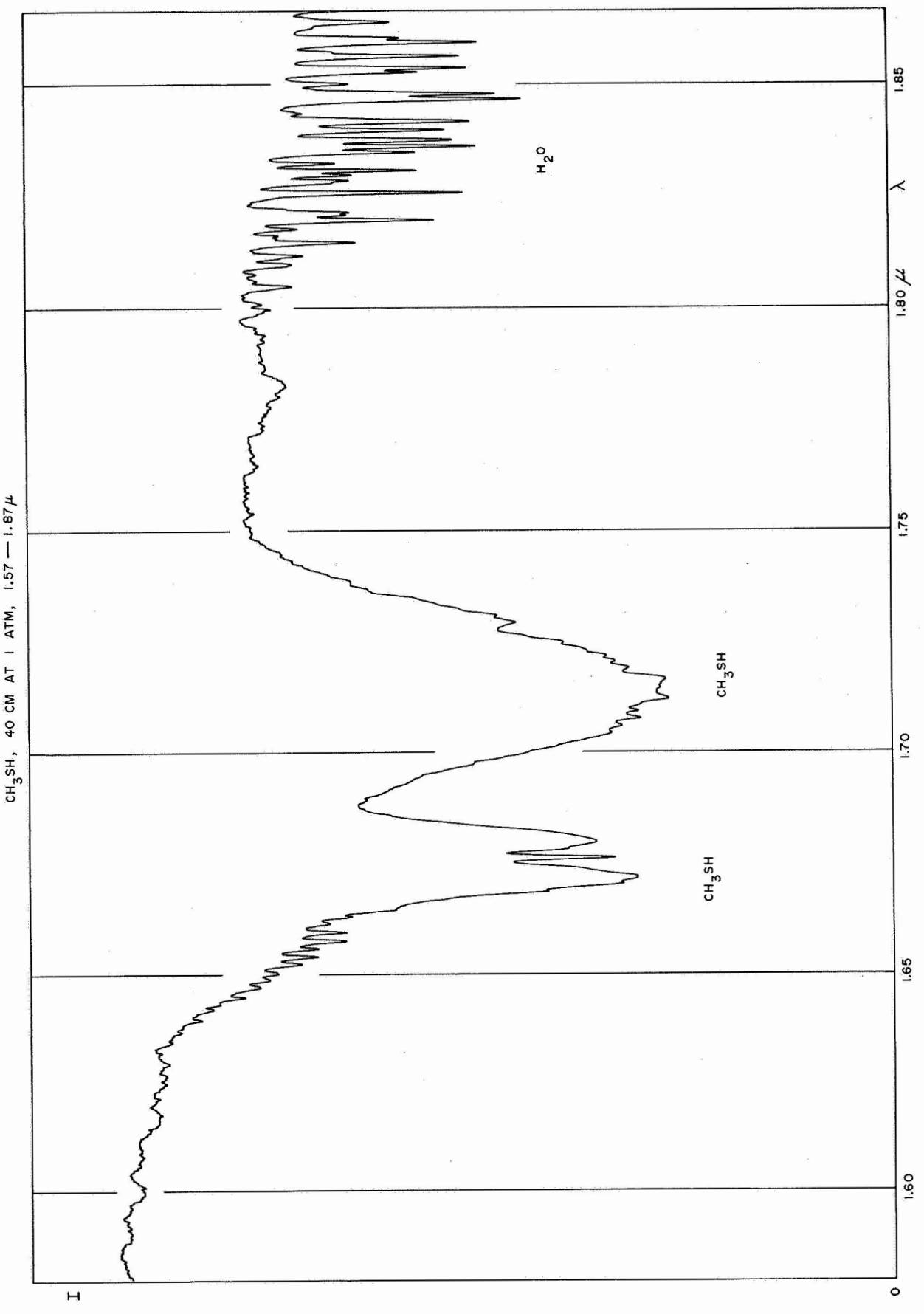
CH_3SH, 40 CM AT 1 ATM, 1.57 — 1.87 μ
I
0
1.60
1.65
1.70
1.75
1.80 μ
1.85
λ
H_2O
CH_3SH
CH_3SH

Fig. 15

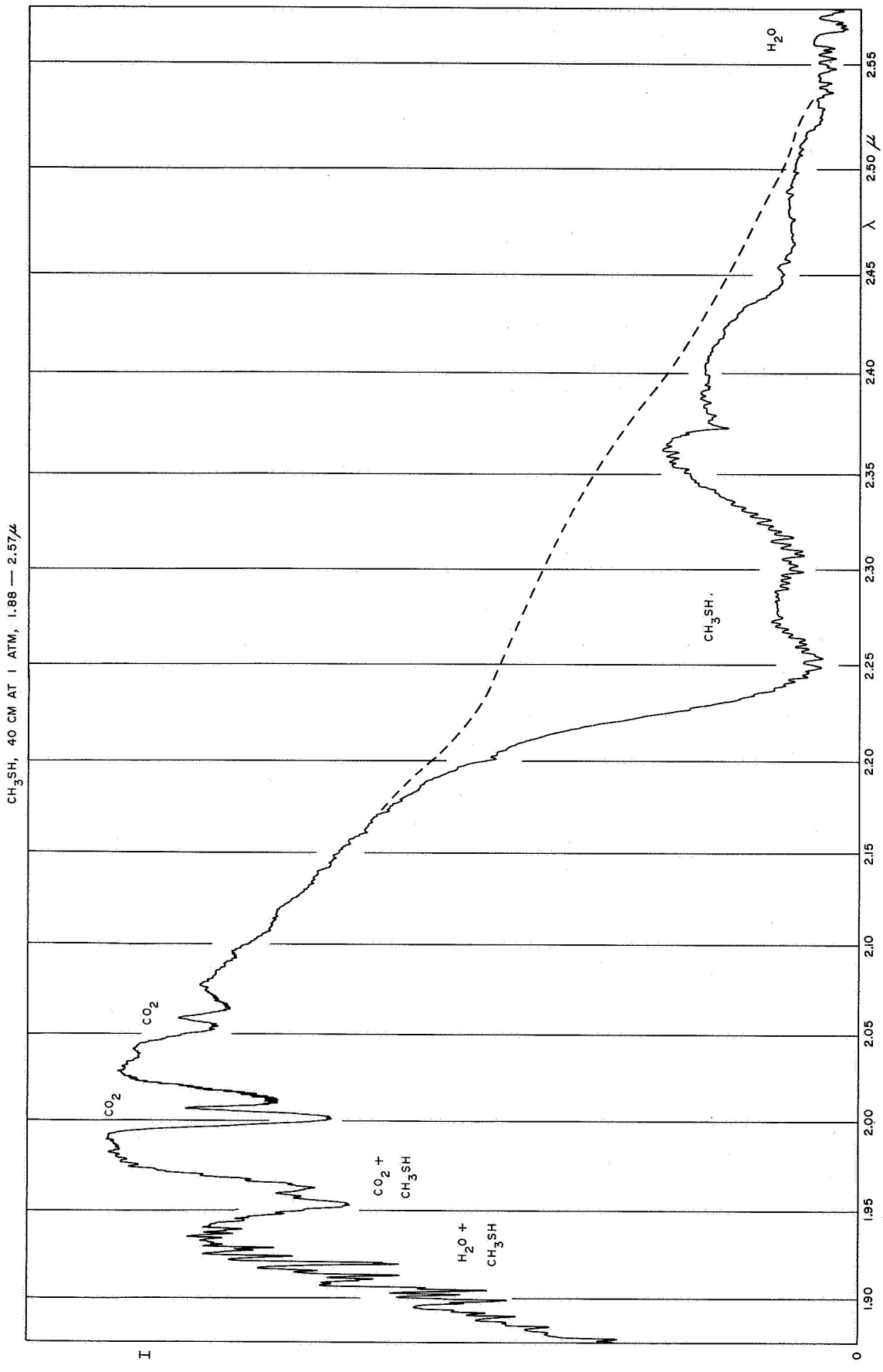
CH_3SH, 40 CM AT 1 ATM, 1.88 — 2.57μ
I
0
1.90
1.95
2.00
2.05
2.10
2.15
2.20
2.25
2.30
2.35
2.40
2.45
2.50 μ
2.55
λ
CO_2
CO_2
CO_2 + CH_3SH
H_2O + CH_3SH
CH_3SH
H_2O

Fig. 16

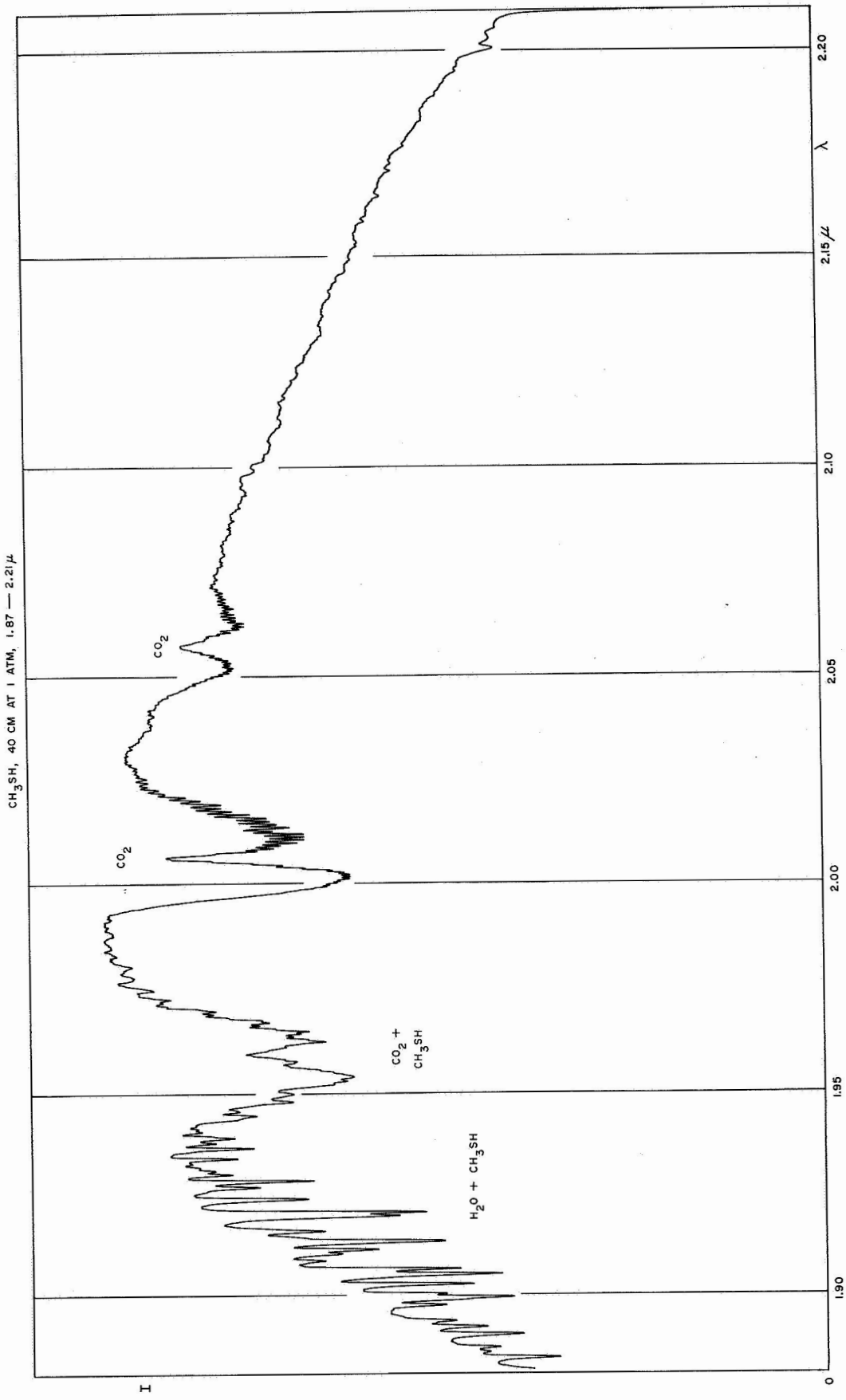
CH_3SH, 40 CM AT 1 ATM, 1.87 — 2.21 μ
CO_2
CO_2
CO_2 + CH_3SH
H_2O + CH_3SH
I
0
1.90
1.95
2.00
2.05
2.10
2.15 μ
λ
2.20

Fig. 17

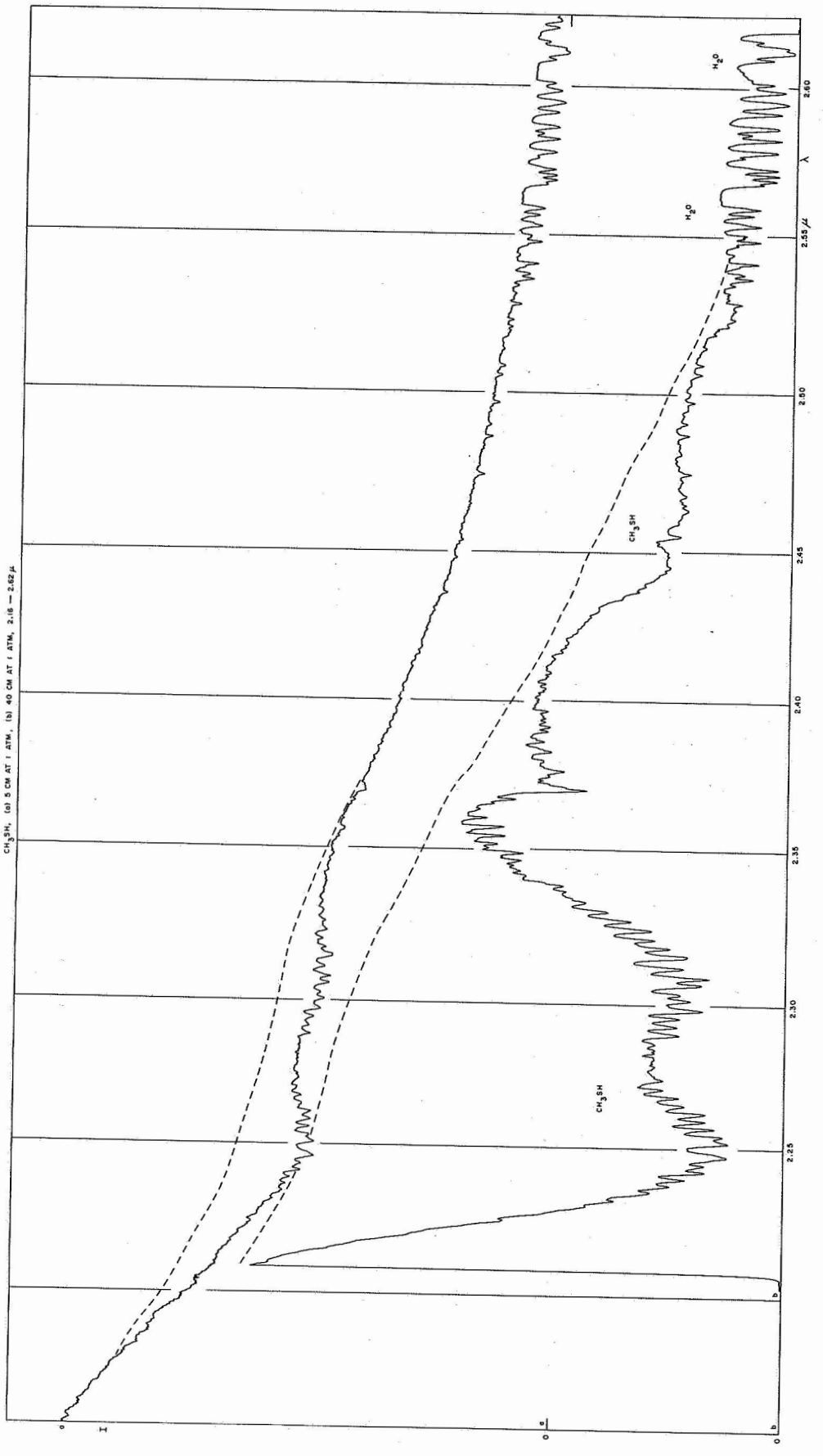
CH3SH, (a) 5 CM AT 1 ATM, (b) 40 CM AT 1 ATM, 2.16 — 2.62 μ
H2O
H2O
CH3SH
CH3SH
2.60
2.55 μ
2.50
2.45
2.40
2.35
2.30
2.25
λ
I
a
b

Fig. 18

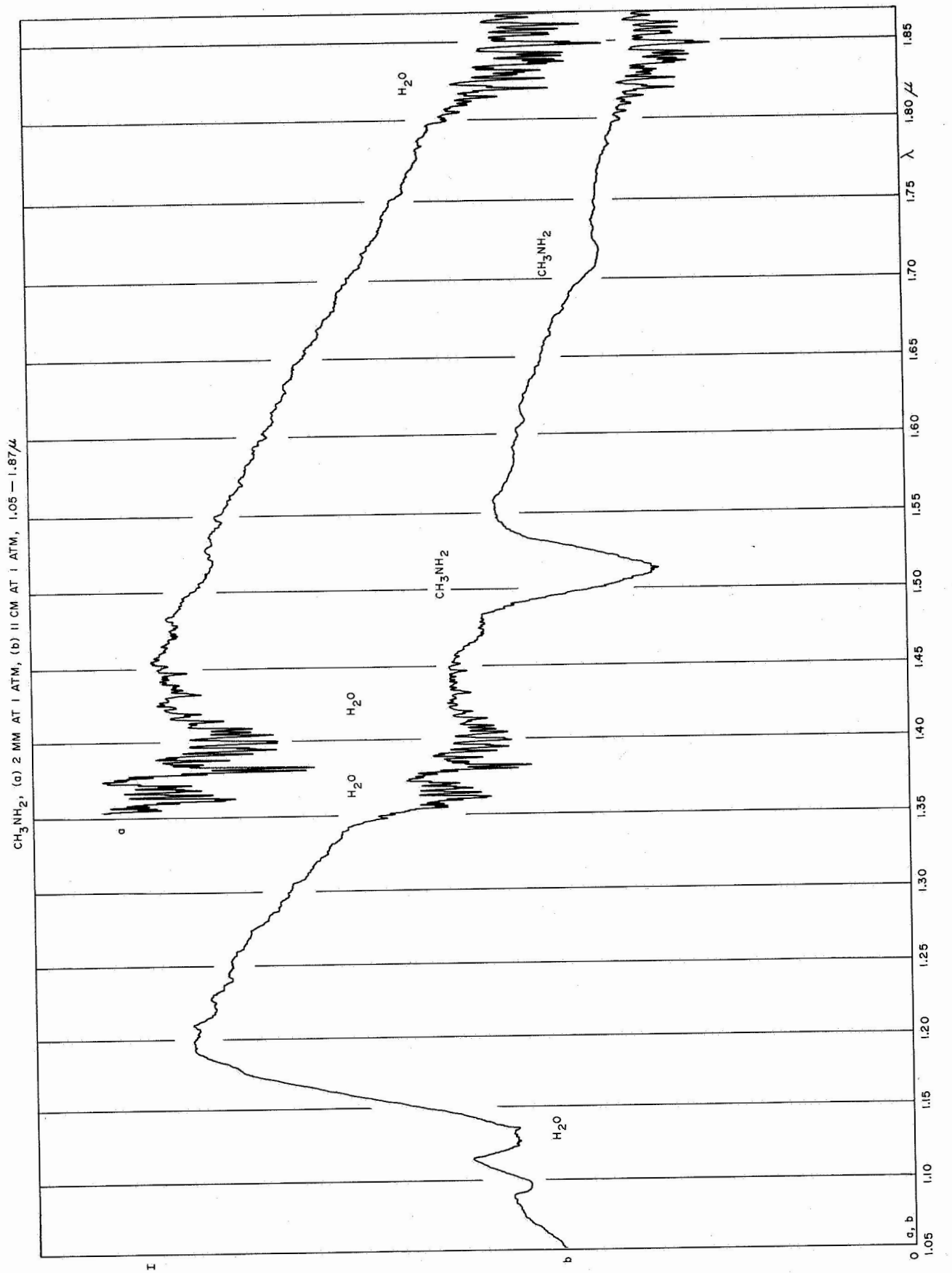
CH_3NH_2, (a) 2 MM AT 1 ATM, (b) 11 CM AT 1 ATM, 1.05 — 1.87 μ
H_2O
CH_3NH_2
H_2O
CH_3NH_2
H_2O
H_2O
a
b
I
0
a, b
1.05
1.10
1.15
1.20
1.25
1.30
1.35
1.40
1.45
1.50
1.55
1.60
1.65
1.70
1.75
λ
1.80 μ
1.85

Fig. 19

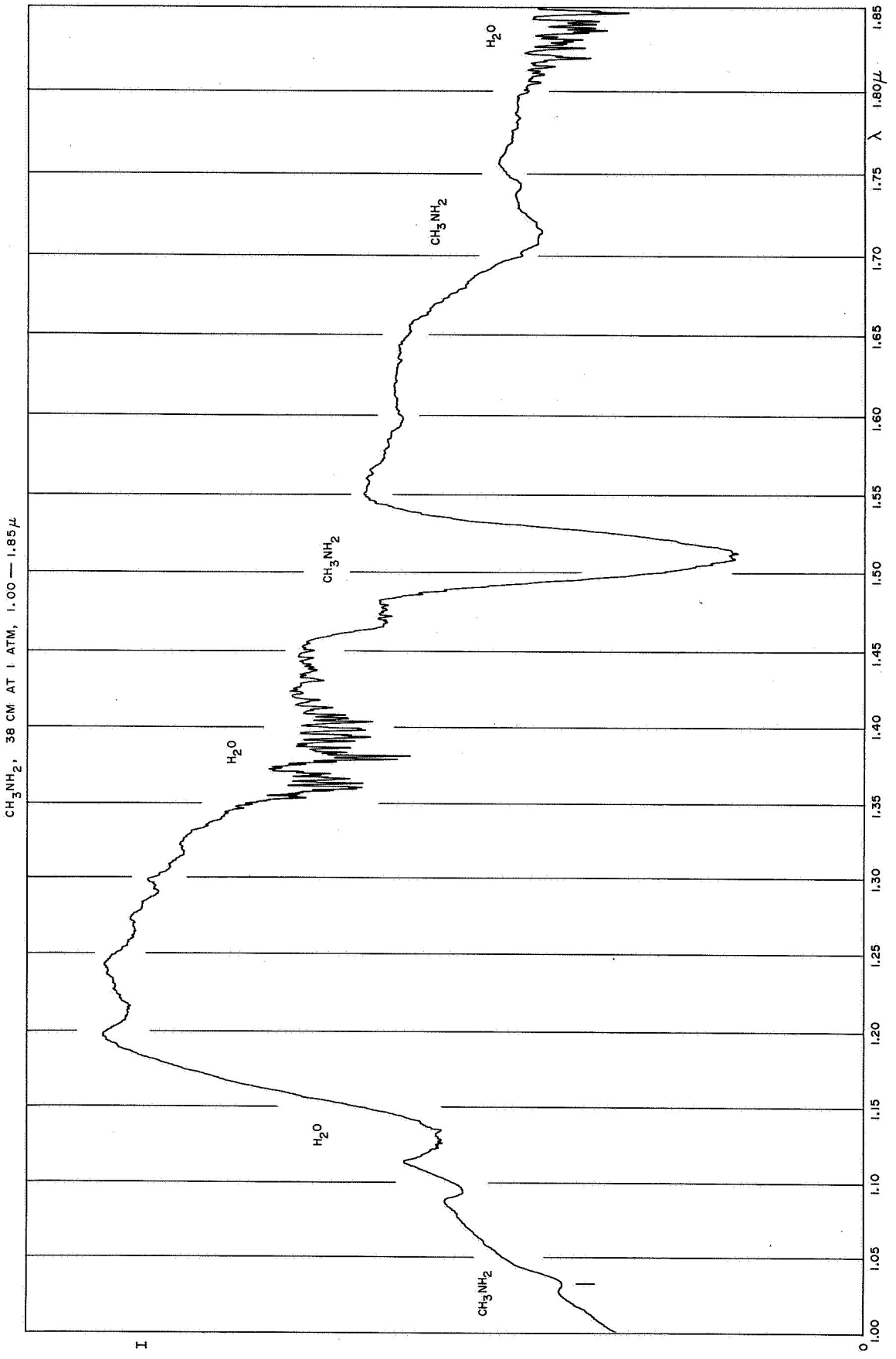
CH_3NH_2, 38 CM AT 1 ATM, 1.00 — 1.85 μ
I
0
1.00
1.05
1.10
1.15
1.20
1.25
1.30
1.35
1.40
1.45
1.50
1.55
1.60
1.65
1.70
1.75
1.80μ
λ
1.85
H_2O
CH_3NH_2
H_2O
CH_3NH_2
H_2O
CH_3NH_2

Fig. 20

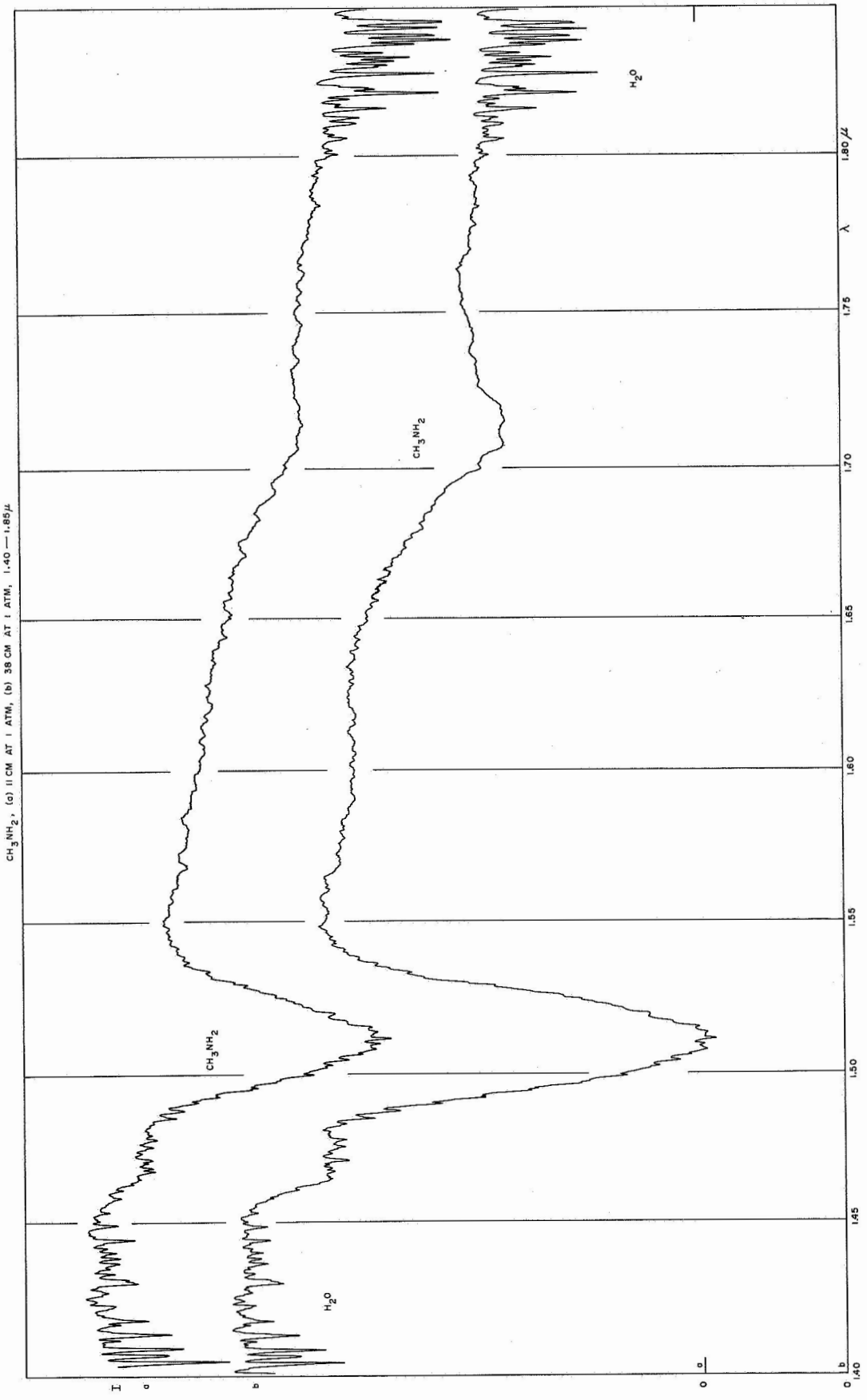
CH_3NH_2, (a) 11 CM AT 1 ATM, (b) 38 CM AT 1 ATM, 1.40 — 1.85μ
CH_3NH_2
H_2O
CH_3NH_2
H_2O
I
a
b
0
a
b
1.40
1.45
1.50
1.55
1.60
1.65
1.70
1.75
1.80 μ
λ

Fig. 21

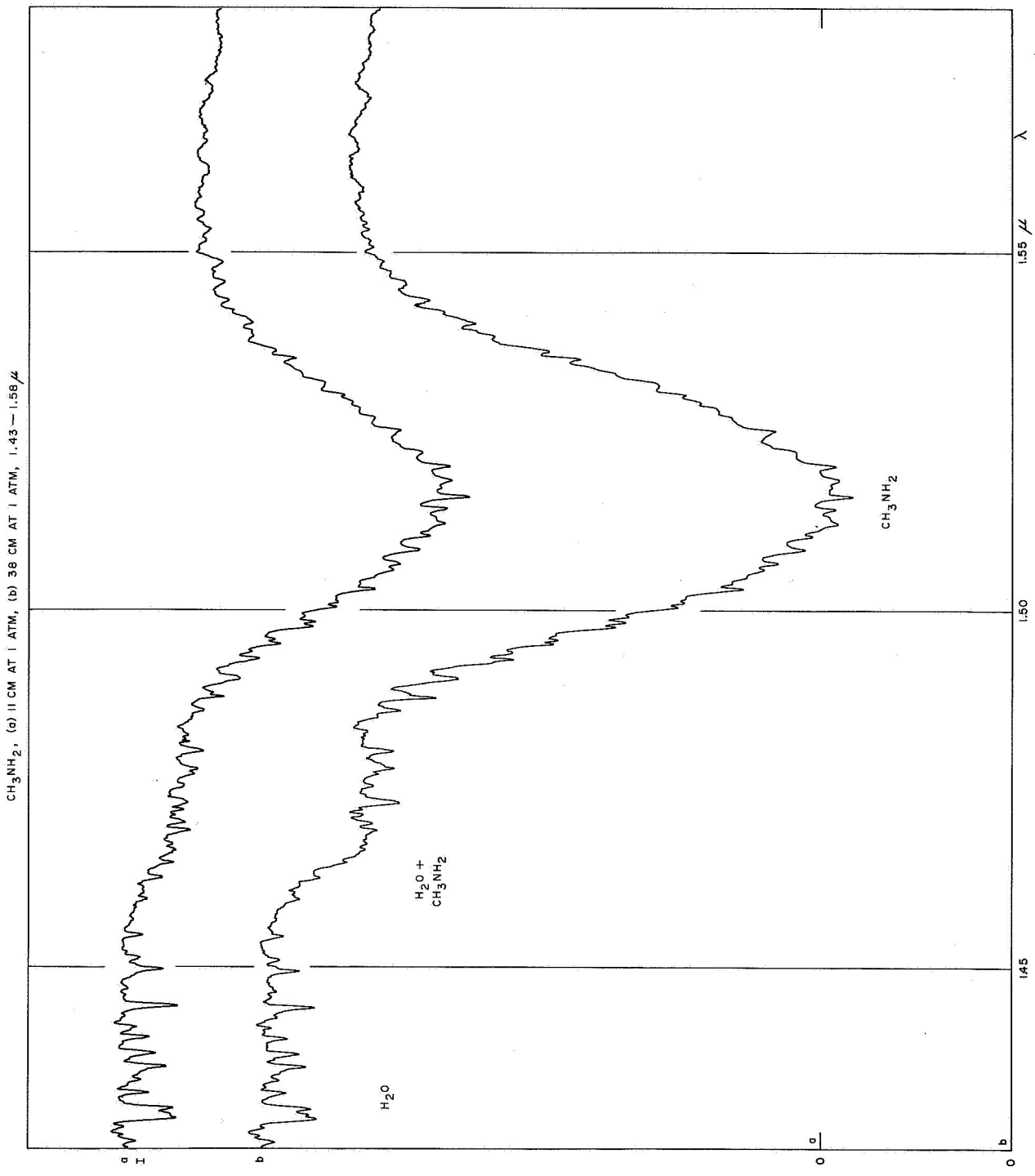
CH_3NH_2, (a) 11 CM AT 1 ATM, (b) 38 CM AT 1 ATM, 1.43 — 1.58 μ
a
b
H_2O
$H_2O + CH_3NH_2$
CH_3NH_2
1.45
1.50
1.55 μ
λ
0
0
a
b

Fig. 22

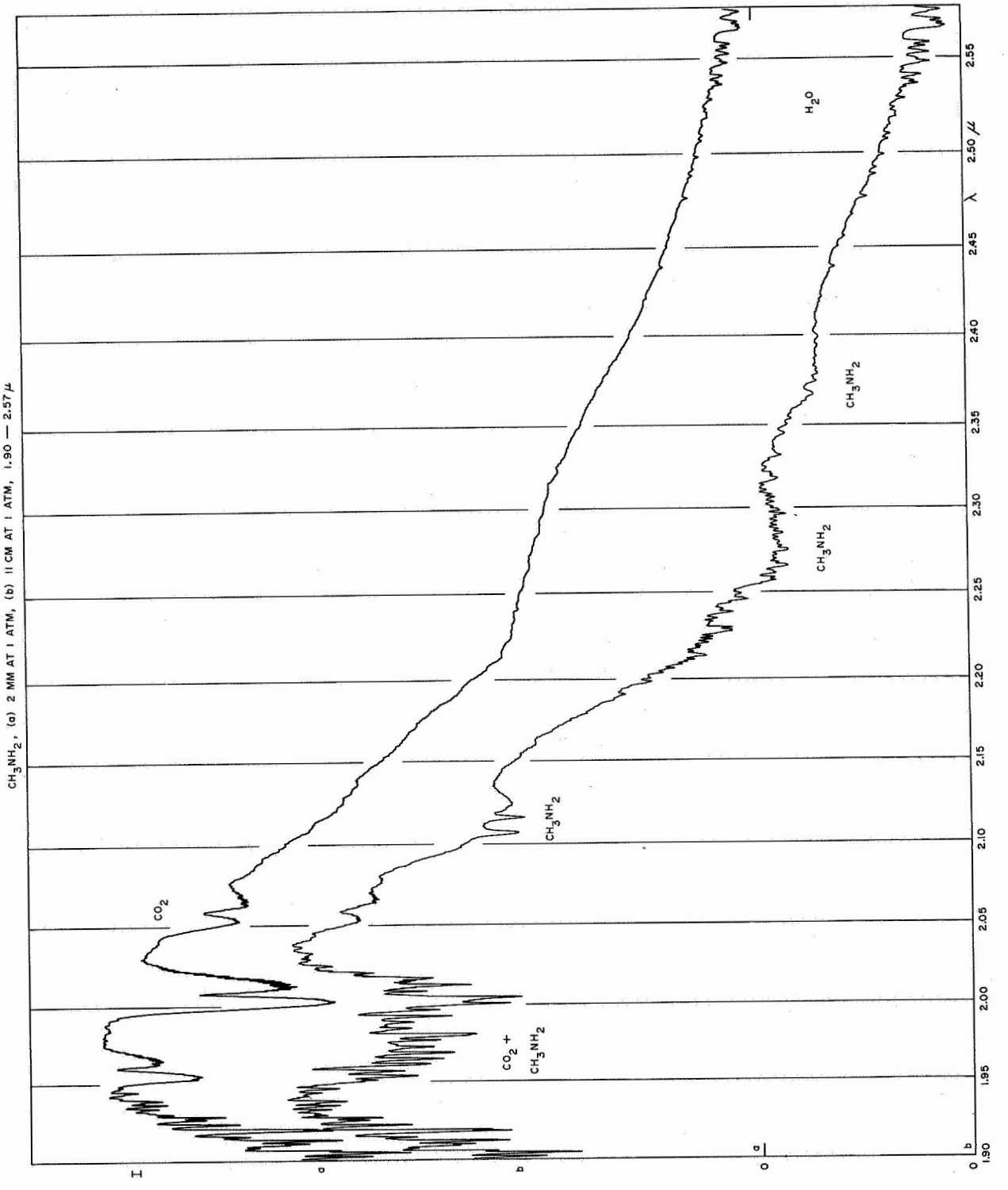
CH_3NH_2, (a) 2 MM AT 1 ATM, (b) 11 CM AT 1 ATM, 1.90 — 2.57 μ
CO_2
CO_2 + CH_3NH_2
CH_3NH_2
H_2O
CH_3NH_2
CH_3NH_2
CH_3NH_2
I
a
b
0
a
b
0
1.90
1.95
2.00
2.05
2.10
2.15
2.20
2.25
2.30
2.35
2.40
2.45
2.50 μ
λ
2.55

Fig. 23

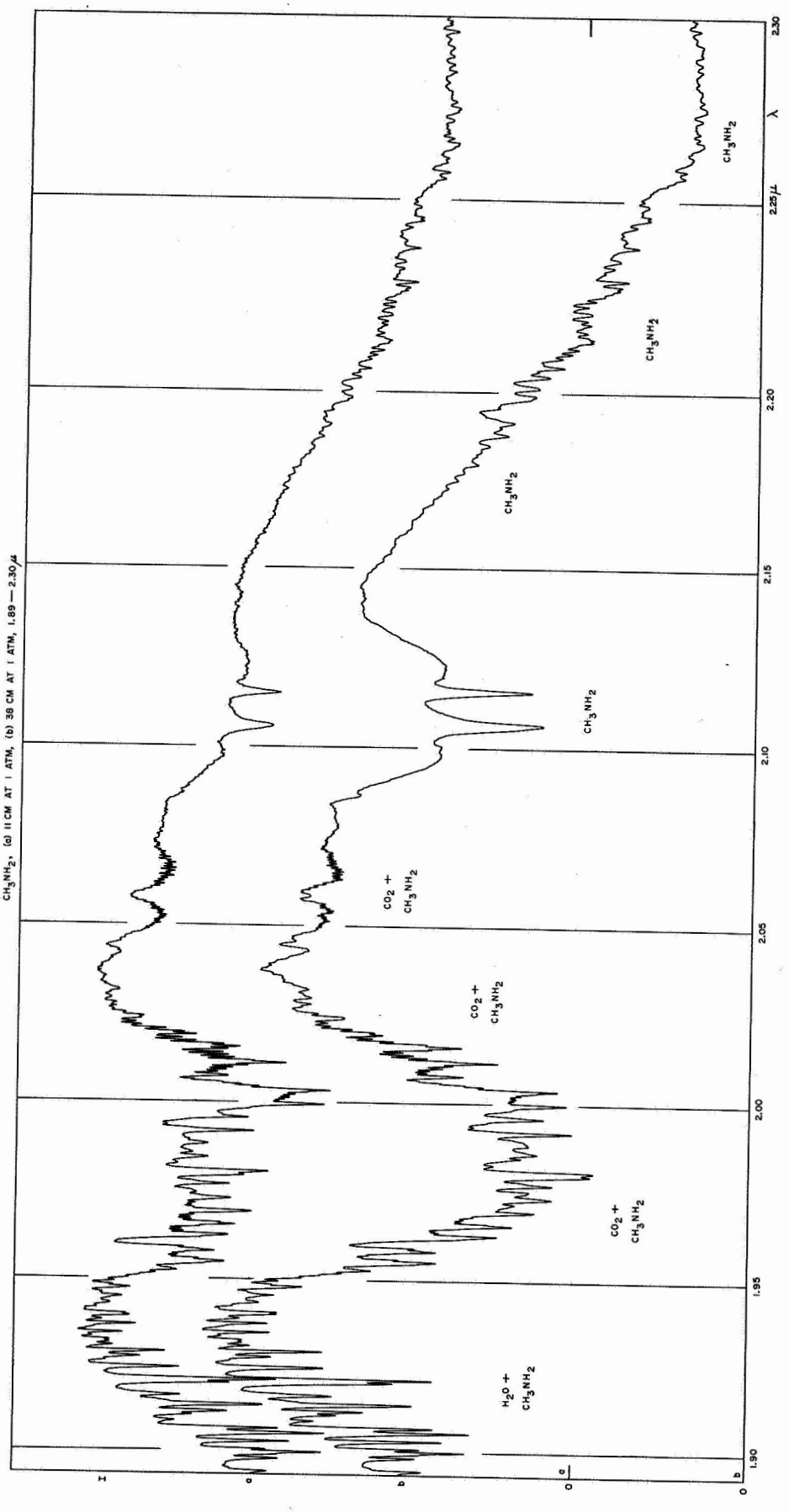
CH_3NH_2, (a) 11 CM AT 1 ATM, (b) 36 CM AT 1 ATM, 1.89—2.30 μ
H_2O + CH_3NH_2
CO_2 + CH_3NH_2
CO_2 + CH_3NH_2
CO_2 + CH_3NH_2
CH_3NH_2
CH_3NH_2
CH_3NH_2
CH_3NH_2
1.90
1.95
2.00
2.05
2.10
2.15
2.20
2.25 μ
2.30
λ

Fig. 24

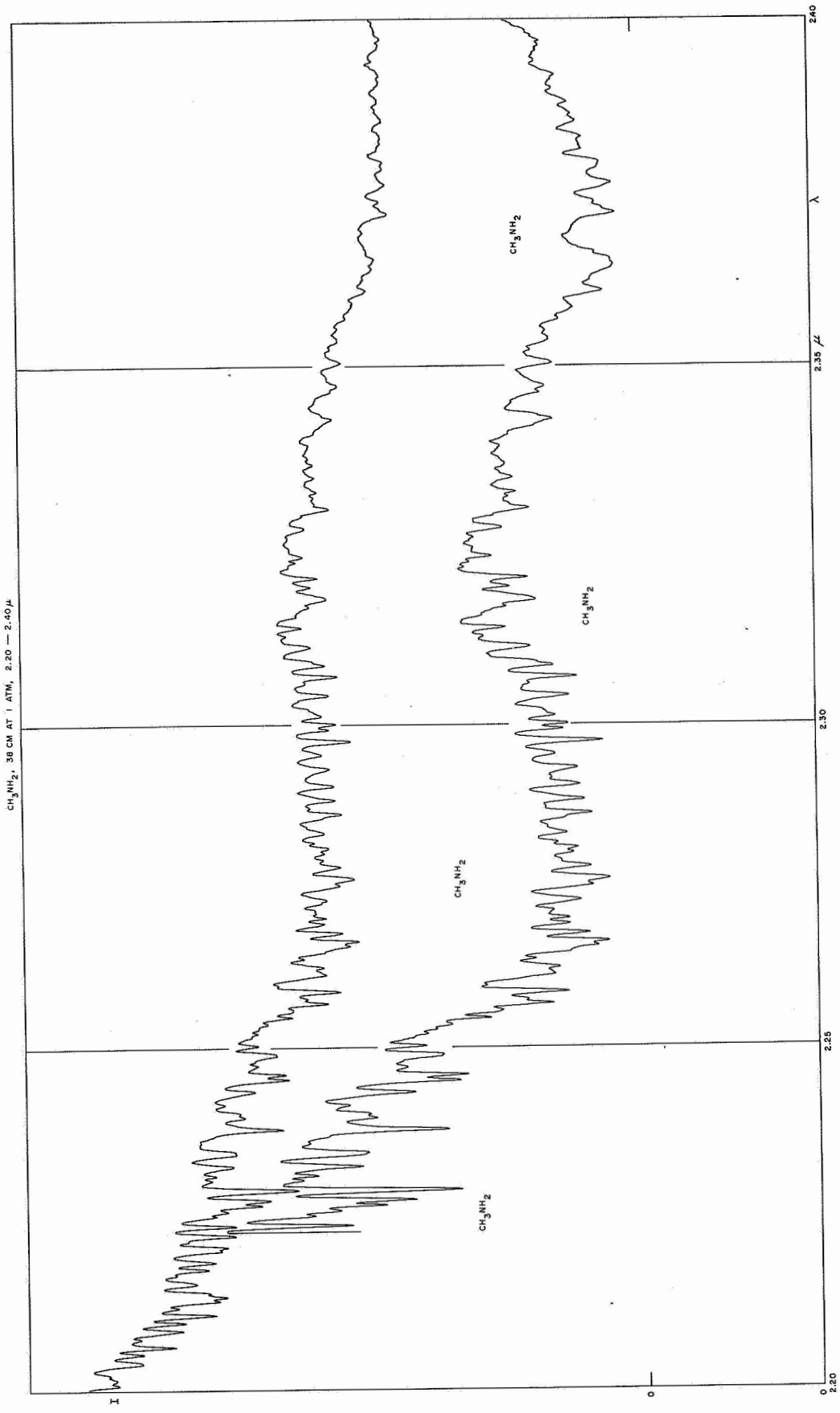
CH_3NH_2, 38 CM AT 1 ATM, 2.20 — 2.40 μ
I
0
0
2.20
2.25
2.30
2.35 μ
2.40
λ
CH_3NH_2
CH_3NH_2
CH_3NH_2
CH_3NH_2

Fig. 25

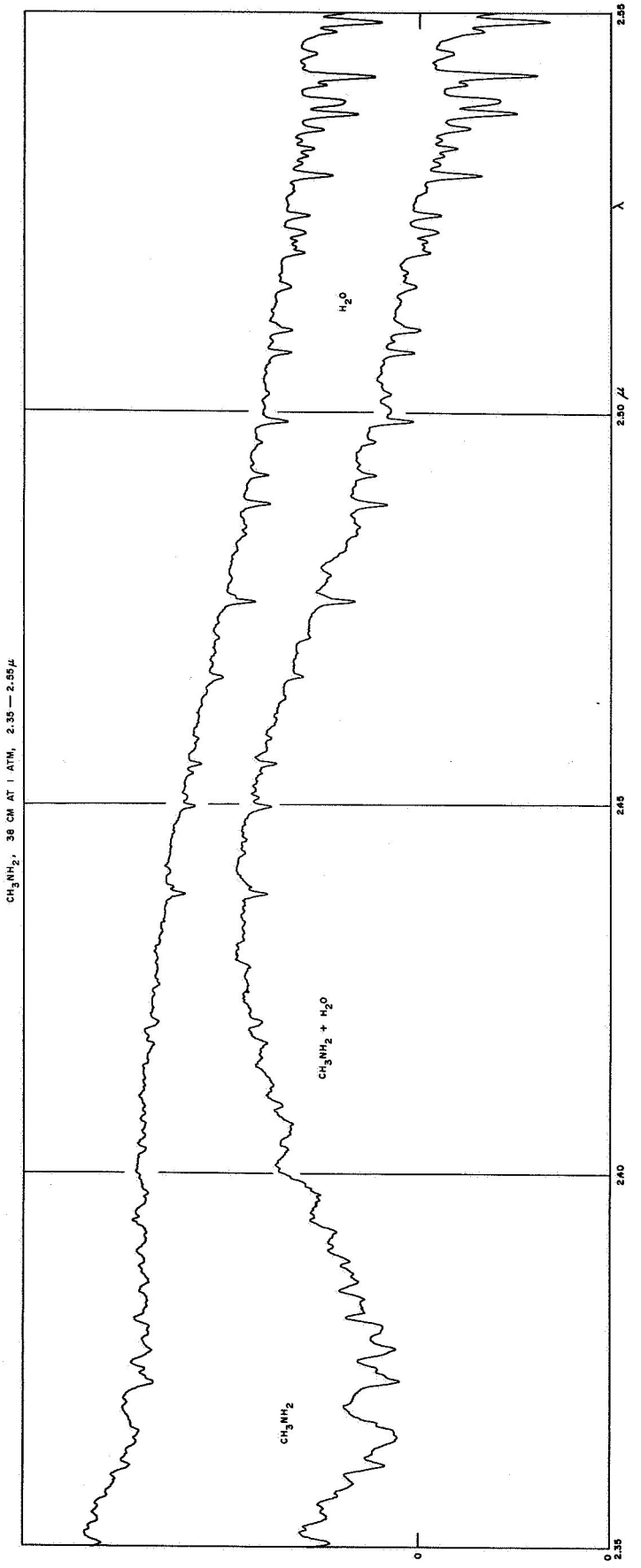
CH_3NH_2, 38 CM AT 1 ATM, 2.35 — 2.55μ
H_2O
$CH_3NH_2 + H_2O$
CH_3NH_2
2.55
2.50 μ
2.45
2.40
2.35
0
λ

Fig. 26

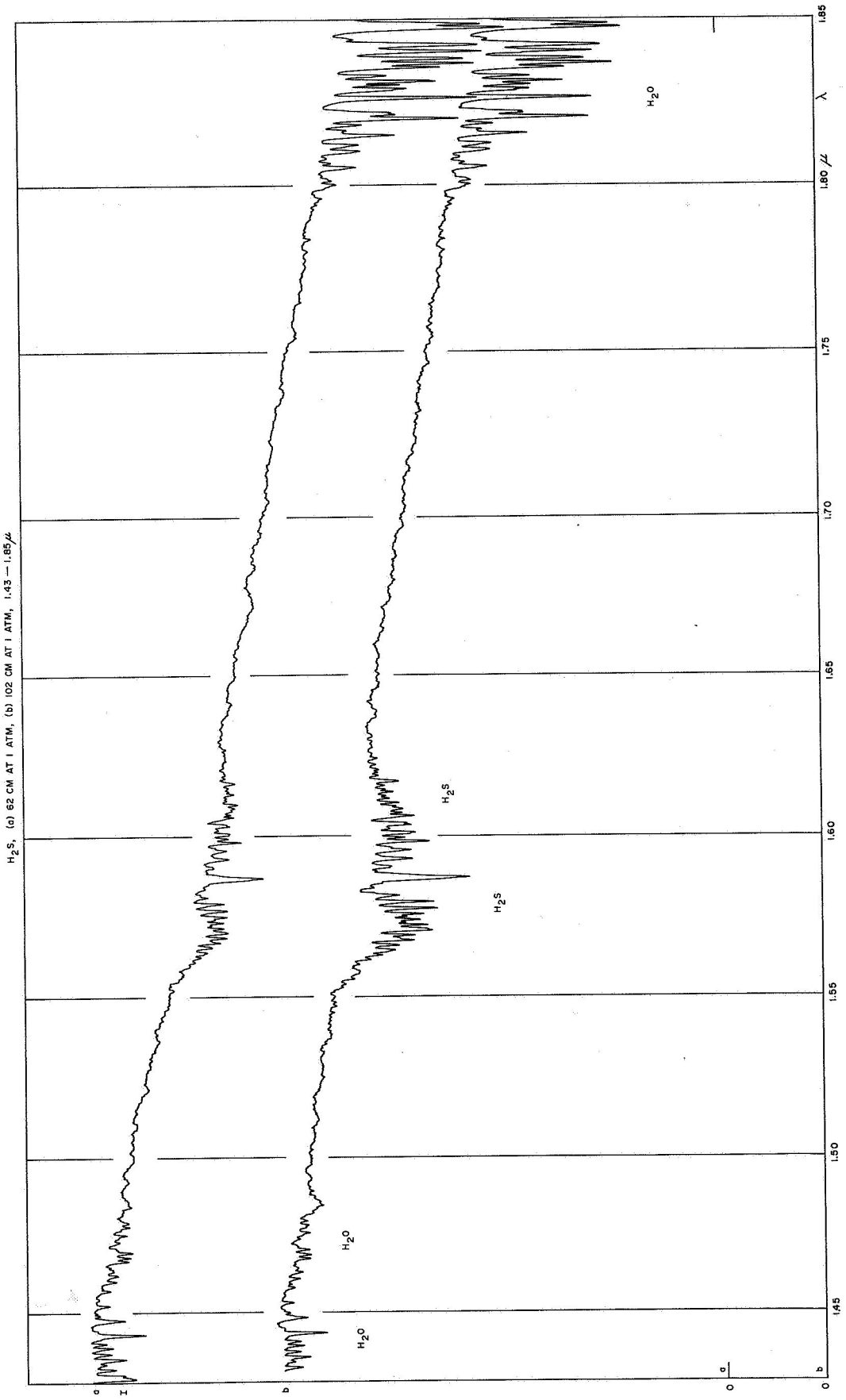
H_2S, (a) 62 CM AT 1 ATM, (b) 102 CM AT 1 ATM, 1.43 — 1.85 μ
H_2O
H_2S
H_2S
H_2O
H_2O
1.45
1.50
1.55
1.60
1.65
1.70
1.75
1.80 μ
λ
1.85
I
a
b
0
a
b
0

Fig. 27

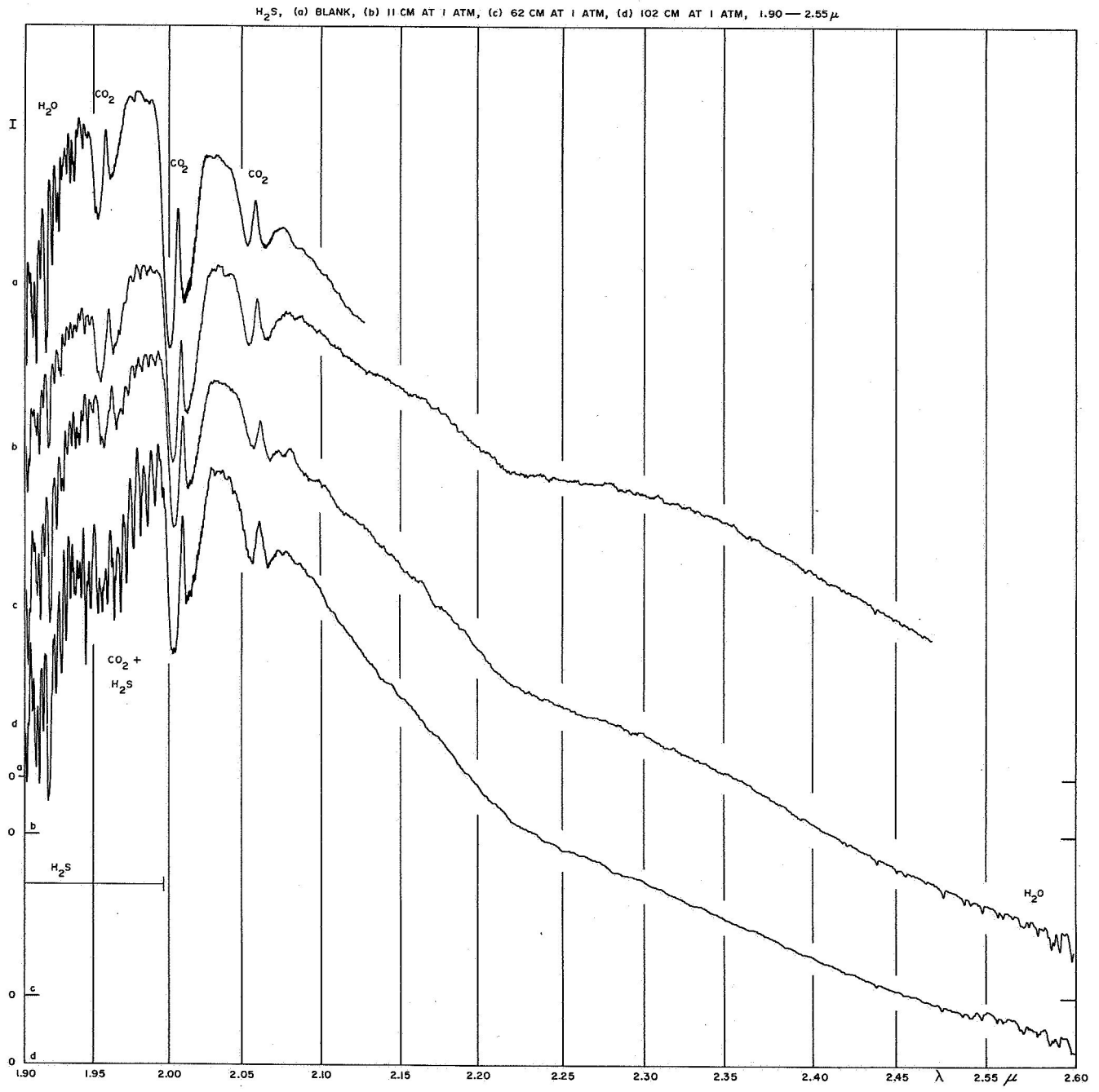
H2S, (a) BLANK, (b) 11 CM AT 1 ATM, (c) 62 CM AT 1 ATM, (d) 102 CM AT 1 ATM, 1.90 — 2.55 μ
H2O
CO2
CO2
CO2
CO2 + H2S
H2S
H2O
I
a
b
c
d
0
1.90
1.95
2.00
2.05
2.10
2.15
2.20
2.25
2.30
2.35
2.40
2.45
λ
2.55 μ
2.60

Fig. 28

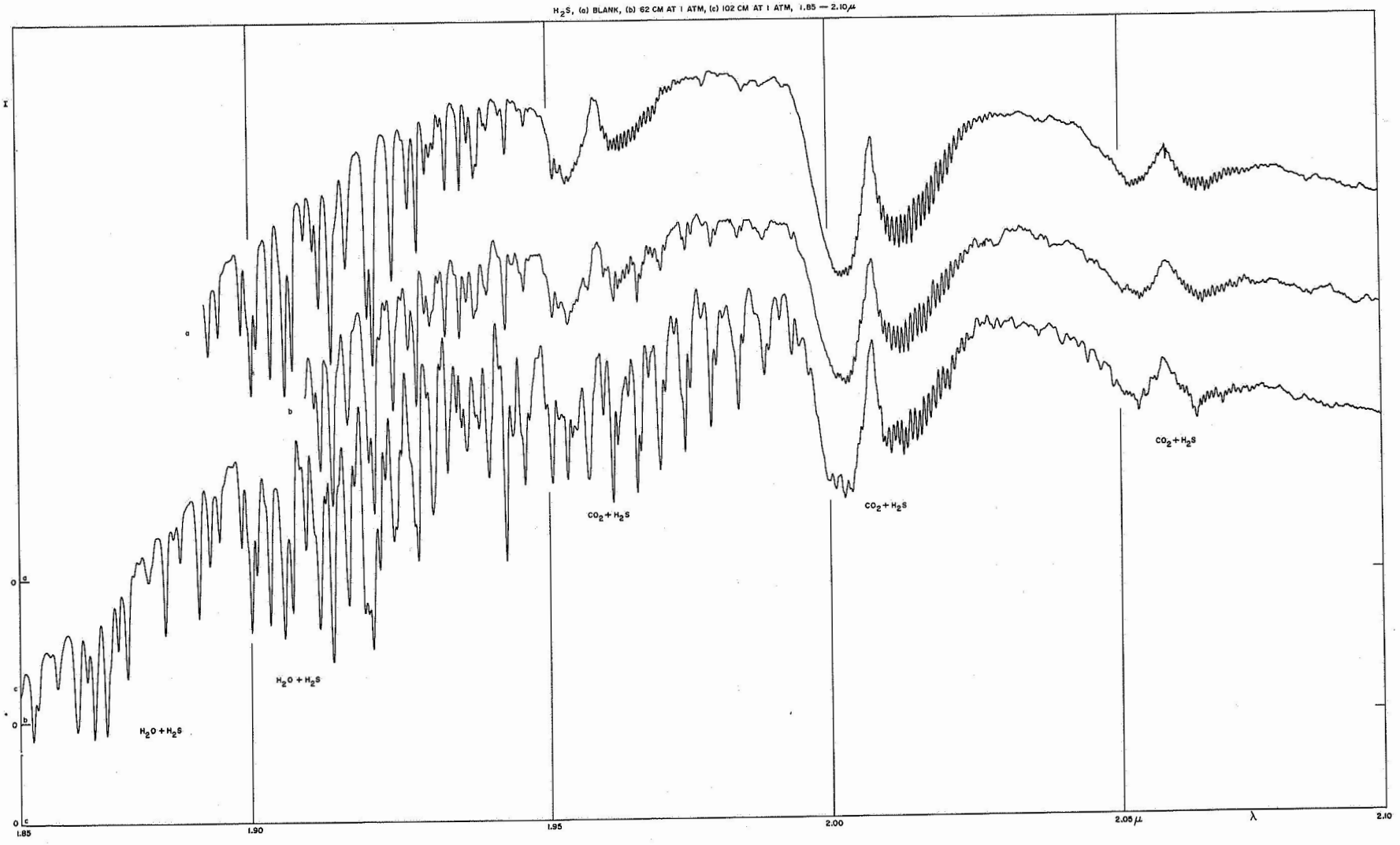
H_2S, (a) BLANK, (b) 62 CM AT 1 ATM, (c) 102 CM AT 1 ATM, 1.85 — 2.10μ
I
a
b
c
$H_2O + H_2S$
$H_2O + H_2S$
$CO_2 + H_2S$
$CO_2 + H_2S$
$CO_2 + H_2S$
1.85
1.90
1.95
2.00
2.05μ
λ
2.10

Fig. 29

No. 80 LUNAR CRATERS COUNTS. I: ALPHONSUS

by WILLIAM K. HARTMANN

March 20, 1967

ABSTRACT

Figures 2 and 4 show the diameter distributions of craters on the east inner wall, the central ridge, and the floor of Alphonsus in the diameter interval 125 m $< D <$ 8 km. The surface density of craters on the floor is about three times that on the wall, and the diameter distributions are parallel over much of this range. Two tenable working hypotheses are discussed to account for this. It is suggested that the central ridge may represent a horst-like structure created during flooding of the floor.

1. Introduction

This paper initiates a series of notes describing results of a crater counting program. The series represents work subsequent to *Comm. LPL,* No. 38, "On the Distribution of Lunar Crater Diameters," (Hartmann 1964*b*). To date, crater diameter distributions have been prepared in LPL for various lunar regions using earth-based, Ranger, Zond III, and Orbiter photography.

Unless otherwise noted, the counts in this series are incremental, the crater frequency F as a function of crater diameter D defined as

$$F(D) = \frac{\text{no. craters in } \Delta\log D \text{ increment}}{\text{km}^2}, \quad (1)$$

where the $\Delta\log D$ increment corresponds to the factor $\sqrt{2}$. Thus, each increment constitutes a 40 percent increase in D, a compromise between construction of highly, perhaps overly, detailed frequency distributions and rapid reduction procedures. Incremental counts have the advantage that counts in each size interval are independent, and the frequency distributions so defined, if linear, have the same slope as cumulative counts. The frequency distributions are plotted as histograms. The individual bars of the histogram typically represent counts of ten to two hundred craters. Dashed bars show counts of lesser statistical weight.

In view of the present state of understanding of the lunar craters, I believe that under-interpretation is preferable to over-interpretation. Therefore, I have avoided, so far as possible, dividing craters by supposed modes of origin and interpreting "fine structure" in the crater distributions.

2. Alphonsus Wall — Observations

Figure 1 shows the region of the Alphonsus east wall photographed with moderate resolution by Ranger IX. Counts were made from a number of frames with both higher and lower resolution than Figure 1. It was found that although all craters with $D < 1$ km were well defined, among larger diameters there were a number of ill-defined, crater-like depressions. If they appeared on other background terrains, they would be mapped as heavily damaged craters. These unusual types were counted separately. Many are included in Figure 1, although they are difficult to detect because they are more prominent at lower resolution. As the resolution increases, the circular structure is lost in the chaos of hummocky rim structure.

Figure 2 shows the distribution of crater diameters in the resolved regime on the Alphonsus wall. Counts of the ill-defined craters are marked with circles; they appear to be overabundant with respect to the smooth curve for the well-defined craters.

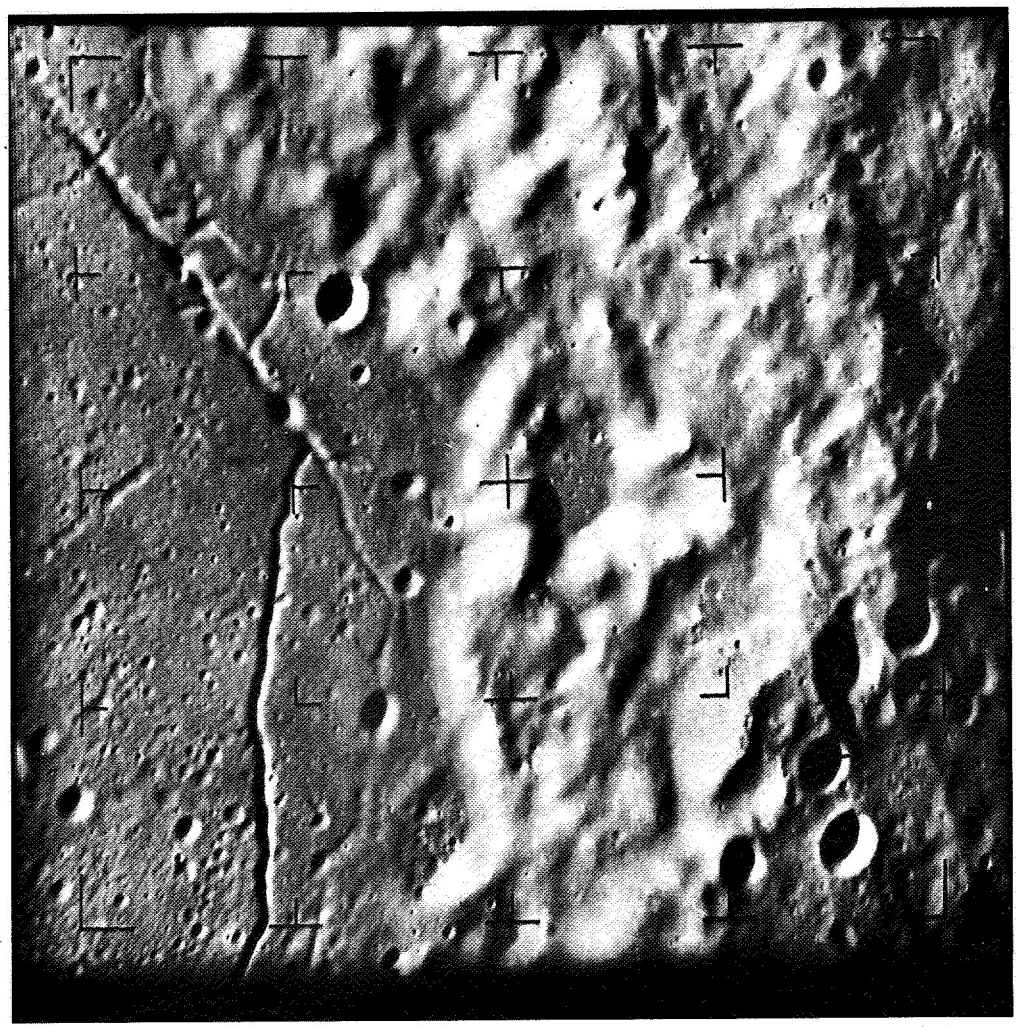

Fig. 1 Inner wall of Alphonsus and a portion of the NE floor. Ranger IX, frame B67.

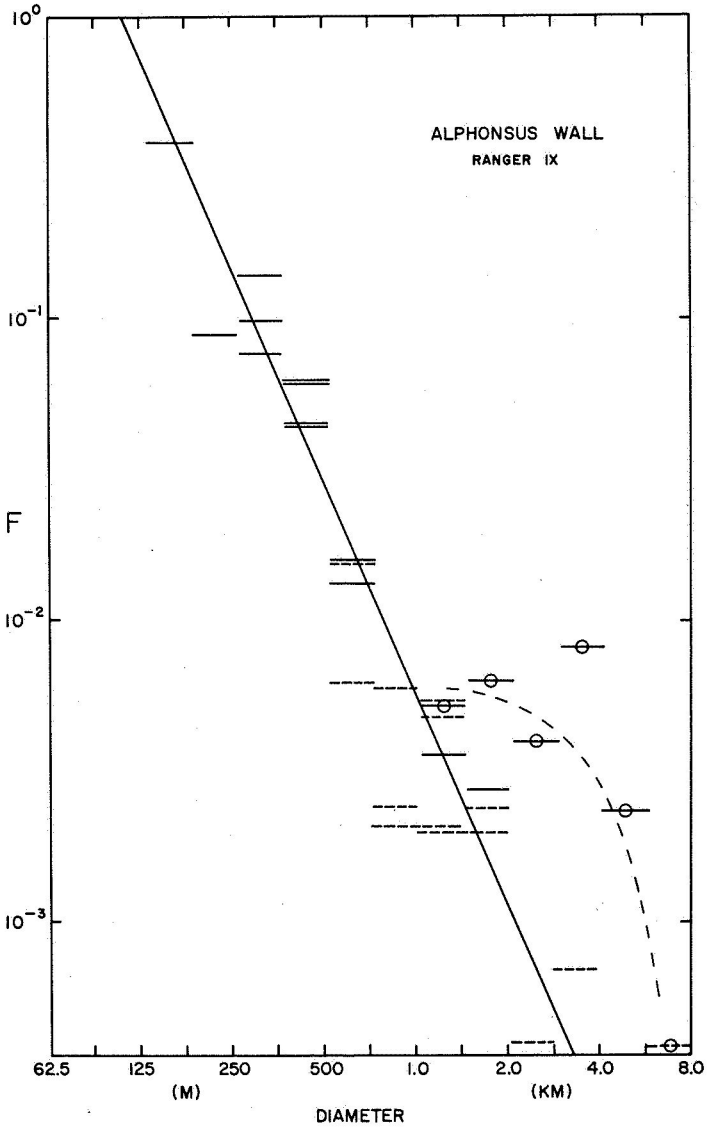

Fig. 2 Diameter distribution of craters on the Alphonsus NE inner wall. Dashed bars are of lesser weight (absolute count ≤ 5 craters). Circled bars include a number of ill-defined crater-like objects, tentatively interpreted as remnants of early craters nearly destroyed by major crater wall slumping. Straight line has slope -2.3.

The distribution of the latter appears to be quite well determined, and a linear relation is satisfactory in this diameter range (125 m to 4 km). The straight line fit in Figure 2 has a slope −2.3.

3. *Floor and Central Ridge — Observations*

Figure 3 shows a moderate-resolution view of the floor and central ridge of Alphonsus. A clear asymmetry in crater density can be seen between the east and west side of the crater floor, divided by the ridge. Closer examination shows smaller anomalous areas.

These asymmetries were neglected in the preparation of Figure 4, which compares the wall, floor, and ridge crater counts, made from many photographs. Among the larger craters (from the lower resolution frames) are some counts from the west side, although Figure 4's crater diameter distribution is an average primarily over the eastern part of the floor. Making counts of craters on the central ridge was difficult because of the small area and moderate ground resolution, but it appears that the ridge contains systematically fewer craters than the floor, yet more than the wall.

From $D = 500$ m to 2 km, the range of the best data, the ridge exhibits about 2.2 times the crater density of the inner wall, and the floor, about 3.0 times the density of the inner wall. These values are thought to be correct to within 15 percent. It should be emphasized that these counts include all identifiable craters, regardless of morphology or origin. At $D = 200$ m there appears to be a convergence of wall and floor counts.

The curve corresponding to the floor craters in Figure 4 parallels that of the wall craters over the range 350 m $< D <$ 3 km, having the slope −2.3. This is in good accord with the data of Shoemaker, *et al.* (1966), who report a value of −2.0 for $D < 500$ m and −2.7 for $D > 500$ m. However, the absolute density of craters counted by Shoemaker, *et al.* is systematically higher than that reported here (after converting to the cumulative format of Shoemaker, *et al.*); the cause of the discrepancy is uncertain.

4. *Interpretation*

The floor of Alphonsus has undoubtedly been flooded in the same sense that the maria have been flooded. Not only in photographs with low (earth-based) resolution, but also in those with moderate to high resolution down to meter scales, the Alphonsus floor structure is nearly indistinguishable from the mare surface structure. The only differences are the well-known higher albedo and a somewhat greater crater density in the kilometer-diameter range. Both of these differences — i.e., a thin veneer of secondary high-albedo material and a longer impact-recording time — suggest a somewhat greater age for the Alphonsus floor than the mare surface. Furthermore, the whole Alphonsus structure appears to be older than the average mare (Alphonsus is classed as pre-mare in the Arthur catalog, Arthur, *et al.* 1965). Alphonsus appears to be one of the typical, very old, damaged, large upland craters. One would expect that immediately after the formation of Alphonsus, the interior surface represented a clean slate for recording impacts. One might also assume that the wall is this same original surface and that the floor has been wiped clean again by the flooding. Hence, if we are here counting primarily impacts, one expects to see a high crater density on the old wall and a lesser density on the younger, mare-like floor. Instead, just the reverse is shown by Figure 4.

Apart from hypotheses requiring extraordinary conditions (walls younger than floor or unusual, thick deposits on the walls), two principal working hypotheses, consistent with the observations, may still be drawn from the literature resulting from the Ranger and Orbiter photography (e.g., Kuiper, Strom, and LePoole 1966; Shoemaker, *et al.* 1966; O'Keefe, Lowman, and Cameron 1967). These will be discussed in turn.

Hypothesis 1. Both the floor and wall of Alphonsus have a steady-state distribution of primary impact craters. The wall has fewer craters because downslope movement of material, or mass wasting, is constantly causing (or has in the past caused) crater erasure. Only the floor represents a sample of craters undisturbed by mass wasting, and it is in a near-saturation state for craters in the size range considered here.

A difficulty with this hypothesis is that the kind of slow mass wasting widely discussed would be expected to erase smaller craters preferentially. Fewer small craters would thus be found than expected from extrapolation of the large-crater counts. This would reduce the steepness of the slope of the wall counts. There is no evidence of this in Figures 2 and 4. The dotted wall curve in Figure 4 parallels or is steeper than the floor counts at all points; thus, there appears to have been no preferential erasure of small craters on the wall.

A related process that may have played a role in the history of the wall is slumping on a large scale.

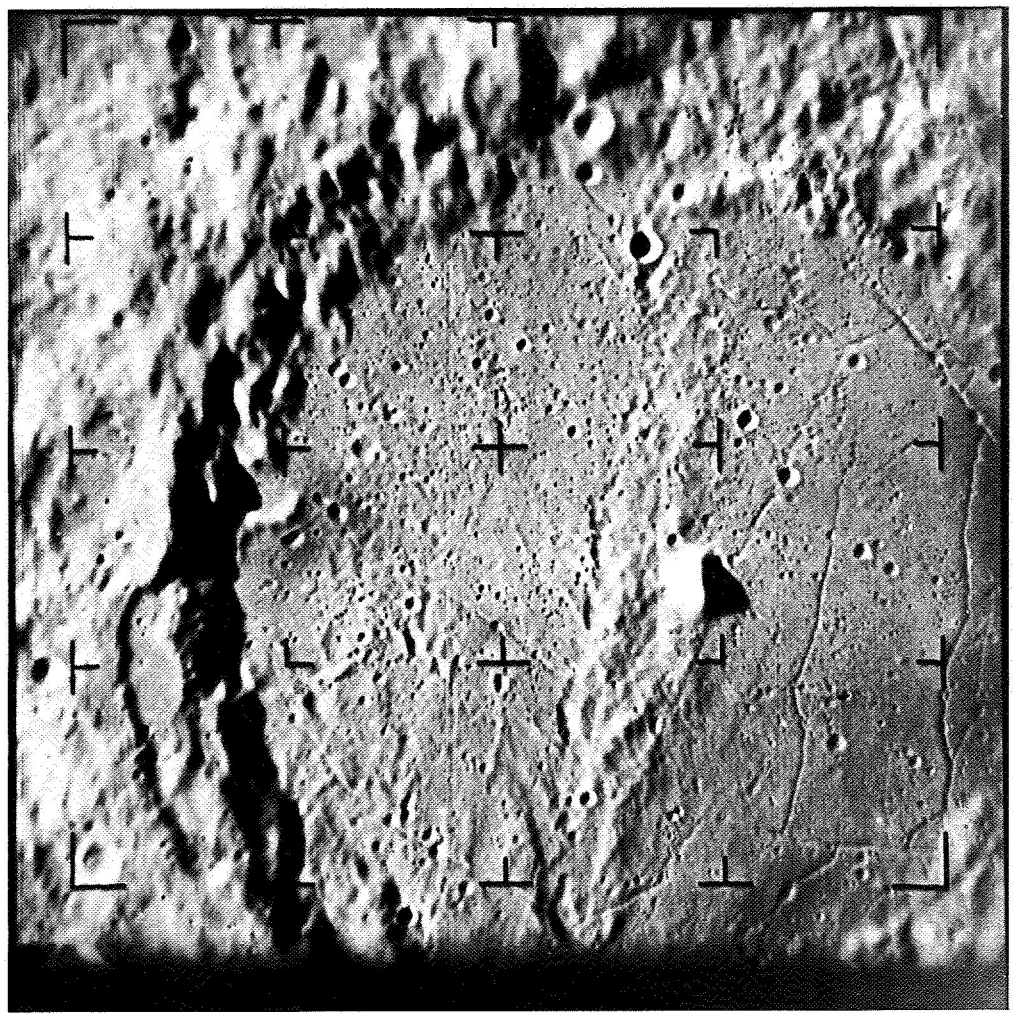

Fig. 3 Interior of Alphonsus, showing the central ridge and asymmetry in crater density between the E and W side. North up. Ranger IX, frame A52.

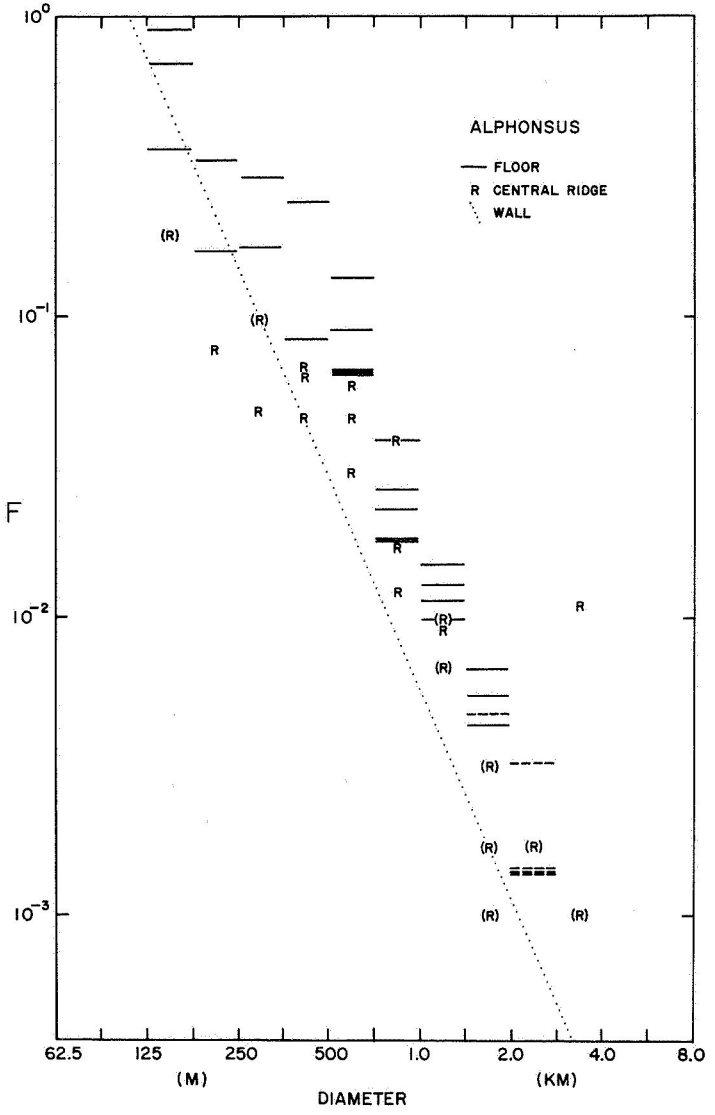

Fig. 4 Diameter distribution of craters inside Alphonsus. Dashed bars and parentheses denote lesser weight (absolute count ≤ 5 craters). Dotted line (wall; after Fig. 2) has slope −2.3.

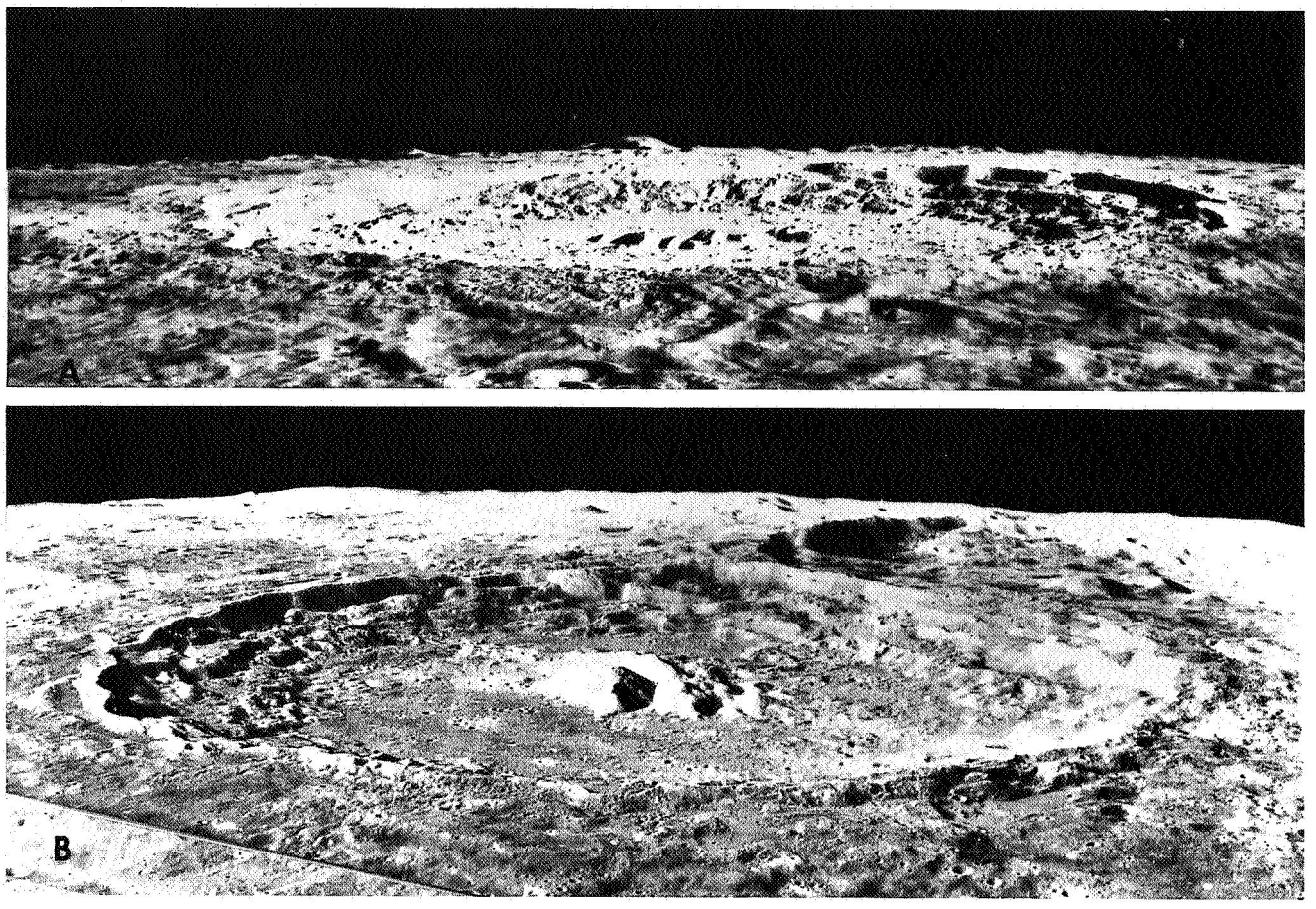

Fig. 5 Terraces and scarps, apparently due to crater wall slumping, in Copernicus (*A*, Orbiter II) and Theophilus (*B*, Orbiter III). (Photographs courtesy of NASA.)

This phenomenon has apparently occurred in Copernicus and Theophilus, producing the well-known steep scarps and flat terraces (Fig. 5). It is pictured as more catastrophic than mass wasting. It would account for the deformed crater-like structures on the Alphonsus wall (as pre-slump craters) and for the overabundance of these craters in Figure 2. Such slumping is not unexpected in large-crater walls, since these mark initially steep relief and loci of isostatic discontinuities produced by crater excavation and rim deposition. However, the sides of well-defined lunar hills also appear to be deficient in craters with respect to adjacent mare regions, even in cases where obvious catastrophic slumping has not occurred, and hence, such slumping does not alone account for the marked crater deficiency.

Hypothesis 2. The wall of Alphonsus represents a slate wiped clean at the formation of Alphonsus, a recorder of impacts ever since. The floor represents another recorder, formed shortly thereafter, but contaminated with a great number of craters of some other mode of origin, presumably internal and peculiar to the mare or mare-like material. Since the floor craters outnumber the wall craters by the factor 3, we would conclude that 67 percent of the floor craters are of non-impact origin. Mass wasting has had only a minor or negligible effect in erasing craters.

This hypothesis is illustrated in Figure 6. The shaded band represents the range of crater densities found in normal large maria. The bars represent the Alphonsus floor and show an excess (by a factor of about 2.5) of craters of $D > 500$ m. Mare craters of $D < 2$ km, which vary in density on different mare surfaces, are interpreted in this hypothesis to be mostly of internal origin peculiar to the maria. The true impact craters are supposed to follow a curve similar to that shown by the dashed line (after Kuiper, Strom, and LePoole 1966). They constitute only a fraction of the total crater densities at diameters $D < 2$ km.

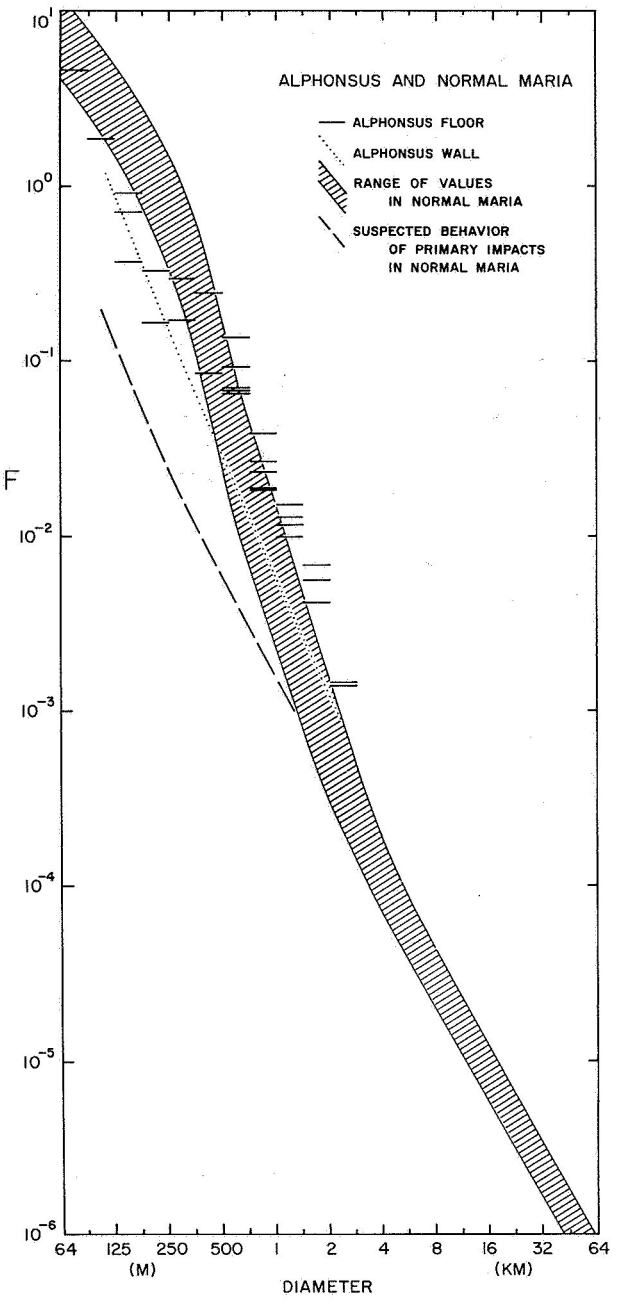

Fig. 6 Comparison of crater diameter distributions in Alphonsus and normal maria. Dashed line schematically shows values proposed by Kuiper, Strom, and LePoole (1966) for primary impacts. Its parallelism with observed counts of all craters on the wall of Alphonsus (dotted line) supports the hypothesis that primary impact craters indeed show this distribution.

Important support for hypothesis 2 comes from the rough parallelism between the wall counts and the dashed line in Figure 6. That is, the craters on the Alphonsus wall have a diameter distribution in the 125-m to 3.5-km range very close to that expected for the supposedly primary impact craters.

On the other hand, a number of observations (Shoemaker, *et al.* 1966; Gault 1967, private communication) indicate that the mare surfaces display near-saturation impact cratering in a loosely consolidated layer of rubble several meters deep. The "sharp" and "soft" craters are held to show merely a continuum of different states of erosion and blanketing. According to this view, the craters on the floor of Alphonsus are nearly all of primary and secondary impact origin in various states of erosion and blanketing, rather than a mixture of endogenous and exogenous craters. Such a view is incompatible with the interpretation of hypothesis 2 and would force one toward some variant of hypothesis 1.

These two hypotheses seem the only two, or the leading two, tenable explanations of the observations of the Alphonsus floor and wall, but it is difficult to choose between them without further data.

The small anomalous regions, illustrated in Figure 7, appear to be deposits superimposed on the cratered background. Two observations support this: (1) in cases where the anomalous region is not distinguished by albedo, it is distinguished by a fuzzy appearance as if camera resolution has failed in a certain area; (2) rilles crossing the anomalous area are filled in. Crater counts attempted in these regions gave no meaningful results because of the small area and insufficient resolution. The areas are associated with prominent single craters of $D \sim 1$ to 3 km. Craters apparently wiped out by the deposits range up to $D \simeq 600$ m. For fresh craters of this size, the depth d is estimated to be 70 m, in accord with the geometric data reported by Heacock (1966). The data of Jaffe (1965) indicate that to erase such a crater by deposition of material, starting from typical, already smoothed morphologies in non-anomalous regions, one would have to add a layer roughly 40 m thick. These figures apply to the example shown in Figure 7*b*, where the volume of the deposit (an elliptical patch 6 x 3.5 km) would be about 3 km^3, while the volume of the main crater would be only about 0.6 km^3. In view of the fact that most ejecta from an impact crater of this size should be piled up in a rim, we conclude that the ejecta blanket is several times more voluminous than could be accounted for in an impact. Hence, the ejecta blanket must be eruptive. The deposited volume estimated above is comparable to that of a large, terrestrial eruption, and is several orders less than the total volume of a magma chamber under a typical terrestrial volcano of moderate size (Williams 1942; Rittmann 1962). The asymmetry of some of these

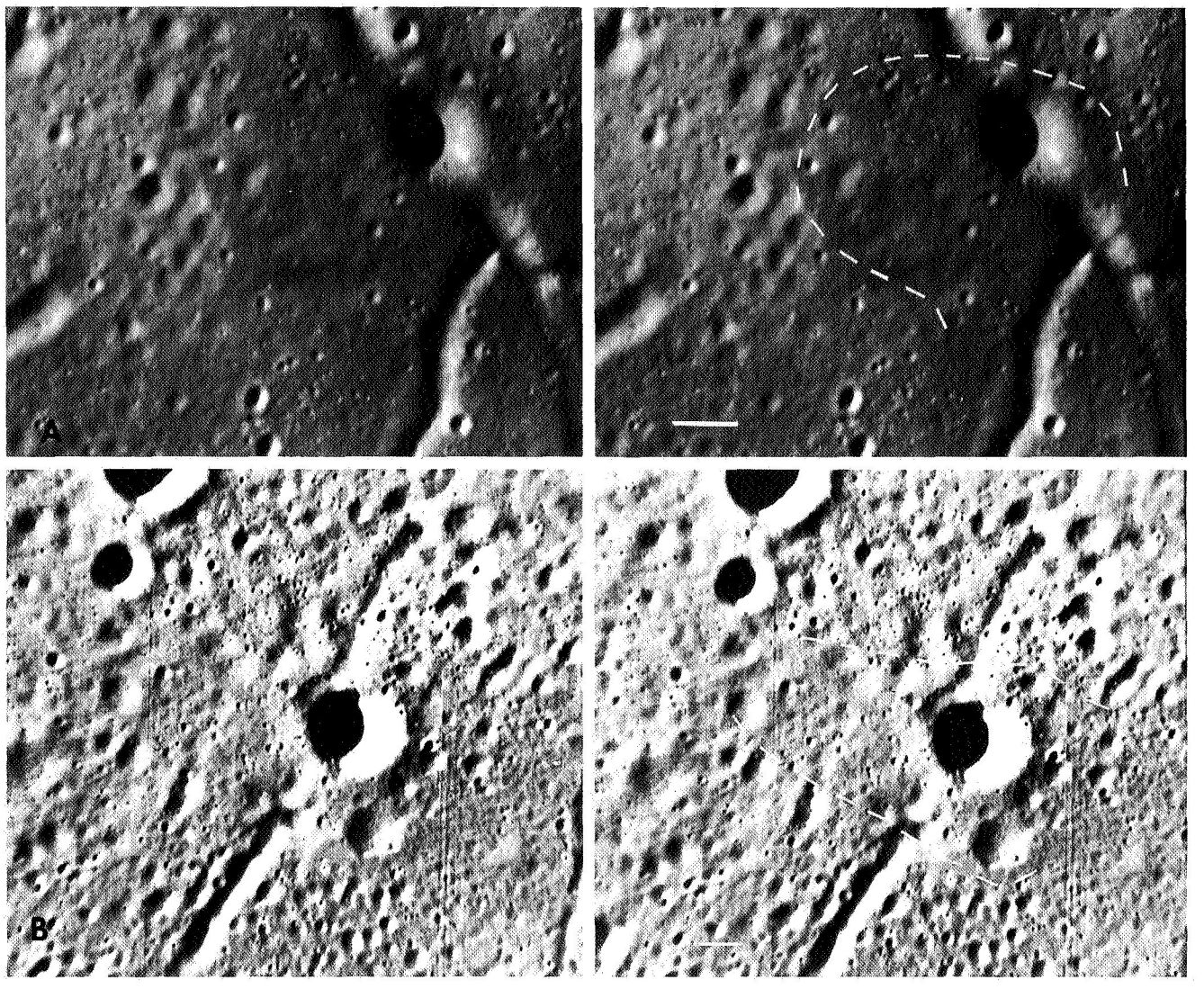

Fig. 7 Local anomalous regions on the floor of Alphonsus. *A*. Dark halo crater. *B*. Region of apparent blanketing with no albedo anomaly. These are interpreted as regions of local eruptive deposition. White bars at bottom indicate 1 km scale.

apparent deposits with respect to the associated crater is also characteristic of an eruptive origin. Finally, the close association of the dark-halo craters with rilles in Alphonsus has long supported the supposition that the halo craters are endogenous (cf. Kuiper, Strom, and LePoole 1966, p. 134).

These evidences for scattered endogenous craters of substantial size on the mare-like floor of Alphonsus support hypothesis 2 — that there is an admixture of endogenous craters there.

Finally, we will consider the central ridge of Alphonsus, which has been interpreted in many different ways. It is accurately aligned with, and considered a part of, the Imbrium radial system as described earlier in these *Communications* (Hartmann 1963, esp. Plate 24.21). Among others, Urey (1966) has described the ridge as consisting of exogenous material dropped onto Alphonsus "from the Imbrian collision itself or of material driven from the wall of Alphonsus by ejecta from the Imbrian collision." He believes that "when it fell it depressed the floor of the crater."

Certain observations suggest to me an endogenous origin. First, along parts of the west side of the ridge stretches a crater chain (see Fig. 4), suggesting that the ridge is defined on at least one side by a fracture. Second is the alignment with the Imbrium radial system, which is held to be primarily tectonic. Third, the ridge divides two provinces of different crater densities, indicating a division in the flooding histories. Hence, it is suggested that this ridge is in the nature of a horst. It has been argued (Hartmann

1963, 1964*a*) that the basin-forming impacts created families of radiating fractures, along which tectonic events occurred, and that subsequent flooding was controlled in part by these fractures. In Alphonsus, the two halves of the floor flooded and subsided somewhat independently. The ridge may have once been partially flooded, but has been left above the subsided units. The herring-bone pattern of the ridge, visible at certain illuminations, suggests the possibility of some shearing.

The interpretation of the central ridge as an old, partially flooded horst is consistent with either hypothesis 1 or 2. In case 1, its crater density intermediate between the wall and floor is ascribed to an intermediate degree of mass wasting on the gentle slopes of the ridge. In case 2, partial flooding has led to the formation of a number of endogenous craters characteristic of the maria, but not as many as on the deeply flooded floor.

Acknowledgment. Mr. Charles A. Wood carried out a number of the crater counts presented in this paper. This work was supported through an NSF Institutional Grant of the University of Arizona.

REFERENCES

Arthur, D. W. G., *et al.* 1965, "The System of Lunar Craters, Quadrant III," *Comm. LPL,* **3**, 61–62.

Hartmann, W. K. 1963, "Radial Structures Surrounding Lunar Basins, I," *Comm. LPL,* **2**, 1–15.

————. 1964*a*, "Radial Structures Surrounding Lunar Basins, II," *Comm. LPL,* **2**, 175–191.

————. 1964*b*, "On the Distribution of Lunar Crater Diameters," *Comm. LPL,* **2**, 197–203.

Heacock, R. L. 1966, "Ranger Block III," *JPL Tech. Rep. 32–800,* pp. 7–34.

Jaffe, L. D. 1965, "Depth of Lunar Dust," *J. Geophys. Res.,* **70**, 6129–6138.

Kuiper, G. P., Strom, R. G., and LePoole, R. S. 1966, "Interpretation of the Ranger Records," *JPL Tech. Rep. 32–800,* pp. 35–248.

O'Keefe, J. A., Lowman, P. D., and Cameron, W. S. 1967, "Lunar Ring Dikes from Lunar Orbiter I," *Science,* **155**, 77–99.

Rittmann, A. 1962, *Volcanoes and their Activity,* (New York: John Wiley and Sons, Inc.).

Shoemaker, E., *et al.* 1966, "Progress in the Analysis of the Fine Structure and Geology of the Lunar Surface from the Ranger VIII and IX Photographs," *JPL Tech. Rep. 32–800,* pp. 249–337.

Urey, H. C. 1966, "Observations on the Ranger VIII and IX Pictures," *JPL Tech. Rep. 32–800,* pp. 339–362.

Williams, H. 1942, *The Geology of Crater Lake National Park, Oregon,* Carnegie Inst. Wash. Pub. 540.

No. 81 LUNAR CRATER COUNTS. II: THREE LUNAR SURFACE TYPE-AREAS

by WILLIAM K. HARTMANN

April 5, 1967

ABSTRACT

Diameter distributions of lunar craters are presented for three type-areas: average mare, the wall of Alphonsus, and "pure upland." These define three distinct distribution curves with parallel branches. Normalizing to the average mare crater density, and considering that the maria show a variation in crater density, we find that the relative crater densities for these three regions are 0.6 to 1.5, 3, and 30, respectively. Because the diameter distributions are parallel, except for mare craters of diameter $D < 2$ km, the craters in these three regions are interpreted to be of predominantly the same origin, from the largest basins ($D > 400$ km) to craters as small as $D = 2$ km. These observations impose boundary conditions on any theory of lunar history.

1. Observations

Figure 1 presents crater counts for three different types of lunar surface: average mare, the wall of Alphonsus, and "pure upland." These data update crater counts presented by the writer in several earlier papers, including "Early Lunar Cratering," synopsized in this issue of the *Communications* (Hartmann 1966).

The counts on lunar maria are based on the four quadrants of the crater catalog of Arthur, *et al.* (1963, 1964, 1965, 1966). The counts were extended to small diameters by using Ranger and Orbiter photographs of representative mare surfaces.

The second type-region, the inner wall of the pre-mare crater Alphonsus, is discussed in Paper 1 of this series (p. 31 of this issue).

"Pure upland" or "pure continental" regions, the third of the type-areas, are regions that show little or no evidence of modification by partial mare flooding or tectonic processes. They are held to be the oldest surfaces for recording cratering events. The pure continental counts of "Early Lunar Cratering" were based on the first three quadrants of the Arthur catalogs. They showed a near-linear distribution on a log-log plot with a break at about $D = 20$ to 30 km. This feature was discussed in *Comm. LPL,* No. 38 (Hartmann 1964). In the course of a more recent study comparing far-side and near-side crater counts, data were gathered on far-side pure upland surfaces. These data indicate that the diameter distribution is linear over a wide range of diameters. The break found on the front side is now thought to be partly a result of some crater-destruction process such as partial flooding, as discussed in *Comm. LPL,* No. 38, and partly a result of observational incompleteness in the catalogs. The new Orbiter data, much more complete at small diameters than the earth-based data, show no break. Therefore, in Figure 1, the earth-based data are omitted for $D < 8$ km, where a slight turndown from the linear relation can already be seen.

2. Variations within Type-Areas

It is well known that apparently homogenous areas of presumably uniform age have non-uniform crater densities. The clusters of craters photographed by Ranger VII in Mare Cognitum are an example. Further, there are systematic variations from mare

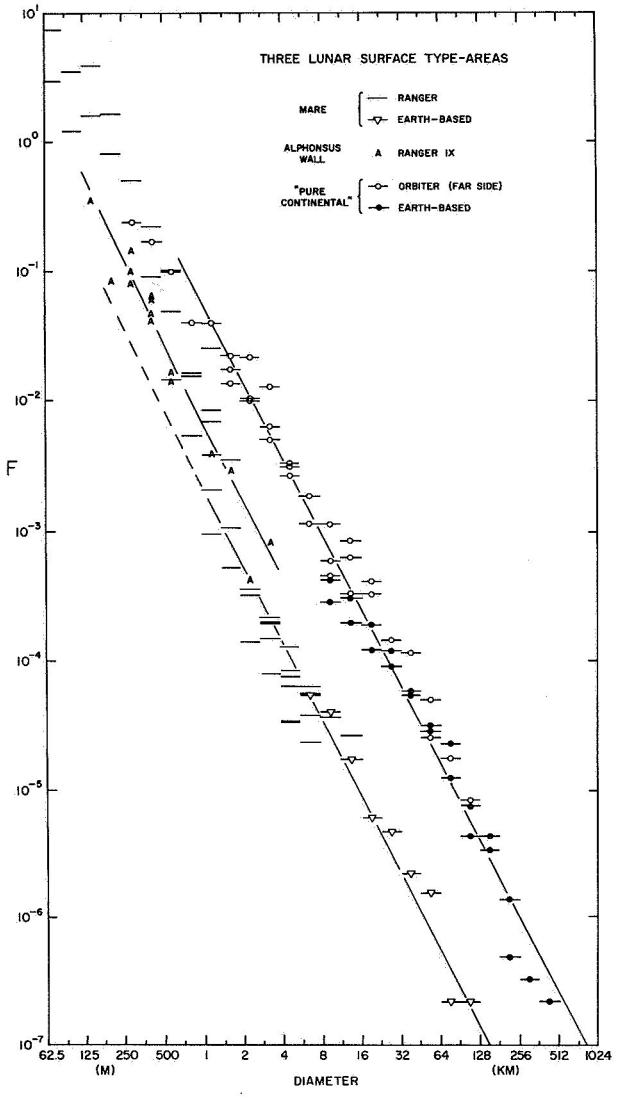

Fig. 1 Diameter distributions of craters in three type-areas of the lunar surface. Mare points represent an average over front-side maria. The dashed line is the inferred run of primary impact craters from Kuiper, Strom, and LePoole (1966) (modified on the basis of Alphonsus wall counts). F is the incremental number of craters per km^2.

to mare. The curve in Figure 1 represents an average over the major front-side maria, but a study of different individual maria, using both published and unpublished data, indicates that the range of variation in crater density amounts to a factor 2.5 from one major mare unit to another. The maria will be discussed in more detail in a later paper in this series.

Finally, even the pure upland areas are somewhat non-uniform, partly because of destructive processes, and possibly, partly because of a variable admixture of endogenous craters. For example, the far-side region studied in Figure 1 has a significant excess of craters in the range 8 km $< D <$ 64 km. Endogenous craters reach this dimension in the Orientale and Nectaris radial crater chains.

3. *Interpretation*

The data for the three regions (Fig. 1) are fitted by three parallel curves. Only the smaller mare craters, $D < 2$ km, define a non-parallel branch with a much steeper slope, as has been known since the flight of Ranger VII (Shoemaker 1965; Kuiper 1965, see *Comm. LPL,* No. 58). The slope of these parallel curves is -2.0 for $D > 1$ km, and steepens to as much as -2.3 at $D = 200$ m.

The parallelism of the curves suggests that for the most part, the craters are of the same origin. The single origin most reasonably applied to all these surfaces is the impact of fragmented cosmic bodies. This is compatible with what is known of the mass distribution of asteroidal fragments (Hartmann 1964). Even the largest mare basins fit the pure upland curve and are interpreted as simply the largest examples of craters. I have argued in "Early Lunar Cratering" that the pure upland craters represent a non-asteroidal, early population of cosmic fragments possibly peculiar to the earth-moon system.

The steep increase in mare craters at $D < 2$ km suggests that another crater-forming mechanism is involved in that range. Critical discussion of crater origins is beyond the scope of this paper, but it should be noted that the attempt of Kuiper, Strom, and LePoole (1966) to select only "sharp," primary impact craters from those of other origins yielded a curve shown schematically by the dashed line in Figure 1. (The dashed line parallels the other data points in this diameter range and may represent the distribution of primary craters more accurately than the original curve determined by Kuiper, Strom, and LePoole.)

The parallelism of the curves enables one to represent, by a simple sequence of numbers, the relative crater density of different regions. Normalizing so that unity is the average crater density on the maria, we have a range of about 0.6 to 1.5 for the major maria, about 3 for the wall of the pre-mare crater Alphonsus, and about 30 for the pure upland surfaces.

These figures place boundary conditions on any theory of lunar history. For example, if one assumes that the rate of crater production has been constant with time, then one must conclude that the maria are 1/30 the age of the uplands, i.e., presumably

1.5×10^8 years. On the other hand, I have argued in "Early Lunar Cratering" that the early cratering rate was much higher, which allows the ages of the maria to be much greater and more variable. This is in better agreement with the apparent great age of lunar structures, judged by the probable thermal history of the moon and by certain stratigraphic relations.

Acknowledgments. Many of the crater counts reported here were prepared by Mrs. Alice Agnieray and Mr. Charles A. Wood. This work was supported by an NSF Institutional Grant of the University of Arizona.

REFERENCES

Arthur, D. W. G., *et al.* 1963, "The System of Lunar Craters, Quadrant I," *Comm. LPL,* **2**, 71–78 ff.

————. 1964, "The System of Lunar Craters, Quadrant II," *Comm. LPL,* **3**, 1–2 ff.

————. 1965, "The System of Lunar Craters, Quadrant III," *Comm. LPL,* **3**, 61–62 ff.

————. 1966, "The System of Lunar Craters, Quadrant IV," *Comm. LPL,* **3**, 1 ff.

Hartmann, W. K. 1964, "On the Distribution of Lunar Crater Diameters," *Comm. LPL,* **2**, 197–203.

————. 1966, "Early Lunar Cratering," *Icarus,* **5**, 406–418 (synopsis in *Comm. LPL,* **5**, 55).

Kuiper, G. P. 1965, "Interpretation of Ranger VII Records," *JPL Tech. Rep. 32–700,* pp. 9–73 (revised version in *Comm. LPL,* **4**, 1–70).

Kuiper, G. P., Strom, R. G., and LePoole, R. S. 1966, "Interpretation of the Ranger VIII and IX Records," *JPL Tech. Rep. 32–800,* pp. 35–248.

Shoemaker, E. M. 1965, "Preliminary Analysis of the Fine Structure of the Lunar Surface in Mare Cognitum," *JPL Tech. Rep. 32–700,* pp. 75–134.

No. 82 THE LEONID METEOR SHOWER OF NOVEMBER 17, 1966

by DAVID R. MCLEAN

April 15, 1967

1. The Observations

On November 17, 1966, a team of observers, led by Dennis Milon of LPL, observed the Leonid meteor shower from Kitt Peak National Observatory. Accurate counts and magnitude estimates of meteors for various regions of the sky were made, and the results have been sent to Dr. Peter M. Millman of the National Research Council of Canada in Ottawa for incorporation into a more comprehensive report.

The first hour of observing, from 8^h30^m UT (1:30 a.m. MST) to 9^h30^m UT, produced a count of only 33 Leonids per hr. However, during the course of the second hour, 9^h50^m to 10^h50^m UT, 192 Leonids were recorded by a single observer. At 11^h10^m, the rate was at least 30 per min and increasing rapidly; at 11^h54^m, the rate was 40 per sec. This rate persisted about 20 min and then dropped back to 30 per min at 12^h40^m UT.

I photographed continually after 11^h00^m UT with a Pentax camera at f/2 and obtained 18 useful frames on 35 mm Tri-X film. The film was developed in D-19 for 12 min. The highest recorded rate was one meteor per sec per frame on a frame exposed for 43 sec.

2. Visual Rate versus Photographic Rate

No magnitude estimates were made during the period of photography because of the high count rates. However, a limiting magnitude for photographs was determined during the Geminid shower, December 13, 1966, when third-magnitude meteors were recorded on two frames. The exposures were on the order of four to five times longer on the Geminid frames, however, than on the Leonid frames. Therefore, the fog level of the Geminid photographs is considerably greater than that of the Leonid, and this may have prevented the recording of fainter Geminids. In any case, third-magnitude meteors on the Geminid frames match the appearance of faint meteors on the Leonid frames. The relative velocity of Leonid meteors is about twice that of Geminids, being 72 and 35 km per sec, respectively (McKinley 1961, p. 147). Thus, for the same angular distance from the radiant, a Geminid has twice the exposure of a corresponding Leonid. The faintest recorded Leonid would thus be about 2.5 mag, that is, 0.7 mag brighter than the matching Geminid (estimates being made to only 0.5 mag).

The dimensions of a single observer's visual field were found by looking straight at a star and

noting which second-magnitude stars could be seen at the very edge of the field. Second magnitude was chosen as representative of the average Leonid meteor. I rotated my head back and forth so that the star would appear, by virtue of the motion, to resemble a meteor. A vertical distance of 100 deg and horizontal distance of 120 deg was found for the dimensions of an ellipse approximating the field of vision. The area of this ellipse is about 9500 sq deg.

The highest photographic rate, one meteor per sec per frame, can be converted to a visual rate. The ratio of the observer's field to that of the camera is $9500/950 = 10$, that is, the eye — assuming it has the same sensitivity as the camera — would see 10 times the number of meteors. Actually, the eye is about twice as sensitive as the camera and thus would see about 20 meteors per sec. This has been confirmed by our results which were compiled by Dr. Millman. The peak visual rate estimated from the photographic rate is therefore 70,000 per hr.

Since the radiant was not more than about 23 deg from the zenith during the intense shower, altitude corrections are never more than 15 percent, according to the equation

$$R_o = R_z \sin (a + l),$$

where R_o is the observed rate, R_z the zenith rate, a the radiant altitude, and l the path length near the horizon, about 6 deg (cf. Prentice 1953).

3. *The Width of the Swarm*

Figure 1 shows the time distribution of meteor counts. This graph shows that the pronounced peak in the flux occurred between 11^h30^m and 12^h30^m UT. The rate at the edge of these limits is 100 per min. The inclination, i, of the orbital plane of the Leonids is 163 deg (McKinley 1961, p. 151). The well-defined width of the swarm is therefore

$$tV \sin i = 3.2 \times 10^4 \text{ km},$$

about 2.5 times the earth's diameter, where t is the time width of the maximum, and V, the earth's orbital velocity. This result is comparable to the value 1×10^5 for the Giacobinid shower found from data for three different years by Davies and Lovell (1955). However, that shower had a weak component corresponding to diameter 3×10^5 km, not found for the Leonids.

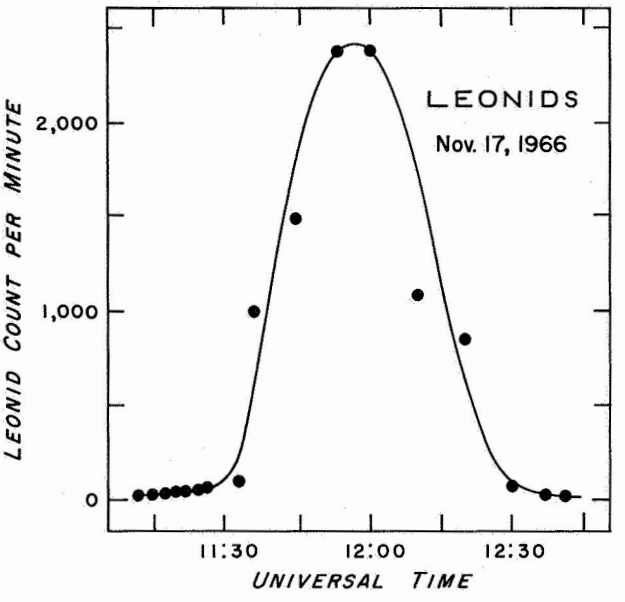

Fig. 1 Count rate as a function of time.

4. *The Photographs*

Figures 2–6 are examples of photographs obtained during the peak of the shower, 11^h30^m–12^h30^m UT.

REFERENCES

Davies, J. G., and Lovell, A. C. B. 1955, *M. N.*, **115**, 23.

McKinley, D. W. R. 1961, *Meteor Science and Engineering* (New York: McGraw-Hill, Inc.).

Prentice, J. P. M. 1953, *J. Brit. Astr. Assoc.*, **63**, 175.

Fig. 2 Leonid radiant showing 30 meteors, including one sporadic. Constellation Leo. Exp. 1 min 20 sec; ~ $12^{h}00^{m}$ UT. Field size, 28° × 34°.

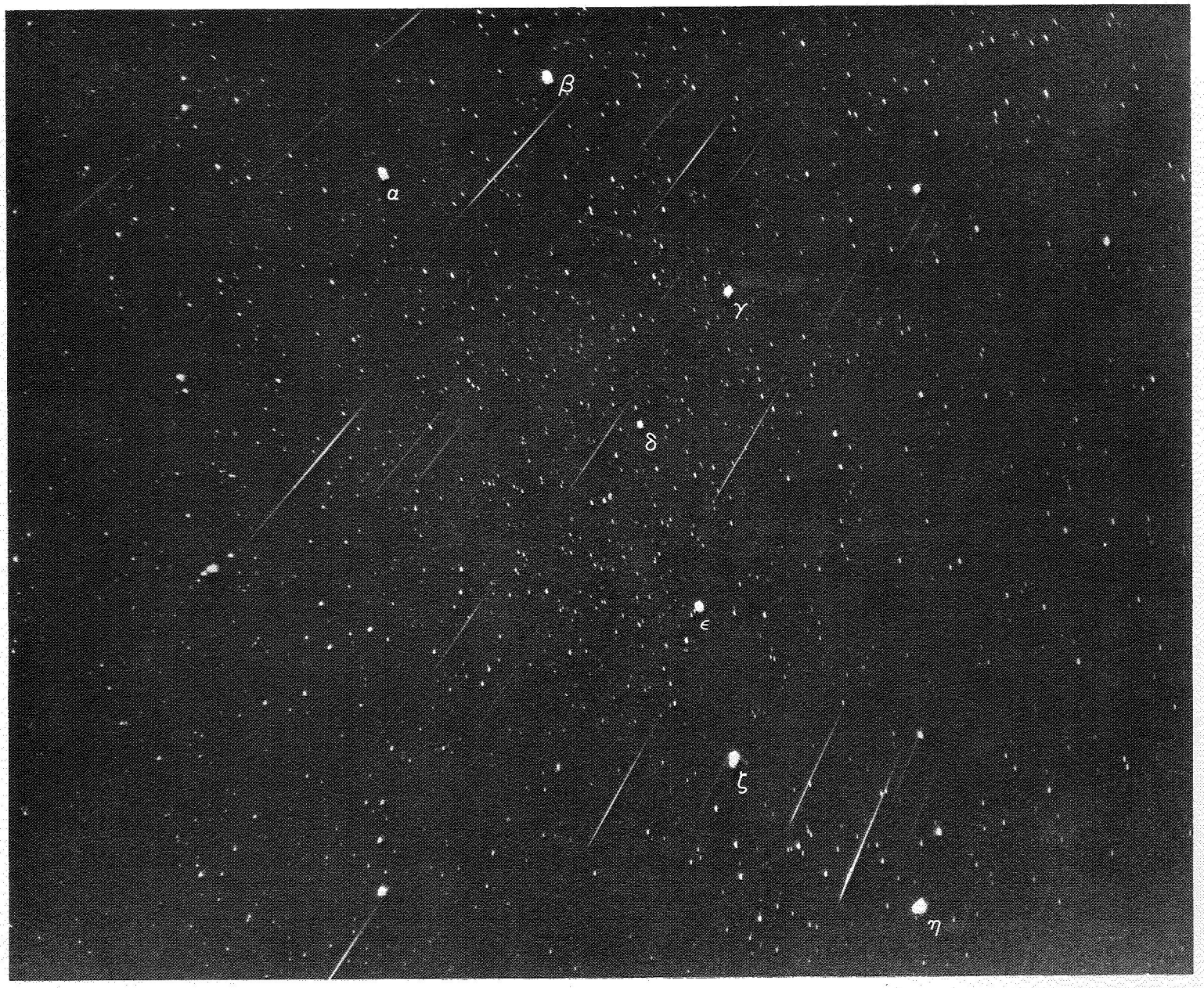

Fig. 3 Ursa Major showing 43 Leonids. Exp. 43 sec; ~ $12^{h}00^{m}$ UT. Field size, 28° × 34°.

Fig. 4 Looking west. Exp. 4 min; ~ 11^h45^m UT. Field size, 28° × 34°.

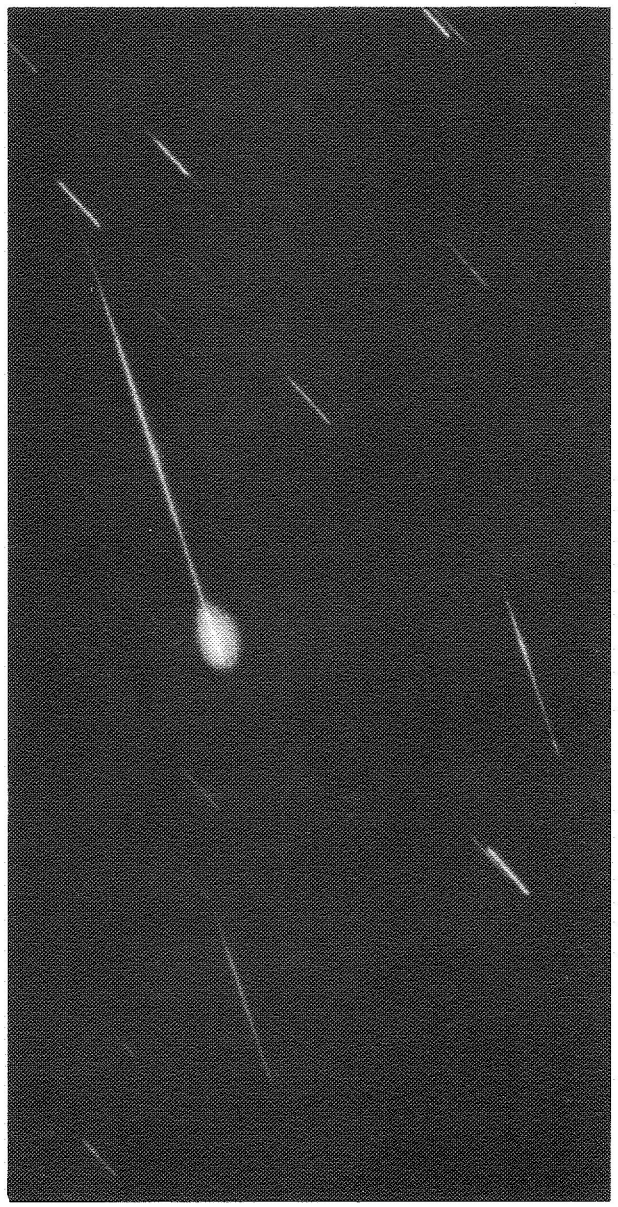

Fig. 5 Enlargement of Fig. 4 showing structure of bolide trail.

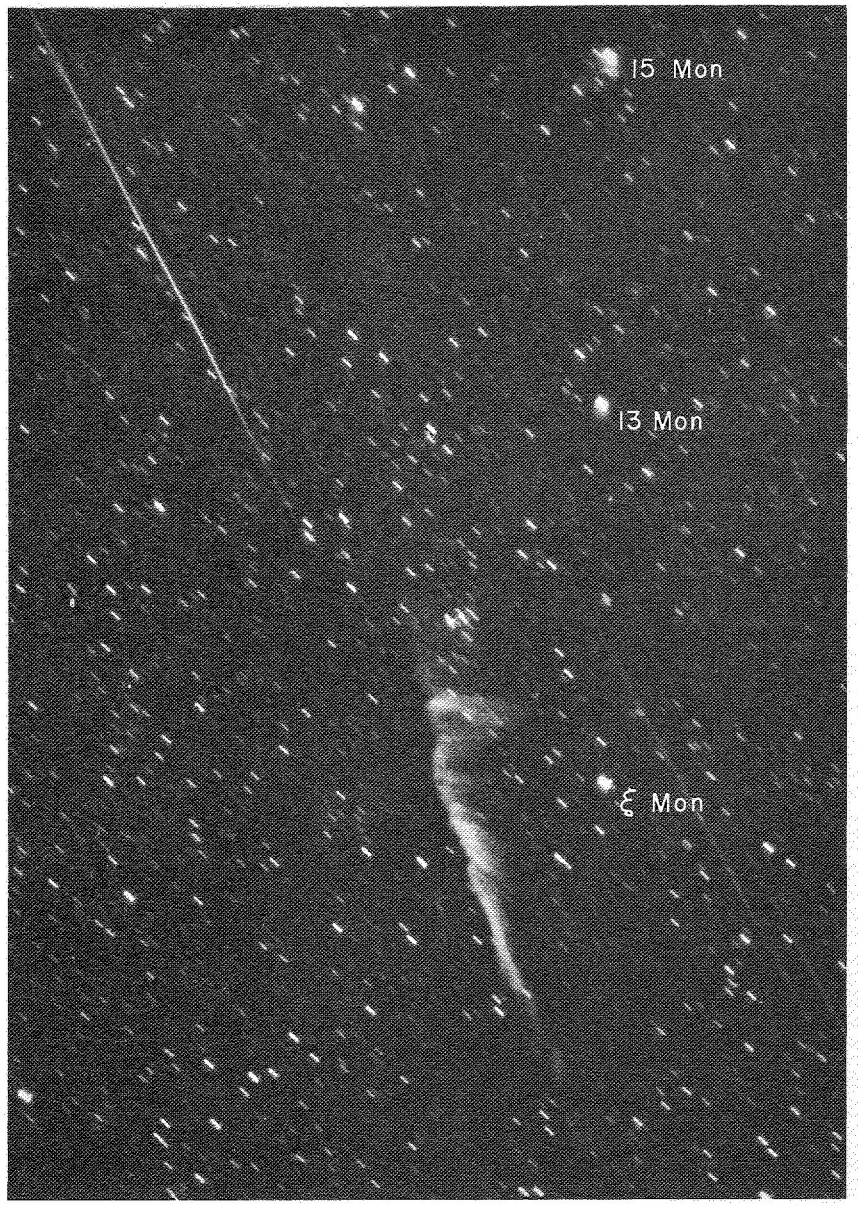

Fig. 6 Long-enduring train of Leonid bolide. Exp. 40 sec beginning 10 sec after bolide passage; ~ 12^h00^m UT. Field size, 8° x 12°.

NO. 83 SURVEYOR I LOCATION*

by E. A. WHITAKER

By attempting to correlate the positions of summits of lunar hills, situated beyond the horizon of Surveyor I, with features given on the Aeronautical Chart and Information Center map of the area, Jaffe *et al.* (*1*) derive a location (Site I) situated well outside the 2 σ uncertainty ellipse based upon the tracking data. Furthermore, the correlation is only partial. By repeating the process with a suitable Earth-based photograph, I find that only one location of Surveyor is possible, well within the tracking-data ellipse.

Figure 1 depicts the NE portion of the large, incomplete ring Flamsteed P (*2*); it was made from two stacked negatives taken with my laboratory's NASA-sponsored 61-in. (153-cm) reflecting telescope at 0315 hours U.T., 2 April 1966. The lines of latitude and longitude were carefully transferred from (*3*). The radial lines represent the directions of horizon features *A–F* (*1*, Fig. 16), the azimuths having been adjusted for the computed inclination of the lunar surface from the plane perpendicular to the line of sight. The small dot indicates the location of Surveyor for optimum correlation between these lines and the various hills, while the ellipse represents the theoretical horizon as seen from Surveyor's camera. Table 1 gives the coordinates of the landing site derived from the preceding correlation and from the tracking data; the former is approximately 2.4 km south of the latter, well within the 2 σ uncertainty ellipse.

*Reprinted with permission from *Science*, Sept. 23, 1966, Vol. 153, No. 3743, pp. 1550–1551.

TABLE 1

SURVEYOR LANDING SITES

DERIVED FROM	SITE	
	SOUTH LATITUDE (deg)	WEST LONGITUDE (deg)
Photo correlation	2.57 ± 0.02	43.34 ± 0.02
Tracking data	2.49	43.32

In order to verify the correctness of the correlations, the heights of several hills in the group were obtained from shadow measurements made on a print similar to Figure 1 (Table 2). These values may be compared with those calculated from the angular dimensions given in (*1*, Table 2) and the assumed

TABLE 2

HEIGHTS (ABOVE THE PLAIN) OF HILLS FROM SHADOW MEASUREMENTS. FEATURE *B* CANNOT BE MEASURED BECAUSE SHADOW FALLS ON HILLS *D* AND *d*.

FEATURE	SHADOW LENGTH (km)	SOLAR ALTITUDE (deg)	HEIGHT (m)
A	.5.4	3.25	300
a	3.0	3.10	160
C	5.0	2.75	230*
D	7.5	2.65	330†
d	6.6	2.60	290†
F	4.5	3.00	230

*Underestimate, because end of shadow falls on hill *D*.
†Overestimate, because end of shadow falls in large, somewhat depressed area.

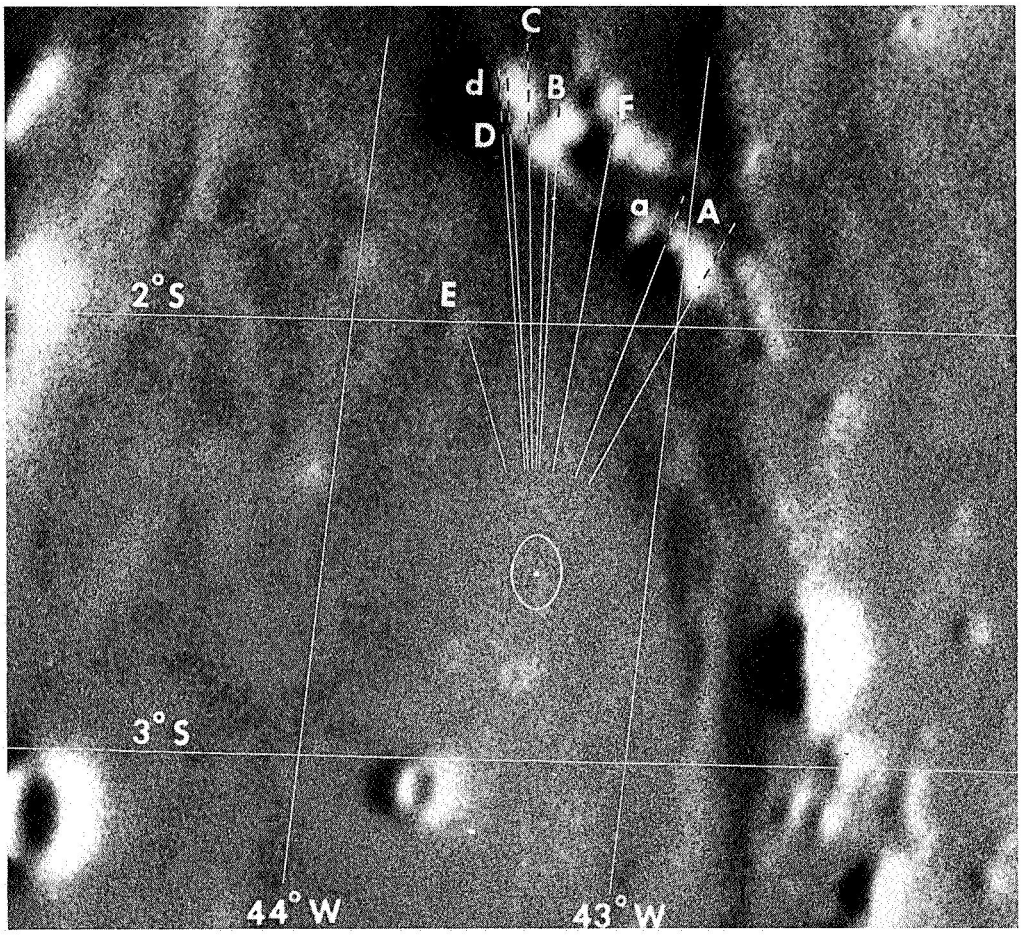

Fig. 1. Northeast portion of Flamsteed P, showing Surveyor location derived from horizon features; 1° ≈ 30 km.

position of Surveyor (Table 3). The agreement is remarkably good in view of the uncertainties of the shadow measurements; differences do not exceed 10 m except where the shadows are cast on rising or falling terrain. Hill *d* appears larger than *D* in Figure 1, but *D* is higher since it casts a longer shadow and thus occults *d* in the Surveyor view. Feature *E* is not identified; the walls of the small crater situated at the location indicated are well below Surveyor's horizon, so this feature is presumably a small object situated relatively close by. The summit of *a* must be almost exactly at horizon level.

TABLE 3

HEIGHTS OF HILLS FROM SURVEYOR DATA. FEATURE *d* IS INVISIBLE TO SURVEYOR.

FEATURE DISTANCE FROM SURVEYOR (km)	HEIGHT		
	SEEN ABOVE HORIZON (m)	BELOW HORIZON (CALC.) (m)	TOTAL (m)
A, 23.4	180	130	310
a, 24.8	≤ 0	≤ 150	≤ 150
B, 31.3	130	240	370
C, 29.8	40	220	260
D, 30.9	80	230	310
F, 30.0	20	220	240

REFERENCES

1. L. D. Jaffe, *et al.* 1966, *Science,* **152**, 1737.
2. D. W. G. Arthur, *et al.* 1965, *Comm. LPL,* **3**, 62.
3. D. W. G. Arthur and E. A. Whitaker 1961, *Orthographic Atlas of the Moon,* ed. G. P. Kuiper (Tucson: Univ. of Arizona Press), sheet E5.

No. 84 "EVIDENCE FOR AN ATMOSPHERE ON IO"* AND "PHOTOMETRIC SEARCH FOR ATMOSPHERES ON EUROPA AND GANYMEDE"† (SYNOPSES)

by A. B. BINDER AND D. P. CRUIKSHANK

ABSTRACT

Photometric observations of eclipse reappearances of satellites Jupiter I, II, and III were carried out in the interval 1962–1965 to search for possible temporary brightening of the satellites after eclipse. If present, this could be attributed to a frost, snow, or haze layer caused by the drop in surface temperature during eclipse. Such an effect was observed on JI (0.09 mag) and JII (0.03 mag), but no effect greater than 0.01 mag was present on JIII. A freezing-out of CH_4 snow onto 20 percent and 10 percent of the satellite surfaces in the first two instances, respectively, is hypothesized to account for the observations.

Although there is no spectroscopic evidence for atmospheres on the four Galilean satellites of Jupiter (Kuiper 1952, p. 368; Owen 1965), their presence has long been suspected because of the moderate albedos and large sizes of the bodies. Continuing the search for these atmospheres, we made photometric observations of the disappearances and reappearances of the satellites into and out of the shadow of Jupiter in 1962–1965. The duration of eclipse is about 2.25 hrs for JI (Io) and about 2.5 hrs for JII (Europa). Because of the satellite orbit inclinations, the eclipse lengths of JIII (Ganymede) and JIV (Callisto) are more variable, about 2.7–3.7 hrs and up to 5 hrs, respectively.

During eclipse, the satellites receive only a minute amount of long-wave radiation from Jupiter's dark side and no direct sunlight. For bodies with tenuous atmospheres, the surface temperature must drop by several tens of degrees during a 2.5 hr eclipse. Kuiper (1965) gives the average radiation temperatures based on absorbed sunlight: JI, 101° K; JII, 88° K; JIII, 110° K; JIV, 117° K. Here we examine the possibility that a satellite's surface temperature drops during eclipse and that part of the hypothetical atmosphere may condense on the surface or in the atmosphere causing an increase in the albedo that can be detected upon reappearance from Jupiter's shadow. The albedo anomaly would persist until the satellite returns to more normal temperatures and the "snow" sublimes or the haze dissipates.

Observations were made with photoelectric photometers with standard B (blue) filters (λ 4500 A) and RCA 1P21 photomultipliers. A diaphragm of 10 sec of arc diameter was used to minimize the scattered light from the nearby disk of Jupiter. It was necessary to observe the sky both north and south of the satellite to obtain sufficient data for scattered-light corrections. The blue filter was chosen because the albedo of the Galilean satellites is lower at shorter wavelengths, making changes in albedo more easily detectable. However, the scattered light from Jupiter also increases and prevents the use of a U (ultraviolet) filter.

Preliminary observations were made with the Steward Observatory 36-in. reflector after Jupiter's opposition in 1962. Later observations were made with the 36-in. and 16-in. reflectors of the Kitt Peak National Observatory.

Figures 1 and 2 show the observations of JI and JII respectively, proving conclusively the existence of a short-lived anomalous brightness upon reap-

*Full text published in *Icarus*, 3, 299–305, 1964.
†Full text published in *Icarus*, 5, 7–9, 1966.

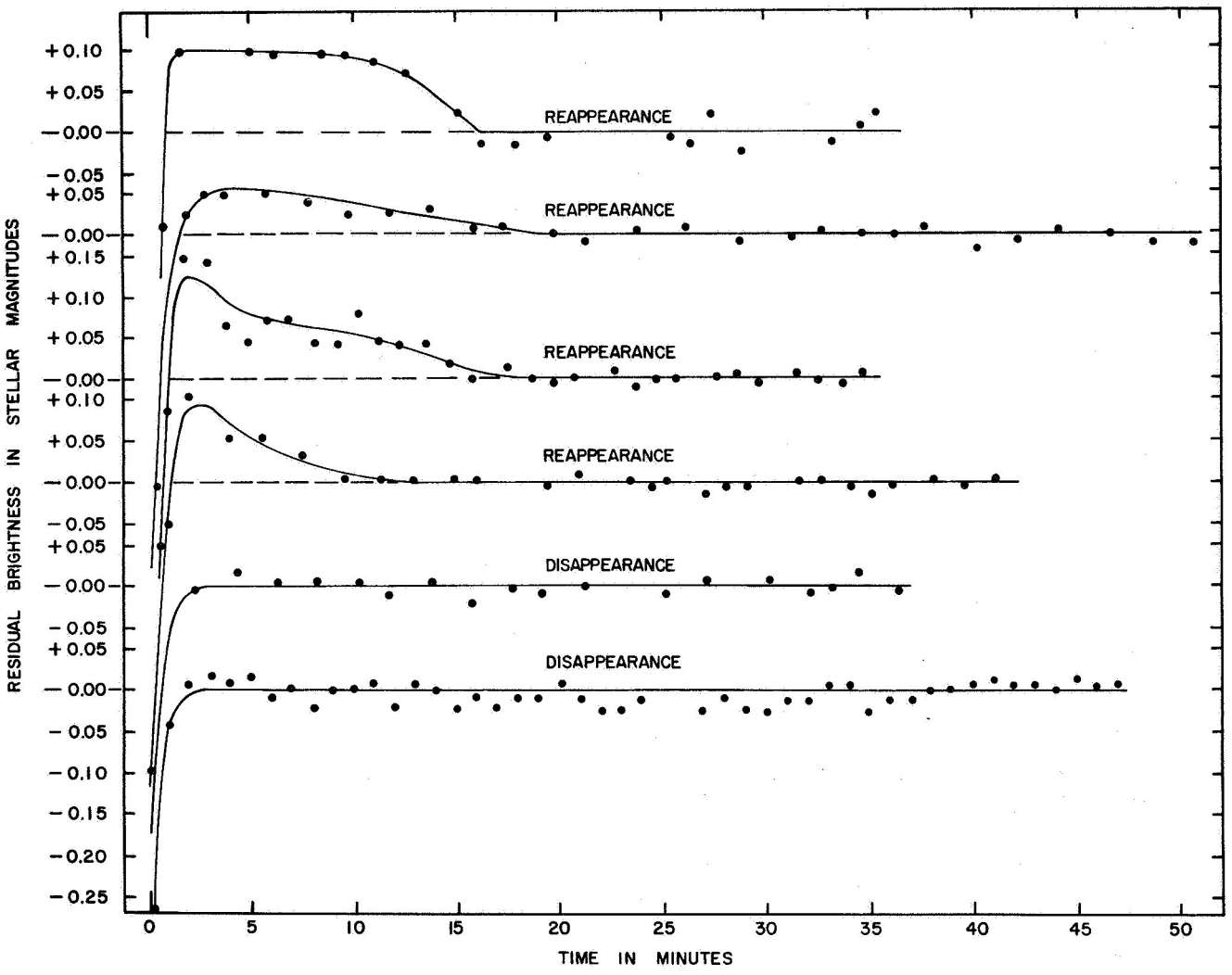

Fig. 1 Anomalous brightening of JI (Io) after eclipse.

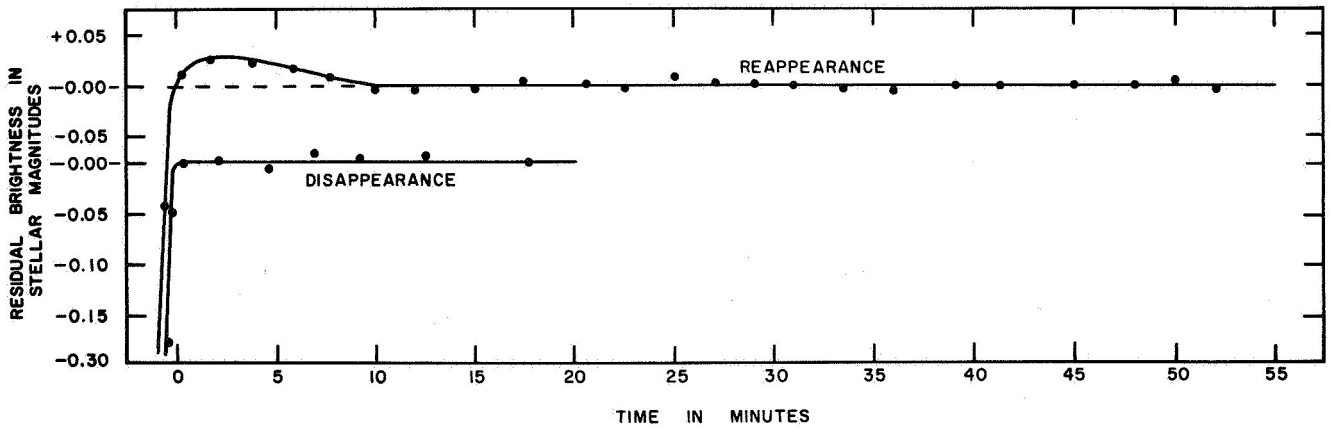

Fig. 2 Anomalous brightening of JII (Europa) after eclipse.

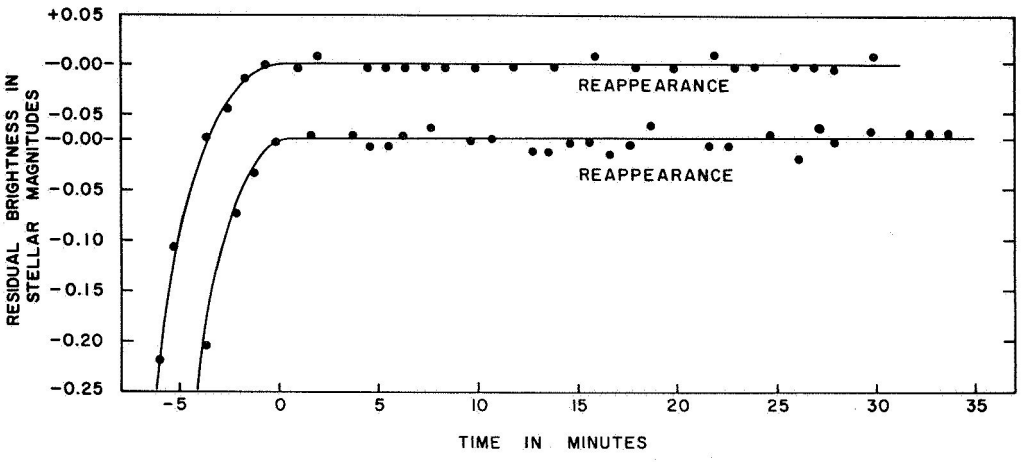

Fig. 3 Eclipse reappearance and disappearance of JIII (Ganymede) showing no anomalous brightening.

pearance after eclipse. Disappearance observations showed no such effect, indicating that scattered light from the bright planet or other systematic errors are not responsible for the excess at reappearance. Figure 3, the best observations of JIII, shows no measurable effect. The decay time of the phenomenon on JI is about 15 min. On JII, it is about 10 min.

Theoretical considerations indicate that of reasonable candidates for the atmospheric gases of these satellites, H_2O, NH_3, N_2, and CH_4, the first two would be frozen out or would have escaped, and the third and fourth would be gaseous. On JII, the presence of CH_4 is questionable, the escape time being near the age of the solar system, unless it is continually being replenished from the crust.

Assuming that some sort of deposited layer of snow or frost condenses out of the atmospheres during eclipse, and that its albedo is 0.8, we compute the fractional area of the planet covered by the deposit. For JI we find 20 percent, and for JII, 10 percent. The albedo of the hypothetical deposit must be greater than 0.67, which is the blue albedo of JII.

It is concluded that atmospheric phenomena have been observed on Io (JI). The single high-quality observation of Europa (JII) leads tentatively to the same conclusion. Two high-quality observations of Ganymede (JIII) give no evidence of atmospheric phenomena.

REFERENCES

Kuiper, G. P. 1952, "Planetary Atmospheres and Their Origin," *The Atmospheres of the Earth and Planets,* ed. G. P. Kuiper (Chicago: Univ. of Chicago Press), pp. 306–405.

———. 1965, "Physics of Planets and Satellites," *Astronomy and Astrophysics, Landolt-Börnstein Numerical Data and Functional Relationships in Science and Technology,* ed. H. H. Voigt (Berlin: Springer-Verlag), New Ser., Group IV, Vol. I, pp. 166–176.

Owen, T. C. 1965, "Saturn's Ring and the Satellites of Jupiter: Interpretation of the Infrared Spectra," *Science,* **149**, 974–975.

NO. 85 "EARLY LUNAR CRATERING"* (SYNOPSIS)

by W. K. HARTMANN

ABSTRACT

The evidence for intense cratering early in the history of the moon is presented. This early cratering rate, averaged over the first seventh of lunar history, was about two hundred times the average post-mare rate, and may have had a peak still much higher. Surface crater densities are thus not proportional to surface age. The large, circular mare basins fit the diameter distribution of the early continental craters and are therefore identified with pre-mare cratering. This cratering is assumed to be due to a high early bombardment rate by objects of uncertain origin. Mars shows no such early intense cratering. Some considerations on the origin of the objects are given.

The evidence for an early intense cratering of the moon comes from the very high density of pre-mare craters in continental or upland regions and the probability that the formation of the maria occurred quite early. Kuiper (1954) proposed early intense bombardment both on the above grounds and on the basis of visual observations of smooth, intercrater upland regions, which he took to be parts of an original, accreted, uncratered crust. This raises the important possibility that the original surface was not marred by major impact features. More recently, the possibility has been raised that smooth upland areas might result from other causes, such as volcanic activity, overlapping ejecta blankets, or early flooding overlain by thin opaque ejecta layers. In 1963, Alter also found evidence that ancient upland features predate the craters, suggesting that the general background has not been due to impact.

During the last fifteen years, Urey has assumed an early intense bombardment for a different reason: that the maria are a mixture of dust and lava flows produced by fusion at the time of impact. This would require that all basin-forming impacts occurred within a time less than the cooling time of the lava fills, i.e., as short as "some thousands of years." The high density of "Archimedian" or post-basin, pre-mare craters, however, testifies that the interval between impact and flooding was appreciable.

Others hold that there is no evidence for early intense bombardment. Disregarding theoretical and meteoritic indications that the mare-forming period was confined to early lunar history, they choose the simplest possible interpretation of the data: the age of any surface is directly proportional to the crater density. This *ad hoc* assumption led Fielder in 1963 to conclude that no major mare is older than 7×10^8 years, thus confining mare formation to the last 15 percent of lunar history. This appears unacceptably recent, in view of the early melting of other planetary bodies.

Figure 1 shows a comparison of crater densities averaged over mare surfaces with crater densities in selected "pure continental" regions. The basins of the large, circular maria fit perfectly onto the continental crater curve, indicating that they are simply the large-diameter extension of continental craters and presumably were formed by the same basic process.

*Full text published in *Icarus*, 5, 406–418, 1966.

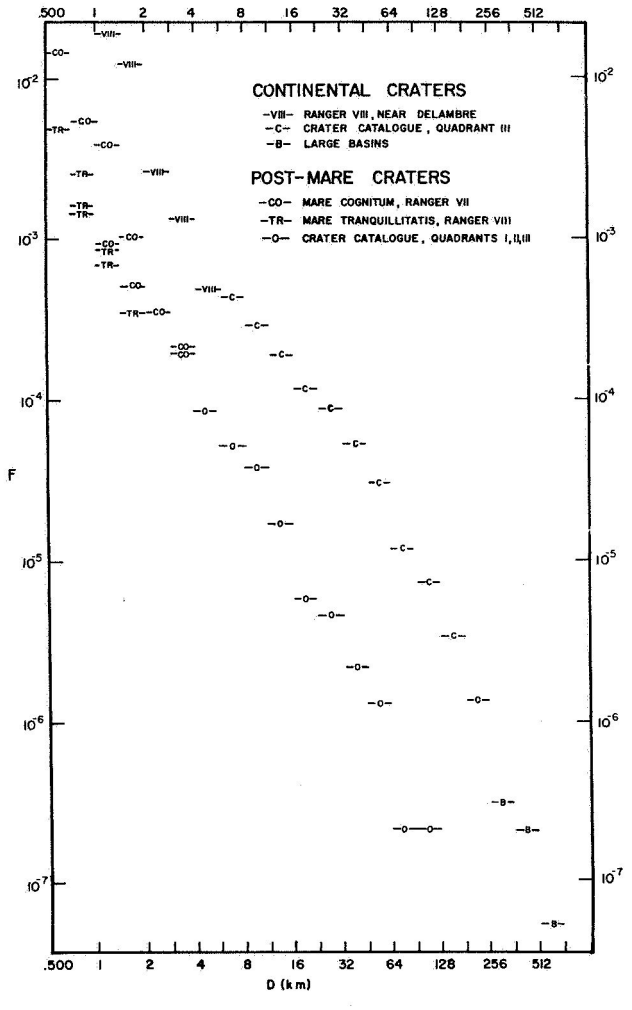

Fig. 1 Comparison of lunar crater densities in pure continental and mare areas. Each bar gives crater counts per km^2 in indicated diameter increment.

The roughly parallel branches of the two curves in Figure 1 indicate that crater density differs by a factor of 32 between the maria and pure continental surfaces. If we suppose that the maria were laid down just after the first seventh of lunar history — a supposition compatible with crater densities on earth and thermal histories of meteorites — we have an *average* cratering rate in this period about two hundred times the post-mare rate. If the maria were formed at a still earlier time, the peak rate would have been higher.

One possible explanation of the high early rate would be to suppose that the continental craters are mostly the result of intense volcanism and outgassing of the moon, i.e., they are of internal origin. But because these early craters are similar in dimension, morphology, and diameter distribution to the post-mare impact craters, an internal origin is tentatively rejected, and it is assumed that the craters were caused by impacts.

Figure 2 shows a schematic sketch of the situation for the very early stages of lunar history.† The "background" flux, labeled "cometary and meteoritic," may at first have declined from an early accretion rate. In later time, approaching the present day, the background flux has probably increased owing to the fragmentation of asteroids.

Within a framework of modern ideas about the early history of the solar system, one may conceive of six hypothetical causes of a high flux: (1) the objects represent the final, dwindling stages of lunar accretion; (2) they were planetesimals left in solar orbit after the formation of the planets; (3) they result from a much higher early ejection rate of comet nuclei from the cometary cloud; (4) they result from a much higher early ejection rate of objects from the asteroid belt; (5) the moon was captured by the earth after the objects struck it in another part of the solar system, for example, near the asteroid belt; (6) the objects represent circumterrestrial debris swept up by the moon as tidal friction forced it outward from the earth.

There are objections to the first four hypotheses. One such objection is that the diameter distribution of large continental craters appears to be incompatible with the mass distribution of asteroids. The last two hypotheses concern the origin of the moon itself, and it appears likely that just as the earth-moon system is unique, so the early cratering history of the moon may be unique. Mars does not appear to show the two-phase surface characteristic of lunar pre-mare and post-mare terrains, yet Mars' surface appears to be very old in terms of crater-retention age. Hypothesis (6) is tentatively favored.

A powerful tool in distinguishing among these hypotheses will be high-resolution space probe photography of planetary surfaces. Mercury will be especially interesting in this respect as it may have both mare and continental regions.

REFERENCES

Alter, D. 1963, "The General Background of the Lunar Surface," *Pub. A. S. P.*, **75**, 30.

†Cf. Fig. 134 in Kuiper, G. P., *et al.* 1966, "Interpretation of the Ranger Records," *Ranger VIII and IX, Part II: Experimenters' Analyses and Interpretations,* JPL Tech. Rept. No. 32-800, p. 217.

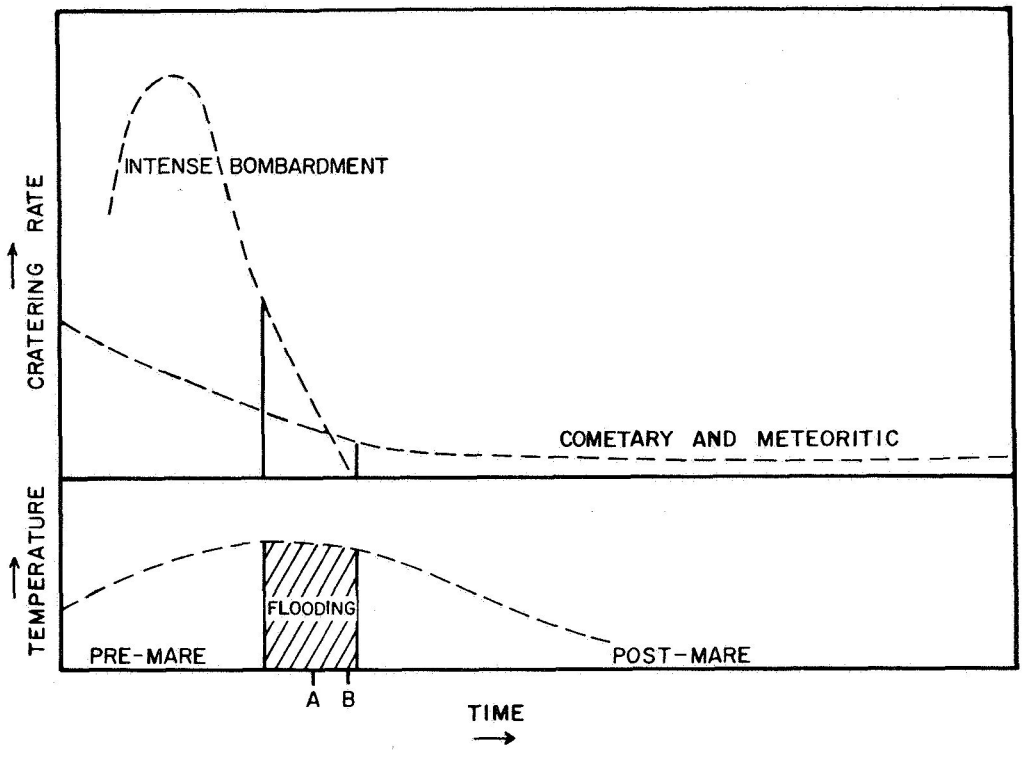

Fig. 2 Schematic diagram of early lunar history. Background flux is shown decreasing from an early accretion rate; it may have since increased as asteroidal fragments became available. Two mare surfaces, formed at *A* and *B*, could show markedly different crater densities as a result of the tail end of the early intense cratering.

REFERENCES — *Continued*

Fielder, G. 1963, "Nature of the Lunar Maria," *Nature,* **198**, 1256.

Kuiper, G. P. 1954, "On the Origin of the Lunar Surface Features," *Proc. Nat. Acad. Sci.,* **40**, 1096.

Urey, H. C. 1952, *The Planets* (New Haven, Conn.: Yale Univ. Press).

————. 1960, "The Duration of the Intense Bombardment Processes on the Moon," *Ap. J.*, **132**, 502.

No. 86 INFRARED PHOTOMETRY OF T TAURI STARS AND RELATED OBJECTS*

by E. E. MENDOZA V.†

We have begun a multicolor photometric study in wavelengths ranging from 0.36 μ in the ultraviolet to 5.0 μ in the infrared for 26 T Tauri stars and related objects. The study is not complete, but the results are so unexpected that a preliminary report is called for.

All of the observations were obtained with the apparatus described by Johnson and Mitchell (1962), and by Low and Johnson (1964), and with the 28-in. and 60-in. infrared telescopes of LPL.

Seven of the objects under study, imbedded in the Orion Nebula, are difficult to observe because they are faint and the sky background is bright and variable. The *UBVRI* photometry for these stars was carried out with two diaphragms of diameter 18″ and 36″, respectively. The sky readings were taken in four prime positions around each object. The internal agreement is good. We find that the values obtained with both diaphragms are the same for *BVRI* magnitudes, which means that the nebular background was negligible compared with stars. However, the *U* magnitudes of three stars (see below) were very different with diaphragm changes; the *U* values were brighter with the larger diaphragm. All the stars were observed in *JKLM* with only the 18″ diaphragm.

The observational data on the multicolor system defined by Johnson (1964) are listed in Tables 1 and 2. The columns of Table 1 contain: first, the name of the star; second through tenth, the *UBVRIJKLM* magnitudes, respectively; eleventh, the spectral types given by Herbig (1962), Joy (1960), and Haro and Chavira (flare types, 1964); twelfth, the number of different nights on which observations were made (first figure corresponds to *UBVRI* observations; middle figure to *JKL*, and last figure to *M*); and last, Notes. Table 2 contains the $U-V$, $B-V$, $V-R$, $V-I$, $V-J$, $V-K$, $V-L$, and $V-M$ colors of stars in Table 1, and those of the Sun (Johnson 1966).

Our photometric data, combined with the spectral types given in Table 1 and the intrinsic colors given by Johnson (1966), show the following:

a) Ultraviolet excesses for the majority of the stars. The strongest excesses are shown by the latest spectral types. For DF Tau, $E_{U-V} = 2.2$ mag.

*Reprinted with permission from *Ap. J.*, 143, 1010–1014, March 1966.

†Also of the Observatorio Astronómico Nacional, University of Mexico.

TABLE 1

MAGNITUDES OF T TAURI STARS AND RELATED OBJECTS

NAME	U	B	V	R	I	J	K	L	M	SP	n	NOTES
BP Tau	12.72	12.89	11.95	10.83	9.85	—	—	—	—	dK5e	1-0-0	
RY Tau	12.20	11.79	10.84	9.94	9.04	—	—	—	—	dGOe	1-0-0	
T Tau	12.44	11.70	10.45	9.33	8.42	7.55	5.53	4.00	2.7	dG5e	13-5-2	1
DF Tau	11.97	12.25	11.42	10.31	9.14	—	—	—	—	dMOe	3-0-0	
DG Tau	12.46	12.84	11.82	10.60	9.52	—	—	—	—	G:e	3-0-0	
UX Tau	11.22	11.83	10.79	9.82	9.04	—	—	—	—	dG5e	2-0-0	
Ton 14	14.97	14.71	13.28	11.47	9.88	—	—	—	—	—	2-0-0	2
UZ Tau	13.74	14.05	12.86	11.21	9.75	—	—	—	—	dMe var	2-0-0	
VY Tau	13.27	13.36	12.49	11.46	10.45	—	—	—	—	—	1-0-0	
UY Aur	12.83	12.97	11.91	10.60	9.53	—	—	—	—	dG5:e	1-0-0	
SU Aur	10.39	9.98	9.09	8.35	7.79	7.2	5.8	4.9	3.5	G2ne III	1-1-2	
RW Aur	10.75	11.00	10.40	9.62	8.90	8.1	6.7	5.6	5.1	dG5e	1-1-1	
CO Ori	12.27	11.62	10.56	9.55	8.76	8.0	6.6	5.6	—	Gpeα	1-1-0	
GW Ori	10.91	10.62	9.66	8.84	8.21	7.5	6.1	5.0	—	dk3e	1-1-0	
P 1353	15.9:	15.6	14.4	13.3	12.7	—	—	—	—	Flare	3-0-0	3,4
EZ Ori	12.84	12.56	11.70	10.89	10.32	9.8	8.7	8.1	—	F9:e V	5-3-0	
P 1553	14.6	14.02	12.86	11.74	10.87	10.1	8.8	8.4	—	Flare	5-2-0	3
P 2078	14.9:	15.0	13.74	12.53	11.58	—	—	—	—	Flare	4-0-0	3,5
P 2172	15.98	15.26	13.93	12.56	11.35	—	—	—	—	Flare	2-0-0	3
P 2305	16.04	14.86	13.54	12.34	11.48	10.7	9.7	8.8	—	Flare	3-1-0	3
P 2347	15.4:	15.03	13.97	12.83	12.13	—	—	—	—	Flare	4-0-0	3,6
V 380 Ori	10.50	10.70	10.26	9.57	8.84	7.9	5.9	4.4	2.9	A1:e	1-1-1	7
P 2441	11.66	11.43	10.75	10.14	9.68	—	—	—	—	F5:e	1-0-0	3
P 2455	17.5	16.18	14.49	12.60	11.12	—	—	—	—	Flare	3-0-0	3
R Mon	12.34	12.45	11.89	11.13	10.22	8.6	5.3	3.1	1.9	Ge	1-1-1	8
LkHα 120	13.37	12.97	11.96	10.98	10.23	—	—	—	—	—	3-0-0	9

NOTES TO TABLE 1

1. The $(U - B)$ range was from +0.63 to +0.83, from January to December 1965. Kuhi (1964) says that a high-dispersion spectrum of T Tau (by Herbig) gives a K1 type.
2. Haro, Iriarte, and Chavira 1953.
3. Parenago 1954.
4. Mean $(U - B)$ of −0.30 and +0.94; see text.
5. Mean $(U - B)$ of −1.00 and +0.83; see text.
6. Mean $(U - B)$ of +0.05 and +0.78; see text.
7. *UBVRI* photometry made with a 36″ diaphragm.
8. *UBVRI* photometry made with a 27″ diaphragm.
9. Herbig 1962.

TABLE 2

COLORS OF T TAURI STARS, RELATED OBJECTS, AND THE SUN

NAME	$U-V$	$B-V$	$V-R$	$V-I$	$V-J$	$V-K$	$V-L$	$V-M$
BP Tau	0.77	0.94	1.12	2.10	—	—	—	—
RY Tau	1.36	0.95	0.90	1.80	—	—	—	—
T Tau	1.99	1.25	1.12	2.03	2.90	4.92	6.45	7.7
DF Tau	0.45	0.83	1.11	2.28	—	—	—	—
DG Tau	0.64	1.02	1.22	2.30	—	—	—	—
UX Tau	0.43	1.04	0.97	1.75	—	—	—	—
Ton 14	1.71	1.43	1.81	3.40	—	—	—	—
UZ Tau	0.88	1.19	1.65	3.11	—	—	—	—
VY Tau	0.78	0.87	1.03	2.04	—	—	—	—
UY Aur	0.92	1.05	1.31	2.38	—	—	—	—
SU Aur	1.30	0.89	0.74	1.30	1.9	3.3	4.2	5.6
RW Aur	0.35	0.60	0.78	1.50	2.3	3.7	4.8	5.3
CO Ori	1.71	1.06	1.01	1.80	2.6	4.0	5.0	—
GW Ori	1.25	0.96	0.82	1.45	2.2	3.6	4.7	—
P 1353	1.5:	1.2	1.1	1.7	—	—	—	—
EZ Ori	1.14	0.86	0.81	1.38	1.9	3.0	3.6	—
P 1553	1.7	1.16	1.12	1.99	2.8	4.1	4.5	—
P 2078	1.2	1.3	1.21	2.16	—	—	—	—
P 2172	2.05	1.33	1.37	2.58	—	—	—	—
P 2305	2.50	1.32	1.20	2.06	2.8	3.8	4.7	—
P 2347	1.4:	1.06	1.14	1.84	—	—	—	—
V 380 Ori	0.24	0.44	0.69	1.42	2.4	4.4	5.9	7.4
P 2441	0.86	0.68	0.61	1.07	—	—	—	—
P 2455	3.0	1.69	1.89	3.37	—	—	—	—
R Mon 0.45	0.45	0.56	0.76	1.67	3.3	6.6	8.8	10.0
LkHα 120	1.41	1.01	0.98	1.73	—	—	—	—
Sun*	0.70	0.64	0.52	0.78	1.06	1.41	1.53	1.40

*$V = -26.74$.

b) Blue excesses for those stars with the largest ultraviolet excesses. For DF Tau, $E = 0.6$ mag.

Earlier UBV photometry of T Tauri stars and related objects (Bretz — see Whitford 1960; Varsavsky 1960; Smak 1964*a*) has shown the same general feature, namely, an ultraviolet excess. At the present time, there is no doubt that these excesses are caused by line and continuum emission in both $U - B$ and $B - V$ colors.

c) Red excesses for the majority of the stars. Notice that DF Tau shows a "deficiency" ($E_{V-R} = 0.2$), most likely caused by the effect of the Hα-line in emission in the V magnitude.

d) Infrared excesses (from 0.9 μ to 5.0 μ) for all the stars. $E_{V-M} = 6.2$ mag for T Tau and $E_{V-M} = 8.5$ mag for R Mon!

If these infrared excesses were caused mostly by interstellar extinction, then the total absorption, $A_v \geqq E_{V-M}$, would be very high and the stars would either be very near (T Tau and R Mon would be closer than 20 pc) or too luminous for their spectral types ($M_v = -7$ mag for R Mon).

The spectral energy-curves for T Tau, R Mon, and the Sun are shown in Figure 1. The ones for V 380 Ori and α Lyr are shown in Figure 2. They

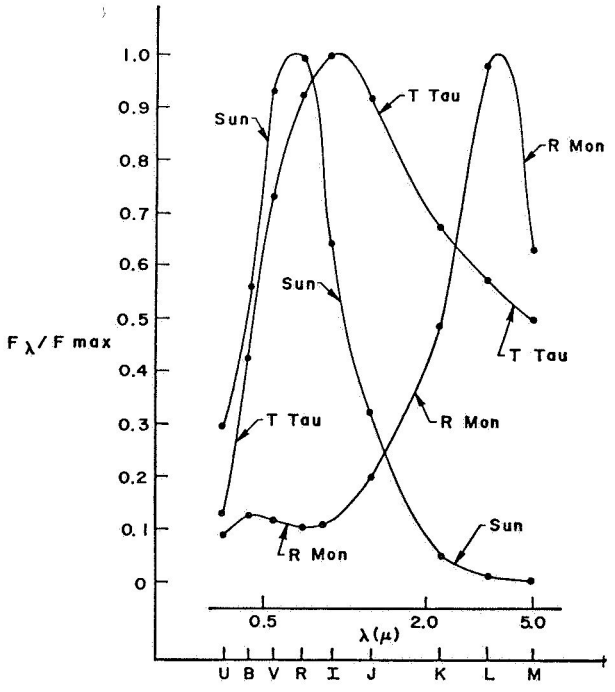

Fig. 1 The spectral energy-curves for the Sun, T Tau, and R Mon. T Tau illuminates NGC 1555 (Hind's nebula). R Mon illuminates NGC 2261 (Hubble's nebula) (see Herbig 1960, 1962).

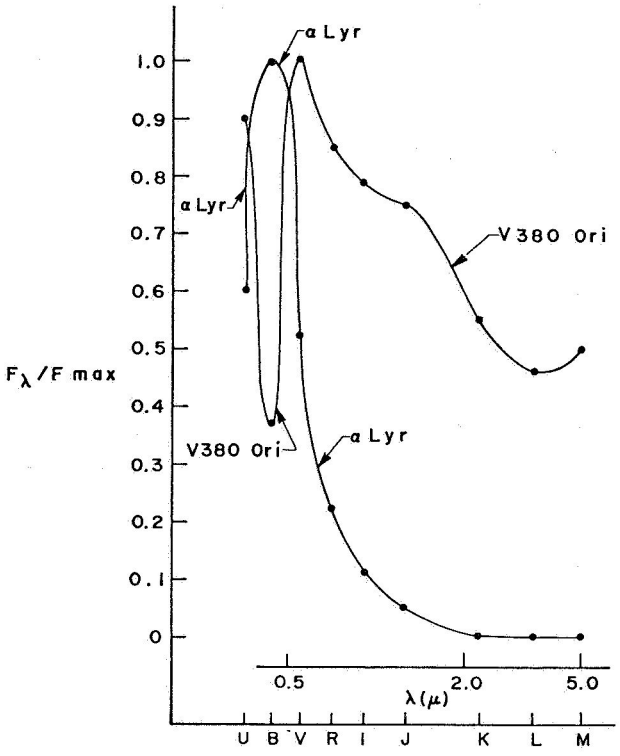

Fig. 2 The spectral energy-curves for α Lyr and V 380 Ori (Al:e), a marginal T Tauri star (Herbig 1962). V 380 Ori illuminates NGC 1999 (Morgan and Sharpless 1946; Herbig 1960).

were computed with the aid of the absolute calibration derived by Johnson (1965*a*) and have been normalized to unity at the maxima. T Tau, V 380 Ori, and R Mon show the strongest infrared excesses. These three objects illuminate bright nebulosity (Herbig 1962). The photometric errors are such that the general features shown in Figures 1 and 2 are not affected appreciably by them.

We have computed the bolometric corrections, B. C., for T Tau, V 380 Ori, and R Mon following the procedure outlined by Johnson (1964). This procedure consists primarily of a simple numerical integration under the spectral energy distribution after conversion to absolute units. The results of this integration are then compared with the corresponding values for the Sun. For this computation, we have assumed that the $N(10\ \mu)$ magnitudes are equal to the $M(5\ \mu)$ magnitudes and that the radiation from wavelengths longer than 14 μ is negligible. Both assumptions probably will cause underestimates of the total radiation flux. The results are given in Table 3. The columns of this table contain: first, the name of the object; second, the bolometric corrections; third, the newly determined distances (John-

TABLE 3

BOLOMETRIC CORRECTIONS FOR THREE T TAURI STARS

NAME	B.C.	r(pc)	M_{bol}
T Tau	−2.6	150	+2.0
V 380 Ori	−2.2	380	+0.2
R Mon	−4.2	690	−2.0

son 1965*b*); and fourth, the absolute magnitude uncorrected for interstellar absorption. Herbig (1960) gives very good reasons for believing that V 380 Ori is at the same distance as the Orion Nebula, and R Mon is at the same distance as NGC 2264. The values of the absolute magnitudes given in Table 3 were computed under these assumptions. For T Tau, we have used the distance of the Taurus cloud (e.g., Smak 1964*a*). These absolute magnitudes most probably are lower values since the apparent bolometric magnitudes might be undercorrected, and no correction for interstellar extinction was made.

We can interpret our photometric data (see Figs. 1 and 2) as follows:

a) As measures for the combination of two or more stars. For example, one solar-type star and one infrared star, like the Neugebauer-Martz-Leighton (1965) Cygnus object or TX Cam (Mendoza V. 1965), would give us a spectral energy-curve very similar to the one shown in Figure 1 for R Mon.

b) The short-wavelength photometry refers to a small core and long-wavelength photometry to a large envelope.

Several long-period variables are known to have companions. For instance, R Hya (M6e) has a K-dwarf companion (Smak 1964*b*). Thus, if assumption (*a*) is correct, it might be that long-period variables are young stars.

We also can see that an infrared star with a spectral energy-curve similar to R Mon (see Fig. 1) at a distance of, say, 690 pc would be several magnitudes above the zero-age main sequence and far to the right in the plane (M_{bol}, T_e). Such a star could be called a protostar (Hayashi 1961) since it is believed that T Tauri stars themselves are very young stars (see, e.g., Huang 1964).

Acknowledgments. We are indebted to Dr. H. L. Johnson for his advice and for the use of observing facilities, to Dr. F. Low for allowing us to use his 5-μ photometer, and to the Organization of American States for a grant. The research has also been supported in part by the National Science Foundation and the Office of Naval Research.

REFERENCES

Haro, G., and Chavira, E. 1964, *ONR Symposium,* Flagstaff, Arizona (in press).
Haro, G., Iriarte, B., and Chavira, E. 1953, *Bol. Obs. Tonantzintla y Tacubaya,* No. 8.
Hayashi, C. 1961, *Pub. Astr. Soc. Japan,* **13**, 450.
Herbig, G. H. 1960, *Ap. J. Suppl.,* **4**, 337.
———. 1962, *Advances in Astronomy and Astrophysics,* ed. Z. Kopal (New York: Academic Press), **1**, 47.
Huang, S.-S. 1965, *Pub. A.S.P.,* **77**, 42.
Johnson, H. L. 1957, *Ap. J.,* **126**, 134.
———. 1964, *Bol. Obs. Tonantzintla y Tacubaya,* No. 25.
———. 1965*a*, *Comm. LPL,* **3**, 73.
———. 1965*b*, *Nebulae and Interstellar Matter,* eds. L. H. Aller and B. M. Middlehurst (Chicago: University of Chicago Press) (in press).
———. 1966, *Ann. Rev. Astr. and Ap.,* ed. L. Goldberg (Stanford, Calif.: Annual Reviews), **4**, 193.
Johnson, H. L., and Mitchell, R. I. 1962, *Comm. LPL,* **1**, 73.
Joy, H. A. 1960, *Stellar Atmospheres,* ed. J. L. Greenstein (Chicago: University of Chicago Press), p. 653.
Kuhi, L. V. 1964, *Ap. J.,* **140**, 1409.
Low, F. J., and Johnson, H. L. 1964, *Ap. J.,* **139**, 1130.
Mendoza V., E. E. 1965, *Bol. Obs. Tonantzintla y Tacubaya,* No. 27.
Mendoza V., E. E., and Johnson, H. L. 1965, *Ap. J.,* **141**, 161.
Morgan, W. W., and Sharpless, S. 1946, *Ap. J.,* **103**, 249.
Neugebauer, G., Martz, D. E., and Leighton, R. B. 1965, *Ap. J.,* **142**, 399.
Parenago, P. 1954, *Pub. Sternberg Astr. Inst.,* Vol. 25.
Smak, J. 1964*a*, *Ap. J.,* **139**, 1095.
———. 1964*b*, *Ap. J. Suppl.,* **9**, 141.
Varsavsky, C. M. 1960, *Ap. J.,* **132**, 354.
Whitford, A. E. 1958, *A. J.,* **63**, 201.

NO. 87 WAVELENGTH DEPENDENCE OF POLARIZATION. V. POSITION ANGLES OF INTERSTELLAR POLARIZATION*

by T. GEHRELS AND A. B. SILVESTER

ABSTRACT

Observations were made of the plane interstellar polarization on 22 stars. Ten of the stars show appreciable wavelength dependence of the position angles; these stars are, generally, at distances greater than 0.6 kpc. Apparently, the light traverses individual clouds that have various particle sizes as well as various orientations of the galactic magnetic field. Variations are also noted in the wavelength dependence of the amount of interstellar polarization.

THE observations were made mostly with the McDonald 82-in. reflector in November 1963 and January 1964. Additional measurements were made at the McDonald 36-in., the Kitt Peak 36-in., the Lowell 21-in. (by S. F. Pellicori), and the Catalina 21-in. (by D. L. Coffeen). The polarimeter and procedures are the same as used before (Gehrels and Teska 1960). Starting with the January 1964 run, the output of the integrators is digitized and punched on paper tape. The program for handling the data at the IBM 7072, of the Numerical Analysis Laboratory at the University of Arizona, was written by Mrs. Tricia Coffeen.

Table I gives the percentage polarization. The stars are in order of galactic longitude, and are identified by the number in the Henry Draper catalogue, the filters by $1/\lambda$ in reciprocals of microns. The probable error of a single observation, determined from repetition, is $\pm 0.07\%$. Colons are used when the probable error of the listed value appears to be greater than $\pm 0.2\%$, or (in Table III) $\pm 3°$. The usual, small, corrections for instrumental polarization (viz., Paper I) are applied at an early stage in the reductions. The depolarization correction factor, determined during the observing run, is 1.01; all polarizations were multiplied by 1.01 before entry in Table I. A few of the stars had already been observed (Paper II); with the present data the weighted means are updated. Similarly, some of the stars will reappear in later papers. When only a single observation is available, a semicolon is used in the tables.

Table II gives a few observations made with the *G* filter/tube combination (Table I of Gehrels and Teska 1960); θ is the position angle in the equatorial reference frame.

Table III lists the observations of position angle θ.

TABLE I. Observed percentage of interstellar polarization.

	Percentage polarization observed at $1/\lambda =$						
HD	1.05	1.19	1.39	1.95	2.33	2.79	3.04
147165	1.12;	1.36;	1.37;	1.68;	1.53;	1.39;	1.35
134335	0.39	0.61	0.58:	0.58	0.78	1.10	0.68
134320	0.69:	0.47	0.49	0.71	0.65:	0.57:	...
207260	1.05;	1.24;	1.30;	1.47;	1.57;	1.49;	1.18;
217476	2.01;	2.23;	2.58;	2.64	2.53;	2.49	2.85:
224014	1.01	1.13	1.32	1.37;	1.18;	1.06;	1.13:
2905	1.14	1.10	1.37	1.41;	1.34;	1.20;	1.19;
7927	2.30	2.47	2.99	3.32;	3.34;	2.89	2.92
12301	2.01	2.37	2.41	2.80	2.72	2.58	2.14
12953	1.96	2.70	2.96	3.48	3.40	3.25	2.94
14489	1.43	1.55	1.80	2.10	2.03	2.01	1.87:
21291	2.37	2.77;	3.13;	...	3.30;	3.02:	2.79;
21389	2.47	2.75	3.18	3.75;	3.61;	3.39	3.15
30614	0.89:	1.13	1.44	1.90;	1.87;	1.74;	1.83;
25291	1.49;	1.59;	1.64;	2.27;	2.12;	2.13	2.00
24398	0.93	1.02	1.16	1.07;	1.02;	0.75;	0.76;
31964	1.45;	1.62;	1.78;	2.09;	2.16;	1.97;	1.97;
36371	1.52;	1.70;	2.04;	2.23;	2.09;	1.83	1.78
37202	1.40;	1.26;	1.21;	1.46	1.53	0.98	0.68
41117	1.95	2.27;	2.50;	2.92	2.81	2.42	2.47
42379	1.88	2.07;	2.63;	3.10	2.81;	2.98	2.44;
37041	0.91	0.94	0.91	0.87	0.58	0.39	0.33

A colon is given for poorer data, and a semicolon is for single observations.

TABLE II. Additional observations of interstellar polarization, made with a filter at $1/\lambda = 1.85$.

HD	$P\%$	θ
224014	1.51;	...
21291	3.40	114°7
21389	3.50;	120.7;
24398	1.33;	59.9;
41117	2.81;	175.0;
42379	2.73;	174.0;

TABLE III. Observed position angles of interstellar polarization.

	Position angles observed at $1/\lambda =$						
HD	1.05	1.19	1.39	1.95	2.33	2.79	3.04
147165	177.7;	174.3;	175.9;	175.9;	178.7;	177.8;	179.9
134335	64.0:	82.0:	62.8:	76.3:	72.6	...	...
134320	64.4:	75.6:	82.0:	75.3	77.7	...	...
207260	44.1;	37.2;	46.0;	39.7;	41.1;	39.3;	46.6;
217476	69.4;	69.5;	68.7;	70.5	70.1;	74.8:	70.0
224014	51.7:	52.3	53.8	51.1;	52.5;	...	...
2905	79.3	80.8	80.2:	83.6;	86.0;	88.3;	92.0;
7927	90.5	91.4	90.8	94.6;	94.8;	94.6	97.8
12301	108.1	109.1	109.6	112.2	112.2	113.0	114.6
12953	103.5	107.5	107.0	110.1	110.8	112.2	112.9
14489	107.3	112.2	110.5	113.8	115.0	116.1	121.1
21291	117.0	115.8	116.4;	...	113.0;	115.1;	117.0;
21389	118.9	119.4	119.6	121.3;	122.0;	121.9	122.3
30614	133.4	136.0	136.9	139.5;	140.1;	140.0;	139.4;
25291	133.3;	132.8;	132.3;	133.4;	132.9;	131.0	134.3
24398	60.7	56.7	60.1	60.3;	60.1;	58.5;	63.6;
31964	143.9;	145.8;	144.4;	143.8;	143.2;	144.7;	146.4
36371	177.6;	176.5;	178.6;	173.5;	172.2;	170.6	168.9
37202	30.4;	31.0;	33.7;	26.0	27.5	23.3	17.6
41117	179.9	177.8;	179.9;	173.2	172.8	174.6:	172.6:
42379	170.0	172.7;	181.0;	164.1:	168.0;	169.9	168.1;
37041	96.7:	104.5:	89.6:	105.6	100.4:	96.6:	...

*Reprinted with permission from the *Astronomical Journal*, Vol. 70, No. 8, Oct. 1965 — No. 1333. *Contributions from the McDonald Observatory, U. of Texas*, Ser. II, No. 4.

TABLE IV. Residuals of position angles.

HD	Observed minus average for each star, at 1/λ= 1.05	1.19	1.39	1.95	2.33	2.79	3.04	Galactic long.	lat.	Dist.[a]
147165	+1°	− 3°	− 1°	−1°	+2°	+1°	+ 3°	319°	+16°	n
134335	−9	+11	− 9	+5	+1	···	···	4	+58	n
134320	−9	+ 1	+ 7	0	+3	···	···	6	+58	n
207260	+2	− 5	+ 4	−4	−1	−3	+ 5	70	+ 6	n?
217476	−1	− 1	− 2	0	0	+5	0	76	− 3	f
224014	−1	0	+ 2	−1	0	···	···	83	− 4	n?
2905!	−5	− 4	− 4	−1	+2	+4	+ 8	89	0	f?
7927!	−3	− 2	− 3	+1	+1	+1	+ 4	95	− 4	f
12301!	−3	− 2	− 2	+1	+1	+2	+ 3	98	+ 3	
12953!	−7	− 2	− 2	+1	+2	+3	+ 4	101	− 2	f
14489!	−6	− 2	− 3	0	+1	+2	+ 7	103	− 4	f
21291	+1	0	+ 1	···	−3	−1	+ 1	109	+ 4	f
21389!	−2	− 1	− 1	+1	+1	+1	+ 2	110	+ 3	f?
30614!	−5	− 2	− 1	+2	+2	+2	+ 2	111	+15	f?
25291	0	0	− 1	+1	0	−2	+ 1	113	+ 6	n
24398	+1	− 3	0	0	0	−2	+ 4	130	−16	n
31964	−1	+ 1	0	−1	−1	0	+ 2	131	+ 2	n
36371!	+4	+ 3	+ 5	−1	−2	−3	− 5	144	+ 1	f?
37202!	+3	+ 4	+ 7	−1	0	−4	−10	153	− 4	n?
41117!	+4	+ 2	+ 4	−3	−3	−1	− 3	157	+ 3	
42379	−1	+ 2	+10	−7	−3	−1	− 3	157	+ 3	f
37041	−2	+ 6	− 9	+7	+2	−2	···	177	−18	f?

[a] In the distance column, *n*ear stands for 0.1–0.6 kpc and *f*ar for 0.8–2.1 kpc. The stars with exclamation marks (!) show appreciable wavelength dependence of the position angles.

The method of calibration is described by Gehrels and Teska (1960).

Table IV shows the wavelength dependence of the position angles. For each star the straight average is determined, and the difference between observed and average value is given in Table IV. Also listed are the galactic longitude and latitude (Lund Pole), and an approximate distance indication.

It is seen in Table IV that the nearby stars generally have no wavelength dependence of the position angles. Some of the farther stars show a certain trend at longitudes 89–111° (Cassiopeia), and a reversed trend is seen at 144–157° (Taurus).

An interpretation, and in fact a prediction, of the wavelength dependence of position angles had already been made by Treanor (1963): "If the existence of a color dependence of polarization on particle size is accepted, physical situations will undoubtedly arise in which this will entail also a color-orientation dependence. The most easily envisaged case is one in which starlight passes through two successive clouds with different orientation of the dust particles relative to the line of sight, and different mean projected particle size." On this interpretation, we may expect interesting detail and sharp reversal of the $\theta-\lambda$ trends when individual clouds are traversed.

Certain variations in the wavelength dependence of the percentage polarization are also noted (Table I). Many stars show the characteristic curve (shown in Paper II), with "a maximum at 6500 Å, decreasing sharply toward longer and gradually toward shorter wavelengths." The interpretation is that the particles have diameters near 0.3 μ and refractive index of that of dirty ices. The characteristic curve is shown by HD 147165 in Table I. HD 37041, however, has a steep rise from the ultraviolet to infrared, showing the presence of larger particles (same refractive index). An indication of large particles is in an excess polarization for filters $1/\lambda=1.05$ and 1.19 (example HD 37202 in Table I). An indication of smaller particles is in an excess in the ultraviolet, for example HD 30614.

REFERENCES

Gehrels, T. 1960, *Astron. J.* **65**, 466 (Paper I), and 470 (Paper II).
Gehrels, T., and Teska, T. M. 1960, *Publ. Astron. Soc. Pacific* **72**, 115.
Treanor, P. J. 1963, *Astron. J.* **68**, 185.

Acknowledgments. The work is supported by the National Aeronautics and Space Administration (NsG-733).

NO. 88 WAVELENGTH DEPENDENCE OF POLARIZATION. VI. MOLECULAR SCATTERING AT THE SKIN OF THE PARTICLES*

by T. GEHRELS

ABSTRACT

The pronounced shape (called "characteristic curve") of the wavelength dependence of interstellar polarization is qualitatively explained with molecular scattering at the surface of interstellar particles.

FIGURE 1 shows the characteristic curve of polarization sometimes observed on interstellar particles (see Paper V); it may be explained as follows. Let Fig. 2 represent an interstellar particle with cross section about 0.3 μ, and assume that the "dirty ice" model is the correct one (refractive index $m \cong 1.3$). Presumably, the particle originated by molecular accretion, and the elongated shape may be caused by chance collision and cohesion of two lumps. The accretion has progressed further, and the skin consists of loosely bound molecules. Figure 1 shows a polarization maximum near 5600 Å, with a slow decline in the ultraviolet, and a steep drop in the infrared.

The shape in the visual and ultraviolet is similar to that for polarization dilution by multiple molecular scattering. That is, single isotropic scattering would show 100% polarization at $1/\lambda = 0$ and at 90° phase, and, by multiple scattering, the polarization decreases as $1/\lambda$ increases. The shape on the right in Fig. 1 is seen in the calculations by Coulson, Dave, and Sekera (1960) for multiple molecular scattering (see Fig. 3 of Gehrels 1962).

How 90°-phase molecular scattering may occur at the skin of interstellar particles is seen as follows. Let the illuminating light source be a star behind the particle of Fig. 2. A molecule at A scatters the incident starlight in all directions, by primary molecular scattering. The light scattered towards the observer by A, but via neighboring molecules B and B', will have predominant vibration perpendicular to the long axis of the particle. The light scattered via A and C (or A and D) has vibrations parallel to the long axis of the particle. However, the light scattered by A towards C is lost to the observer, while that scattered towards D reaches the observer, if at all, only after further multiple scattering. Because of the elongated shape of the particle, the electric vector maximum is predominantly perpendicular to the long axis of the particle.

Longward of a characteristic wavelength in the infrared, the molecular scattering (dependent on λ^{-4}), rapidly decreases in strength; the light mostly bypasses the particle with only inappreciable scattering by the accreted molecules. The characteristic wavelength depends on the particle size and refractive index. In Fig. 1 for $2a = 0.3\,\mu$, for example, the discontinuity occurs near $1/\lambda = 1.3$.

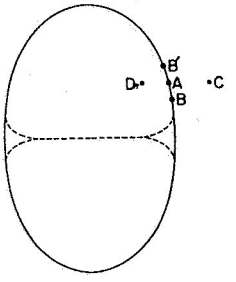

FIG. 2. Cross section perpendicular to the line of sight through an interstellar particle.

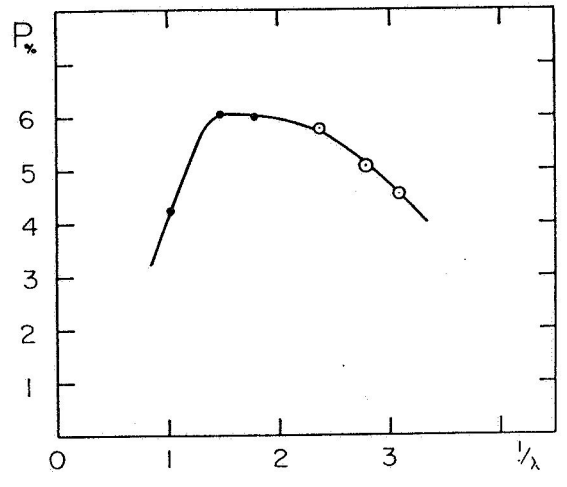

FIG. 1. Observed percentage interstellar polarization. The abscissas are in reciprocals of microns. Computations for refractive index $m \cong 1.3$ and particle diameter $2a \cong 0.3\,\mu$ reproduce this curve.

The accreted molecules presumably are lightly packed, but they may not be independent scatterers. However, independent scattering is not a required condition, and at least the polarization is not affected by interference effects (p. 87 of van de Hulst 1957; also see p. 396). Whether or not loose binding of the surface molecules is essential, remains to be seen.

The present interpretation attempts to explain small-scale phenomena. It is compatible with the theoretical work on light scattering by small particles, of Mie and others, that treats the particle as a whole. Particularly the discontinuity at $1/\lambda = 1.3$ in Fig. 1 is not obvious in the usual calculations (Chap. 15 of van de Hulst

*Reprinted with permission from the *Astronomical Journal*, Vol. 71, No. 1, Feb. 1966 — No. 1336.

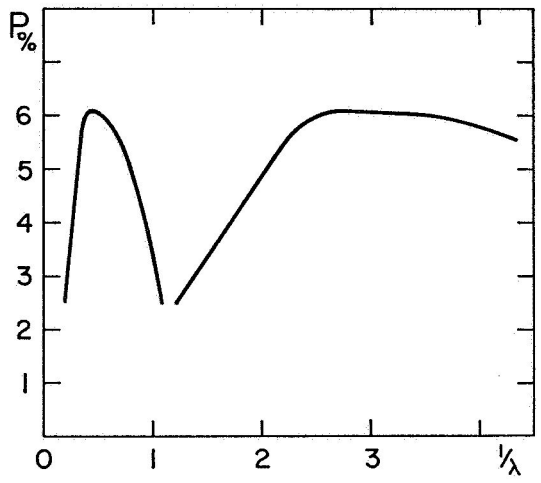

FIG. 3. Percentage interstellar polarization computed for refractive index $m=1.3$ and particle diameters $2a=1.1\,\mu$ (curve on the left) and $2a=0.17\,\mu$ (right).

1957), but it is understood with the above interpretation on molecular scattering.

Figure 3 gives the characteristic curves for $2a=1.1$ and $0.17\,\mu$. They are computed for long cylinders with refractive index near 1.3 (van de Hulst 1957, Chap. 15). The curves are normalized so that the maxima agree with that of Fig. 1.

An alternate fit to the observed variety in interstellar absorption (Johnson 1965) and polarization (Paper V) is with a variety of refractive indices. The curves of Fig. 3 could then have $m\cong 2.1$ (left) and 1.2 (right) for $2a=0.3\,\mu$ (and Fig. 1 still is for $m=1.3$). From the present observations of interstellar absorption and interstellar polarization we cannot decide if there is a variety in $2a$, in m, or in both.

REFERENCES

Coulson, J. L., Dave, J. V., and Sekera, Z. 1960, *Tables Related to Radiation Emerging from a Planetary Atmosphere with Rayleigh Scattering* (University of California Press, Berkeley and Los Angeles).
Gehrels, T. 1962, *J. Opt. Soc. Am.* **52**, 1164.
Gehrels, T., and Silvester, A. B. 1965, *Astron. J.* **70**, 579 (Paper V).
Hulst, H. C. van de 1957, *Light Scattering by Small Particles* (John Wiley & Sons, Inc., New York).
Johnson, H. L. 1965, in *Nebulae and Interstellar Matter*, Vol. 7 of *Stars and Stellar Systems*, edited by L. H. Aller and B. M. Middlehurst (University of Chicago Press, Chicago).

Acknowledgments. The work is supported by the National Aeronautics and Space Administration (NsG-733).

NO. 89 WAVELENGTH DEPENDENCE OF POLARIZATION. VII. INTERSTELLAR POLARIZATION*

by T. GEHRELS AND A. S. MELTZER†

ABSTRACT

Observations were made of the interstellar polarization on eight selected stars with the Kitt Peak 36-in. reflector. The telescope was found, in 1961, to be free of instrumental polarization thanks to careful aluminization procedures.

THIS paper is one in a continuing series in this Journal. Eight stars were especially selected to be as far away and as faint as possible with the available equipment, and also to have uniform color characteristics. The observations of these eight stars are presented here. A detailed discussion of the results, and of those obtained on brighter stars, will be made in a following paper.

1. Filter Tracings

The filters used in this program were traced anew, with the Cary 14 spectrophotometer of the Kitt Peak National Observatory. We thank the Observatory for the use of this fine instrument and we thank Mr. S. F. Pellicori who made all tracings.

Table I describes the tubes and filters and the resulting wavelengths. Table I of Gehrels and Teska (1960) is hereby superseded. The principal changes are the addition of a filter near 1.19 μ^{-1}, especially important for the interstellar polarization, and the use for shorter wavelengths of an EMI 6255*S* phototube which has a quartz window. The R_1 filter of Table I is temporary and will be replaced by an interference filter that does not have a "tail" of transmission out to 1 μ.

The values of the effective wave numbers are defined by

$$\left(\frac{1}{\lambda}\right)_{\text{eff}} = \frac{\int I(1/\lambda)1/\lambda d(1/\lambda)}{\int I(1/\lambda)d(1/\lambda)}.$$

The average color of the stars of the present paper was taken into account for sec$z$= 1.0 at 7000 ft altitude, and the sensitivity curves of the phototubes (as provided by the manufacturer) were used, as well as the tracings of our filter transmissions. The values of $(1/\lambda)_{\text{eff}}$ have an estimated probable error of ± 0.03.

2. Instrumental Polarization

About 10 stars were observed with the Kitt Peak 36-in. reflector in order to determine the instrumental polarization. As usual in this program, the stars were chosen from the Behr (1959) catalogue with the polarization, $p < 0.0008$ mag. Even if these small polarizations are real, the average observed polarization should be zero because the 10 selected stars show a nearly uniform distribution of position angles.

The average of the observed polarizations with the

TABLE I. Filters and phototubes.

Filter	$(1/\lambda)_{\text{eff}}$	Eff. wavel.[a] in μ	Multiplier[b] phototubes	Description of the filters[b]
N	3.04	0.33	EMI 6255*S*	st. th. C.S. 7–54; plus 8.7 mm thickness of a solution: 98% $NiSO_4 \cdot 6\ H_2O$, 420 g/liter, and 2% $CuSO_4 \cdot 5\ H_2O$, 260 g/liter; plus $\frac{1}{16}$-in. thickness of fused silica.
U	2.79	0.36	EMI 6255*S*	2 mm UG 2, plus 2 mm $CuSO_4 \cdot 5\ H_2O$, 260 g/liter, plus $\frac{1}{16}$-in. of fused silica.
B	2.33	0.43	EMI 6255*S*	st. th. C.S. 5–57, plus st. th. GG 13.
G_1	1.95	0.51	EMI 6255*S*	2 mm C.S. 3–71, plus 2 mm BG 18.
G_2	1.85	0.54	RCA 7102	2 mm C.S. 3–71, plus 2 mm BG 18.
R_1	1.39	0.72	RCA 7102	$\frac{1}{3}$ st. th. C.S. 2–64, plus $\frac{1}{2}$ st. th. C.S. 1–58.
R_2	1.19	0.84	RCA 7102	$\frac{1}{3}$ st. th. C.S. 2–64, plus st. th. C.S. 5–57.
I	1.05	0.95	RCA 7102	st. th. C.S. 7–56.

[a] The reciprocal of $(1/\lambda)_{\text{eff}}$.
[b] EMI = Electra Megadyne Inc.; RCA = Radio Corporation of America; C.S. = Corning Specification; UG, etc., are Jena glass filters; st. th. = stock thickness.

*Reprinted with permission from the *Astronomical Journal*, Vol. 71, No. 2, March 1966 — No. 1337. *Contributions from the Kitt Peak National Observatory*, No. 146.

†Rensselaer Polytechnic Institute.

Kitt Peak 36-in., in 1961, is less than 0.002 mag. for all filters. The residual effect, if real, is probably intrinsic to the polarimeter or to the observing method. The instrumental polarization of this telescope in 1961, therefore, is negligible. This near-zero result, over the full range of wavelengths 0.3–1.0 μ, is compared with that of other telescopes in Fig. 1 of Gehrels and Teska (1963).

The aluminization of the mirrors of the Kitt Peak 36-in. had been done carefully with: (1) the glow discharge used sparingly; (2) the use of liquid-nitrogen baffling to eliminate backstreaming of oil vapors; and (3) having the glow discharge as well as the aluminum deposition normal and symmetrical to the surface of the mirrors. Pellicori recently made an additional suggestion, that is to aluminize the secondary while mounted in the hole of the primary, and to mount the secondary on the telescope after rotation of 90° with respect to the primary.

3. Star Selection

Eight stars were chosen from the Hiltner (1956) catalogue, with four selection rules as follows:

(1) $+0.29<(B-V)<+0.42$, and $-0.65<(U-B)<-0.53$.
(2) The amount of polarization $p>0.033$ mag.
(3) $V<8.0$ mag. This still is rather faint for high precision with the present equipment, especially for the N and the I filters. In order to improve the precision, a special effort was made to observe the amount of polarization rather than the position angle. For example, if the position angle for a star in the catalogue was 133°, the analyzer orientations would be as follows: 135° and 225°, 120° and 210°, 150° and 240°, and 133° as a seventh angle. Finally, each star was observed several times (on the average, three times with each filter).
(4) An attempt was made to include a wide range of values of the polarization–extinction ratio $p/3E_{B-V}$. To a first approximation, this ratio can serve as an indicator of orientation of the grains responsible for the polarization. If the ratio is small this may be due either to p itself being small or to E_{B-V} being large (or both). Small $p/3E_{B-V}$ indicates, if the same grains are responsible for both extinction and polarization, that they are poor polarizers. This would be the case, for example, if the grains were poorly aligned. On the other hand a large value of $p/3E_{B-V}$ indicates a high degree of alignment of the particles.

Table II lists the stars in order of galactic longitude; the Henry Draper catalogue number is used for identification. The spectral type, V, $B-V$, $U-B$, and $p/3E_{B-V}$ are all taken from the Hiltner (1956) catalogue.

TABLE II. Selected stars.

HD	Sp.	V	$B-V$	$U-B$	$p/3E_{B-V}$
193443	O9 III	$7^m.24$	$+0^m.41$	$-0^m.54$	0.016
207538	B0 V	7.31	.33	.64	24
218342	B0 IV	7.38	.41	.55	19
6675	B0.5 III	6.90	.31	.64	20
18326	O8	7.82	.38	.63	34
22253	B0.5 III	6.53	.33	.56	22
24431	O9 IV–V	6.72	.38	.61	20
43753	B0.5 III	7.90	+0.30	−0.64	0.034

4. Observations

The observations were made mostly with the 36-in. reflector of the Kitt Peak National Observatory during the fall of 1961. Additional observations were made with the McDonald 36-in. reflector, January 1962, and with the McDonald 82-in. in November 1963. The polarimeter is the same as used before in this series of papers. It has been described by Gehrels and Teska (1960; 1963). All reductions were made by Ann Silvester, to whom we are indebted for her careful work.

Table III gives the weighted mean of the observed percentage polarization. From internal agreement it appears that the probable error, of the results without a colon in Table III, is ±0.08% (nearly independent of wavelength). Colons are given when the precision appears of the order of ±0.4% or worse. A depolarization correction-factor of 1.01 was applied before entry in the table.

TABLE III. Observed interstellar polarization.

	Percentage polarization observed at $1/\lambda=$						
HD	1.05	1.19	1.39	1.95	2.33	2.79	3.04
193443	1.54:	1.03:	2.00:	1.70	1.84:	1.71:	1.30:
207538	1.51:	1.58	1.92	2.12	2.23	2.12:	1.72:
218342	1.85:	1.75	2.07	2.14	1.88	2.04	2.09:
6675	1.48	1.46	1.69	1.66	1.44	1.44	1.73
18326	2.51	2.51	3.88:	3.03	3.15	2.89	3.09
22253[a]	1.36	1.35	1.48	1.63	1.58	1.76	1.67
24431	1.57	1.60	1.34	2.14	1.87	2.12:	1.90
43753	2.18:	2.65	2.84:	2.80	2.59	2.28	2.51

[a] HD 22253 was also observed at $1/\lambda=1.85$; $P=1.94\%$, $\theta=113:°$.

Table IV gives the weighted mean of the position-angle observations. The probable error, of the results without a colon, is ±4°. (Section III describes the reason for poor precision of the position angle.)

TABLE IV. Observed position angles of interstellar polarization.

	Position angle observed at $1/\lambda=$						
HD	1.05	1.19	1.39	1.95	2.33	2.79	3.04
193443	34:°	58:°	71°	52°	43°	74°	64:°
207538	49	55	57:	59	59	56	63
218342	61:	56	53	54	54	50	67:
6675	110	125	127	130	121	116	130
18326	118	109	120:	115	119	116	119
22253	128	129	128	125	122	113	112
24431	125	121	120	113	119	117	110
43753	176:	164	150:	166	168	166	161

5. *Wavelength Dependence*

Table V shows the wavelength dependence of the percentage polarization; the normalization method of Treanor (1963) is followed. For each star, the straight average of the polarizations at $1/\lambda = 1.95$ and 2.33 is set equal to 100.0, and the resulting normalized percentage for each filter is listed in Table V.

The limited precision of the numbers in Table V should be kept in mind. Without colons, the probable error is about $\pm 4\%$, and with colons it is $\pm 20\%$ or worse. Only two conclusions, therefore, appear established: all stars show a drop in the infrared, and in the ultraviolet there may or may not occur a decline in the amount of polarization.

TABLE V. Normalized interstellar polarizations.

	Normalized percentage polarization at $1/\lambda =$						
HD	1.05	1.19	1.39	1.95	2.33	2.79	3.04
193443	87:	58:	113:	96	104:	97:	73:
207538	69:	73	88	97	103	97:	79:
218342	92:	87	103	106	94	101	104:
6675	95	94	109	107	93	93	112
18326	81	81	126:	98	102	94	100
22253	85	84	92	102	98	110	104
24431	78	80	67	107	93	106:	95
43753	81:	98	105:	104	96	85	93

It is noted that HD 6675 has hardly any dispersion in the percentage polarization. HD 22253 clearly shows dispersion in the position angle of interstellar polarization. No correlation is apparent between any of the observed features and the ratio of polarization to extinction (last column of Table II).

In a following paper (Coyne and Gehrels 1966), an analysis will be made of all stars observed in this program to date.

REFERENCES

Behr, A. 1959, *Nachr. Akad. Wiss. Göttingen, Math.-Phys. Kl.*, No. 7, 185.
Coyne, G. V., and Gehrels, T. 1966, *Astron. J.* (to be published).
Gehrels, T., and Teska, T. M. 1960, *Publs. Astron. Soc. Pacific* **72**, 115.
——. 1963, *Appl. Opt.* **2**, 67.
Hiltner, W. A. 1956, *Astrophys. J. Suppl.* **2**, 389.
Treanor, P. J. 1963, *Astron. J.* **68** 185.

Acknowledgments. The work is supported by the National Aeronautics and Space Administration (NsG-733).

NO. 90 WAVELENGTH DEPENDENCE OF POLARIZATION. VIII. INTERSTELLAR POLARIZATION*

by G. V. COYNE S. J. AND T. GEHRELS

ABSTRACT

Eighteen stars were observed primarily with an ultraviolet and an infrared filter in order to verify the previous discovery of a dependence of position angle on wavelength. The effect is confirmed. Observations were also made at five other wavelengths in the range 0.3–1.0 μ. The variability of the polarization of μ Cephei, discovered by K. A. Grigoryan in 1958, appears confirmed. These observations were made with the Catalina 21-in. and Steward Observatory 21-in. reflectors. The current data are combined with those previously reported in this series of papers, so that the total number of stars now is 36. The interpretation is in terms of the traverse of several discrete clouds having different particle sizes and different particle orientations. If the refractive index is 1.3, for example, various particle diameters occur in the range 0.17–0.4 μ. (Smaller particles may be present but they can be observed only at shorter wavelengths.) In a few regions, particle diameters near 1 μ are also found. (Larger particles can be observed only at longer wavelengths.) In general, there is no uniform law of the dispersion of interstellar polarization.

1. *Introduction*

LITTLE is known about the wavelength dependence of plane interstellar polarization. The present observational status was reviewed by Martel (1964). The topic was discussed at the IAU Colloquium on Interstellar Grains (Greenberg 1966) held at Troy, New York, in August 1965.

Circular interstellar polarization has been observed by Serkowski (1965b) for two stars that have no plane polarization and four stars that have strong plane polarization; no ellipticity exceeding 0.05% was found.

In this paper we present additional observations of the wavelength dependence of plane polarization on 18 stars. They were observed primarily at two wavelengths ($1/\lambda = 1.05$ and 2.79) in order to confirm the rotation of position angle with wavelength reported in Paper V. Observations at other wavelengths were also obtained, and all of the new observations are combined with the observations of Papers II, V, and VII (see Reference section).

A discussion is made of the variations for individual stars of the percentage polarization versus wavelength, and of the rotation of position angle. The correlation of percentage polarization and position angle with distance and with galactic longitude are also discussed.

An attempt is made to fit the calculations of van de Hulst (1957), for light scattering by long cylinders, to the observations. This, however, is only a first approximation, using single-particle sizes rather than size distributions and restricting the refractive index to that of dirty ices ($m \simeq 1.3$).

2. *The Observations*

Most of the observations reported here were obtained during the summer of 1965 with the Catalina 21-in. and the Steward 21-in. reflectors. The Catalina telescope is at 2510 m altitude in the Santa Catalina Mountains north of Tucson and is operated by the Lunar and Planetary Laboratory of The University of Arizona. The Steward telescope is in Tucson at 757 m altitude and it is operated by the Astronomy Department of The University of Arizona. The polarimeter is the same as used before (Gehrels and Teska 1960). The tubes and filters which define the effective wavelengths are described in Table I of Paper VII. We are indebted to Mrs. Tricia Coffeen, who assisted with much of the observing and who made the majority of the reductions.

In order to obtain corrections for instrumental polarization, at least six nonpolarized stars ($P < 0.023\%$) were observed twice. As usual, the resulting small corrections were applied at each analyzer angle before the computation by least squares of the cosine curve was made.

Table I gives the instrumental effects of the two telescopes. P is the percentage polarization (division by 46.05 gives the amount in magnitudes), and θ is the position angle in the equatorial reference frame. Under the $1/\lambda = 1.90$ heading is listed the average of observations at $1/\lambda = 1.85$ (green filter with RCA 7102 phototubes) and at $1/\lambda = 1.95$ (same filter with EMI 6255*S*). It is seen in Table I that the instrumental polarization is small even for the Steward mirrors for which no special precautions, to reduce polarization, in the aluminization had been taken.

The calibration of the polarization position angles (Gehrels and Teska 1960, p. 121) was carried out in the course of the observing runs.

TABLE I. Observed instrumental polarization.

Telescope		Amount and position angle observed at $1/\lambda =$ 1.05	1.19	1.39	1.90	2.33	2.79	3.04
Catalina	P (%)	0.09	0.13	0.09	0.07	0.13	0.14	0.21
	θ (deg)	90	107	106	87	94	99	102
Steward	P (%)	0.18	0.14	0.12	0.12	0.14	0.13	0.19
	θ (deg)	172	173	165	169	173	10	174

*Reprinted with permission from the *Astronomical Journal*, Vol. 71, No. 5, June 1966 — No. 1340.

TABLE II. Observed percentage of interstellar polarization. 1965 observations.[a]

HD	Percentage polarization observed at $1/\lambda=$ 1.05	1.19	1.39	1.95	2.33	2.79	3.04
147165	0.90	1.12;	1.96:	1.60	1.44	1.23	...
187929	1.16	1.42	1.64	1.50	1.65	...	...
198478	1.96;	1.84;	2.11;	2.94	2.65	2.31;	2.52;
206936	0.85	1.11:	1.55	2.28	2.44	...	...
207260	1.24	1.00	1.35	1.67	1.55	1.45	1.01;
217476	1.62	1.64:	2.14	...	...	...	...
224014	1.09	...	...	1.33	1.34	1.12	...
2905	0.95	...	...	1.62	1.49	1.28	1.40
7927	2.07	...	...	3.35	3.66	3.11	...
14489	1.54	...	...	...	...	2.43:	...
21291	2.54	2.64	3.24	3.56:	3.60	3.48:	2.73
21389	2.72	...	...	4.07:	3.61	...	...
30614	...	...	...	1.70	1.59	1.56	1.06:
25291	1.54	1.57	1.83	1.85	2.00	...	...
24398	0.95	0.92	1.08	1.19	1.19	0.96:	0.55
31964	1.46	1.58	1.89	2.01	1.88	2.02	1.28:
36371	...	...	1.56:	2.22	2.20	1.69	...
37202	1.36;	1.06;	1.21;	...	...	1.08;	...

[a] Semicolons are used for single observations and colons for uncertain observations.

The depolarization correction factor was determined anew, for all filters with $1/\lambda<2.3$, and it was found to be 1.004 ($\pm$0.001 p.e.), independent of wavelength; the observed polarizations have been multiplied by 1.004 before entry in the tables. This determination of the depolarization is made with a Polaroid sheet immediately in front of the *polarimeter*, and it does not, therefore, include any depolarization effects of the telescope mirrors (we thank Mr. F. F. Forbes for a discussion of depolarization effects).

In 1965, the observations were primarily made with the *I* and *U* filters (see Table I of Paper VII) using, for both filters, one and the same phototube box (RCA 7102); these observations were to test the wavelength dependence of the position angles. As an incidental part of the work in 1965, observations were also made at the other wavelengths.

TABLE III. Observed position angles of interstellar polarization. 1965 observations.

HD	Position angles observed at $1/\lambda=$ 1.05	1.19	1.39	1.95	2.33	2.79	3.04
147165	164°7:	168°8:	176°6;	0°9:	179°9	8°8:	...
187929	91.4	90.5	90.0	88.7	95.9	...	...
198478	7.3:	1.3;	5.1:	3.3	2.8	0.6;	9°8:
206936	22.2	22.7	24.9	30.8	32.0	...	...
207260	48.8:	44.2:	41.6:	41.6	42.1	46.2	49.9;
217476	70.1	67.1	69.3	...	...	...	...
224014	58.5:	...	...	56.4	58.0:	53.4:	...
2905	80.9	...	...	82.9	84.9	84.8	90.9;
7927	91.0	...	...	92.5	...	94.2	...
14489	116.1:	...	...	...	...	110.5:	...
21291	115.9	115.2	115.9	116.5	116.8	117.3	107.6:
21389	118.9	...	...	120.3	120.9	...	...
30614	136.8	...	...	136.6	138.0	135.5:	137.0
25291	132.8	141.3:	133.2	131.8	133.1	...	...
24398	61.1	58.6	63.9	61.7	61.8	63.2:	72.7
31964	144.9	144.9	145.8	146.2	145.0:	144.4	143.3;
36371	...	...	176.4;	179.3:	178.8:	173.8	...
37202	...	28.2;	34.0;	...	...	...	...

TABLE IV. Observed percentage of interstellar polarization. All observations combined.

HD	Percentage polarization observed at $1/\lambda=$ 1.05	1.19	1.39	1.95	2.33	2.79	3.04
147165	1.10	1.18	1.55:	1.65	1.49	1.30	1.35
161056	2.89	...	4.24;	4.08	3.98;	3.00	3.07;
154445	2.62	...	3.75;	3.68	3.42;	2.87	2.60;
134335	0.39	0.61	0.58:	0.58	0.78	1.10	0.68
134320	0.69:	0.47	0.49	0.71	0.65:	0.57:	...
187929	1.16	1.42	1.64	1.50	1.65	...	...
183143	4.21;	...	5.99	6.08;	5.68	5.18:	4.28:
193443	1.54:	1.03:	2.00:	1.70	1.84:	1.71:	1.30:
198478	1.94	1.84;	2.45:	2.89	2.68	2.33	2.39
206936	0.85	1.11	1.55	2.28	2.44	...	...
207538	1.51:	1.58	1.92	2.12	2.23	2.12:	1.72
207260	1.08	1.15	1.30	1.60	1.56	1.48:	1.09;
217476	1.95:	2.18:	2.49:	2.64	2.53	2.49	2.85:
218342	1.85:	1.75	2.07	2.14	1.88	2.04	2.09:
224014	1.02	1.13	1.32	1.39	1.25	1.08	1.13:
2905	1.10	1.10	1.37	1.51	1.40	1.24	1.31
6675	1.48	1.46	1.69	1.66	1.44	1.44	1.73
7927	2.28	2.47	2.99	3.33	3.36	2.90	2.92
12301	2.01	2.37	2.41	2.80	2.72	2.58	2.14
12953	1.96	2.70	2.96	3.48	3.40	3.25	2.94
14489	1.44	1.55	1.80	2.10	2.03	2.05	1.87:
18326	2.51	2.51	3.88:	3.03	3.15	2.89	3.09
21291	2.39	2.72	3.16	3.48	3.43	3.09:	2.78
21389	2.49	2.75	3.18	3.72:	3.61	3.39	3.15
30614	0.89:	1.13	1.44	1.83	1.76	1.68	1.50:
22253	1.36	1.35	1.48	1.69:	1.58	1.76	1.67
25291	1.50	1.59	1.71	2.11	2.08	2.13	2.00
24431	1.57	1.60	1.34	2.14	1.87	2.12:	1.90
24398	0.93	0.98	1.13	1.20	1.11	0.88:	0.67
31964	1.46	1.60	1.83	2.04	2.00	1.99	1.76:
36371	1.52;	1.70;	1.87:	2.23	2.14	1.81	1.78
37202	1.37	1.23	1.21	1.46	1.53	1.01	0.68
41117	1.95	2.27;	2.50;	2.85	2.81	2.42	2.47
42379	1.88	2.07;	2.63;	2.92:	2.81;	2.98	2.44;
43753	2.18:	2.65	2.84:	2.80	2.59	2.28	2.51
37041	0.91	0.94	0.91	0.87	0.58	0.39	0.33

Table II lists the amounts of polarization observed in 1965. The stars are identified by their number in the Henry Draper catalogue, and they occur in the order of increasing galactic longitude. Corrections for red leaks of the ultraviolet filters have not been applied in any of our reductions of interstellar polarization. We have assumed that the effective wavelength for the ultraviolet filter with RCA 7102 tubes is the same as with EMI 6255S, so that $1/\lambda=2.79$. Furthermore, we have combined (Tables IV and V, below) a few observations made at $1/\lambda=1.85$ into those reported at $1/\lambda=1.95$, and at 1.46 (Paper II) into those at $1/\lambda=1.39$; resulting errors in the final values are always less than 0.03%.

The weighted mean values are listed in our tables, where the weights are equal to the reciprocal of the mean of the least-squares residuals. In practice, this is more realistic than applying the *square* of the mean residual. The number of observations per least-squares solution is small (of the order of 6 usually, and only

TABLE V. Observed position angles of interstellar polarization. All observations combined.

HD	Position angles observed at $1/\lambda =$ 1.05	1.19	1.39	1.95	2.33	2.79	3.04
147165	176°4:	170°1:	176°1	177°8:	179°2	183°9:	179°9
161056	68	...	65 ;	66	62 ;	68	63 ;
154445	89	...	86 ;	89	86 ;	89	87 ;
134335	64.0:	82.0:	62.8:	76.3:	72.6	...	...
134320	64.4:	75.6:	82.0:	75.3	77.7	...	...
187929	91.4	90.5	90.0	88.7	95.9	...	...
183143	0 ;	...	179	1 ;	1	0 :	0 ;
193443	34 :	58 :	71	52	43	74	64 :
198478	2.3:	1.3;	3.0:	2.0	1.4	1.3	6.4:
206936	22.2	22.7	24.9	30.8	32.0	...	...
207538	49	55	57 :	59	59	56	63
207260	44.9:	39.9:	44.9:	41.0	41.6	42.0:	48.3
217476	69.5	69.3	68.8	70.5	70.1;	74.8:	70.0
218342	61 :	56	53	54	54	50	67 :
224014	52.3:	52.3	53.8	53.5:	54.9:	53.4:	...
2905	79.6	80.8	80.2:	83.2	85.5	86.4	91.8
6675	110	125	127	130	121	116	130
7927	90.6	91.4	90.8	93.7	94.8;	94.6	97.8
12301	108.1	109.1	109.6	112.2	112.2	113.0	114.6
12953	103.5	107.5	107.0	110.1	110.8	112.2	112.9
14489	108.1:	112.2	110.5	113.8	115.0	115.5:	121.1
18326	118	109	120 :	115	119	116	119
21291	116.9	115.6	116.3	115.8	114.6	115.5	115.5:
21389	118.9	119.4	119.6	121.1	121.8	121.9	122.3
30614	134.2	136.0	136.9	138.4	139.1	138.4:	138.4
22253	128	129	128	122	122	113	112
25291	133.2	133.8:	132.7	132.8	133.0	131.0	134.3
24431	125	121	120	113	119	117	110
24398	60.8	57.4	61.0	60.8	61.0	61.5:	67.6:
31964	144.3	145.2	145.0	145.3	144.2	144.2	145.5
36371	177.6;	176.5;	177.8	175.9:	175.2:	171.0	168.9
37202	30.4;	30.6	33.8	26.0	27.5	23.3	17.6
41117	179.9	177.8;	179.9;	174.9	172.8	174.6:	172.6:
42379	170.0	172.7;	181.0;	169.5:	168.0;	169.9	168.1;
43753	176 :	164	150 :	166	168	166	161
37041	96.7:	104.5:	89.6:	105.6	100.4:	96.6:	...

in the case of I and U observations in 1965 of the order of 18) and the mean residual is, therefore, statistically not a good indicator (for details of the least-squares solutions, see Gehrels and Teska 1960).

Table III lists the weighted mean value of the position angles observed in 1965.

Table IV gives the combination of all our observations of the percentage polarization. The results of Papers II, V, and VII, and those of the present Table II are included. The probable error, determined from repetition of observations, of the values without a colon in Table IV is $\pm 0.08\%$.

Table V gives the combination of all our observations of the equatorial position angle. The probable error of the values without a colon is $\pm 0°.9$ (when the polarization is about 2%), except for the stars from Paper VII, marked with asterisks in Table IX, for which the probable error is $\pm 4°$. The relative weights in Table II–V are with the reciprocal of the mean residual, as described above. Colons are used in the tables when the values appear uncertain by about three times the probable error. Semicolons are used to indicate that there is only one observation.

Table VI has some of the fundamental data for the observed stars. The *Catalogue of Bright Stars* (Hoffleit 1964) was used as a general reference, and especially for the parallactic distances; "neg" indicates zero or negative parallax. The photometric data are from Johnson and Mitchell (personal communication). We are indebted to Mitchell for several helpful discussions. The intrinsic photometric data for the classical Cepheid η Aquila were taken from Kraft (1963). The values of the ratio of total to selective absorption, $R=A_v/E_{B-V}$, were obtained from Fig. 41 of Johnson (1966). The absolute magnitudes are from Blaauw (1963). When in the second column the BD number is given, the star is not in the bright-star catalogue and the photometric data then are from Hiltner (1956), or Serkowski (1965a). Because the present distance determinations are poor—as seen in the lack of agreement of the parallactic and photometric distances—it is more practical to designate a few well-established distances by "near" and "far." The distances in the footnote of Table VI are based on the R values of Johnson, whereas in Paper V the old value $R=3$ was used. For reference in Sec. IV we have P_{vis} in Table VI, which is equal to the weighted mean (colons and semicolons halfweight) of the polarizations at $1/\lambda=1.39$, 1.95, and 2.33 in Table IV. "Var." in the last column of Table VI indicates that the brightness is variable.

3. *Intrinsic Variations*

Because of motion of dust clouds and stars in the galaxy, the interstellar polarization is not invariable. Small changes in particle characteristics can cause strong changes in the observed polarization. Furthermore, in some cases we may be observing a polarization that is intrinsic to the star, or caused by material that is close to the star. Since the discovery of interstellar polarization in 1949, too few years have passed to expect sufficient changes in the relative motions of clouds and stars. But a quick reconnaissance of the problem may be useful, and the comparison of the work of various observers is always interesting.

Tables VII and VIII give the difference between our observations, made mostly in the years 1961–1965, with those of other observers. The catalogues were used of Hiltner (1956 and references given in that paper), Hall (1958, the "Hall" columns), and Behr (1959). The "Serkowski 1960–65" observations were supplied directly to us by Serkowski who applied a depolarization correction to the ones with the Belgrade refractor (publications are by Serkowski 1965a, 1965b, 1966a, 1966b, and Kruszewski 1962). Hall's measurements were compared with those of our blue filter ($1/\lambda=2.33$), Hiltner's with our green filter ($1/\lambda=1.95$), Behr's with the weighted (colons and semicolons halfweight) mean of our green and blue filters, while the average is listed for the differences of Serkowski's yellow filter with our green, his blue with ours, and—in 1965—his ultraviolet with ours.

The systematic difference between the various observers is determined by taking the straight average. The mean residual—without regard to sign—is also

TABLE VI. Various data on the stars observed in this program.

HD	Name	Galactic long	Galactic lat	Sp	V	$B-V$	E_{B-V}	R	Distance in kpc Phot.	Par.	Rel.[a]	P_{vis}	Remarks
												%	
147165	σ Sco	351°	+17°	B1 III	2m89:	+0m14	0m40	3.6	0.15	···	*n*	1.57	Sp. bin. Var.
161056	BS 6601	19	+12	B3 Vn	6.2	···	0.61:	3.6	0.14:	···	*n*	4.10	
154445	BS 6353	19	+23	B1 V	5.6	···	0.51:	3.6	0.30:	···	*n*	3.63	
134335	BS 5640	38	+59	gK1	5.8	···	···	···	···	···		0.66	
134320	46 Boo	39	+60	gK2	5.6	···	···	···	···	···		0.61	
187929	η Aql	41	−13	F6: Ib	3.50:	+0.80	0.13:	3.6	0.24:	0.20	*n*	1.60	Class. Ceph
183143	+18°4085	53	+ 1	B7 Ia	6.87	+1.24	1.30	3.6	0.72	···	*f*	5.88	
193443	+37°3879	76	0	O9 III	7.24	+0.41	0.71	3.6	1.19	···	*f*	1.81	
198478	55 Cyg	86	+ 2	B3 Ia	4.87	+0.43	0.57	3.9	0.78	0.08		2.72	Double
206936	μ Cep	101	+ 4	M2 Ia	4.13:	+2.26	0.62	4.6	0.45	0.08		2.09	Var.
207538	+59°2420	102	+ 4	B0 V	7.31	+0.33	0.63	4.6	0.58	···		2.09	
207260	ν Cep	102	+ 6	A2 Ia	4.29	+0.51	0.46	4.6	0.86	0.11		1.49	Var. ?
217476	BS 8752	108	− 3	G0 Ia	5.13	+1.55	0.85	4.9	0.62	neg.	*f*	2.58	
218342	+62°2170	111	+ 3	B0 IV	7.38	+0.41	0.71	5.0	0.53	···		2.03	
224014	ρ Cas	115	− 4	G0 Iap	4.59:	+1.26	0.56:	5.2	0.86:	0.06		1.32	Var.
2905	κ Cas	121	0	B1 Ia	4.16	+0.14	0.36	5.4	0.58	···		1.43	Var. ?
6675	+68°74	124	+ 7	B0.5 III	6.90	+0.31	0.59	5.6	0.46	···		1.60	
7927	φ Cas	127	− 4	F0 Ia	4.99	+0.68	0.49	5.6	1.41	neg.	*f*	3.23	
12301	53 Cas	131	+ 3	B8 Ib	5.58	+0.38	0.41	5.7	0.59	···		2.64	
12953	BS 618	133	− 3	A1 Ia	5.68	+0.61	0.58	5.8	0.84	···	*f*	3.28	
14489	9 Per	136	− 5	A2 Ia	5.17	+0.37	0.32	5.8	1.45	···	*f*	1.98	
18326	+59°578	138	+ 2	O8	7.82	+0.38	0.69	5.9	0.78:	···	*f*	3.25	
21291	BS 1035	142	+ 3	B9 Ia	4.21	+0.41	0.42	5.9	0.58	···		3.36	Var. ? Double
21389	BS 1040	142	+ 2	A0 Ia	4.54:	+0.56	0.55	5.9	0.48	···		3.46	Sp. bin.
30614	α Cam	144	+14	O9.5 Ia	4.29	+0.03	0.33	6.0:	0.50:	neg.		1.68	
22253	+56°824	145	+ 2	B0.5 III	6.53	+0.33	0.61	6.0	0.33	···		1.56	
25291	BS 1242	146	+ 5	F0 II	5.08	+0.50	0.30	6.0	0.14	···	*n*	1.97	
24431	+52°726	150	0	O9 IV–V	6.72	+0.38	0.69	6.0	0.34	···		1.78	
24398	ζ Per	162	−17	B1 Ib	2.85	+0.12	0.34	6.1	0.20	0.14	*n*	1.15	Var. ?
31964	ϵ Aur	163	+ 1	F0 Iap	3.00:	+0.54	0.35:	6.1	0.75:	0.25		1.96	Ecl. sp. bin.
36371	χ Aur	176	+ 1	B5 Iab	4.77:	+0.35	0.45	6.0	0.47	···		2.12	Sp. bin.
37202	ζ Tau	186	− 6	B2 IVp	3.03:	−0.19	0.05:	6.0	0.16:	neg.		1.40	Sp. bin. Shell
41117	χ^2 Ori	190	− 1	B2 Ia	4.63	+0.28	0.46	5.9	0.55	0.04		2.76	Var. ?
42379	+21°1143	190	+ 3	B1 II	7.37	+0.35	0.58	5.9	0.62	···	*f*	2.79	
43753	+23°1297	190	+ 5	B0.5 III	7.90	+0.30	0.58	5.9	0.68	···	*f*	2.72	
37041	θ^2 Ori	209	−19	O9.3 Vp	5.10:	−0.11	0.19:	5.2	0.55:	neg.		0.79	Sp. bin.

[a] In the relative-distance column, *n*ear stands for 0.1–0.3 kpc and *f*ar for 0.6–1.5 kpc.

given at the bottom of Tables VII and VIII. The values in brackets were not included for these determinations.

HD 206936 is already now suspected of intrinsic variation. On the other hand, HD 224014 is well observed and good agreement is seen. Additional and repeated observations are obviously needed. We are indebted to Dr. Serkowski for a discussion on this topic. The variations of HD 206936, μ Cephei, were first noticed by Grigoryan (see Serkowski 1965a, p. 85).

4. *Wavelength Dependence*

Table IX is designed to reveal any dependence of position angle on wavelength and to show any differences among the stars in this dependence. For each star the weighted (half-weight for colons and semicolons) mean value of the position angles is determined and the difference with the values of Table V is listed in Table IX. The stars marked with an asterisk have a much lower precision in the position angle as the observations had been made mainly for the percentage polarization (Paper VII).

Table IX shows that at least one-third of the stars show a marked dispersion of position angles, they are indicated with exclamation marks. The findings of Paper V are thereby confirmed. More stars may have some dispersion of the position angles, detectable at better precision and/or greater wavelength range. As for the dependence on galactic longitude, the effect is not so often found from Ophiuchus through Cygnus. But in the range of $120°<\text{long}<145°$ (Cassiopeia), 7 of the 10 observed stars show an increase in position angle with increasing $1/\lambda$. There is a sudden reversal as 5 of the 10 stars within the range $144°<\text{long}<191°$ (from Perseus to Orion) show a decrease of θ with increasing $1/\lambda$.

Table X lists normalized values of the percentage polarization. For each star the straight average of the polarizations at $1/\lambda=1.95$ and 2.33 is set equal to 100.0. The probable errors of the values without a colon now are about ±4%. Colons and semicolons are transferred from Table IV.

Table X shows a variety of shapes in polarization-wavelength dependence (see also the third and fourth columns of Table XI, Sec. V). Paper II concluded to a general shape ("characteristic curve") with a maximum near $1/\lambda=1.5$ or 1.6, a gradual decrease toward greater $1/\lambda$ value and a sharp drop toward smaller $1/\lambda$. Nearly half of the stars show this same general shape although some may have the maximum apparently shifted, in most cases towards larger value of $1/\lambda$.

HD 37041 is peculiar. The maximum of the amount of polarization occurs near $1/\lambda=1.2$. In addition to HD 37041, HD 37202 also shows an abnormally large decrease towards the ultraviolet. A few stars show an abnormally large decrease toward the infrared; HD 206936 is noteworthy in this respect.

Some of the stars of Table X show a rise to a *second* maximum near the limits of the observed wavelength range. For example, such a secondary rise occurs in the ultraviolet for HD 22253, and in the infrared for HD 37202. HD 6675 has little wavelength dependence of polarization.

An intercomparison of Tables IX and X is now made. In the case of HD 2905, the maximum in percentage polarization coincides with the mean value of the position angle. In other cases, such as HD 206936, the percentage polarization maximum coincides with the maximum value of the position angle. For HD 206936 the abnormally low value of percent polarization at $1/\lambda=1.05$ corresponds to a large difference of

TABLE VII. Our percentage polarization minus that of other observers.

HD	Hall 1949–54	Hiltner 1949–54	Behr 1956–58	Serkowski 1960–65
147165	+0.06	...	+0.08	+0.16
161056	(−1.09;)	...	...	+0.09
154445	+0.10;	...	...	−0.04
134335	...	...	+0.07	...
134320	...	...	+0.04	...
187929	...	...	−0.05	...
183143	(−0.91)	+0.09;	+0.03	+0.04
193443	+0.50:	+0.13	...	...
198478	−0.45	+0.08	−0.08	+0.10
206936	...	(+0.67)	...	(+2.01)
207538	+0.02	0.00	...	...
207260	−0.10	−0.10	...	−0.05
217476	−0.14	−0.31	...	−0.21
218342	+0.36	+0.25	...	...
224014	−0.09	+0.01	+0.08	+0.01
2905	−0.12	+0.04	+0.17	...
6675	−0.08	0.00	...	...
7927	+0.14	−0.08	+0.15	+0.08
12301	−0.09	+0.45	−0.12	−0.03
12953	−0.10	+0.07	...	−0.07
14489	+0.05	−0.16	...	...
18326	+0.57	−0.19	...	...
21291	+0.11	+0.03	+0.07	+0.07
21389	−0.21	+0.27:	(+0.48)	+0.20
30614	+0.10	...	...	...
22252	+0.01	−0.15:	...	...
25291	...	...	+0.11	...
24431	−0.43	+0.25	...	...
24398	+0.14	−0.14	+0.02	...
31964	...	...	+0.07	−0.08
36371	−0.44	...	+0.16	+0.08
37202	+0.19	...	...	...
41117	−0.18	...	(+0.62)	+0.21
42379	−0.60;	+0.16:	...	...
43753	+0.43	+0.08	...	...
37041	−0.11	...	...	...
Syst. Diff.	−0.01	+0.04	+0.05	+0.04
Mean Res.	0.21	0.14	0.09	0.09

TABLE VIII. Our position angle minus that of other observers

HD	Hall 1949–54	Hiltner 1949–54	Behr 1956–58	Serkowski 1960–65
147165	+ 3°	...	0°	− 1:°
161056	0;	...	...	− 6
154445	− 2;	...	...	− 2
134335	...	...	−4	...
134320	...	...	−4	...
187929	...	...	−4	...
183143	+ 2	+2°;	+3	+ 2
193443	−10	−4	...	...
198478	− 3	−3	0	− 2
206936	...	(−7)	...	(+17:)
207538	− 1	−2	...	...
207260	+ 6	−5	...	− 4
217476	− 3;	+1	...	− 1
218342	− 4	−4	...	...
224014	+ 5:	+3:	−1	− 1
2905	+ 2	0	−2	...
6675	− 4	+7	...	...
7927	− 1;	+1	0	+ 1
12301	+ 1	+2	+2	+ 2
12953	+ 2	+2	...	+ 1
14489	− 3	0	...	...
18326	0	−2	...	...
21291	0	−1	0	− 3
21389	− 2	0	+1	+ 1
30614	− 2	...	...	...
22253	0	−5	...	...
25291	...	...	+2	...
24431	− 2	−5	...	...
24398	+10	−1	−1	...
31964	...	...	+1	+ 1
36371	− 4:	...	−1	0
37202	+ 5	...	...	...
41117	− 4	...	−2	0
42379	− 8;	−1:	...	...
43753	+ 7	+5	...	...
37041	− 2:	...	...	...
Syst. Diff.	− 0.4	−0.5	−0.6	− 0.8
Mean Res.	3.3	2.5	1.6	1.8

TABLE IX. Residuals of position angles.

HD[a]	Observed minus average for each star, at $1/\lambda=$ 1.05	1.19	1.39	1.95	2.33	2.79	3.04
147165!	− 2°:	− 8°:	− 2°	0:°	+ 1°	+ 6°:	+ 2°
161056	+ 2	···	− 1;	0	− 4;	+ 2	− 3;
154445	+ 1	···	− 2;	+1	− 2;	+ 1	− 1;
134335	− 8:	+10:	− 9:	+5:	+ 1	···	···
134320	−11:	0:	+ 7:	0	+ 2	···	···
187929	0	− 1	− 1	−3	+ 5	···	···
183143	0;	···	− 1	+1;	+ 1	0:	0:
193443*	−24:	0:	+13	−6	−15	+16	+ 6:
198478	0:	− 1;	+ 1:	0	− 1	− 1	+ 4:
206936!	− 4	− 4	− 2	+4	+ 5	···	···
207538*!	− 8	− 2	0:	+2	+ 2	− 1	+ 6
207260	+ 3:	− 2:	+ 3:	−1	− 1	0:	+ 6
217476	− 1	− 1	− 1	0	0;	+ 5:	0
218342*	+ 6:	+ 1	− 2	−1	− 1	− 5	+12:
224014	− 1:	− 1	+ 1	0:	+ 2:	0:	···
2905!	− 5	− 3	− 4:	−1	+ 1	+ 2	+ 8
6675*	−13	+ 2	+ 4	+7	− 2	− 7	+ 7
7927!	− 3	− 2	− 2	0	+ 2;	+ 1	+ 5
12301!	− 3	− 2	− 2	+1	+ 1	+ 2	+ 3
12953!	− 6	− 2	− 2	+1	+ 2	+ 3	+ 4
14489!	− 6:	− 2	− 4	0	+ 1	+ 1:	+ 7
18326*	+ 2	− 7	+ 4:	−1	+ 3	0	+ 3
21291	+ 1	0	+ 1	0	− 1	0	0:
21389!	− 2	− 1	− 1	0	+ 1	+ 1	+ 2
30614!	− 3	− 1	0	+1	+ 2	+ 1:	+ 1
22253*!	+ 6	+ 7	+ 6	0	0	− 9	−10
25291	0	+ 1:	0	0	0	− 2	+ 1
24431*!	+ 7	+ 3	+ 2	−5	+ 1	− 1	− 8
24398	0	− 4	0	0	0	+ 1:	+ 7:
31964	− 1	0	0	+1	− 1	− 1	+ 1
36371!	+ 4;	+ 2;	+ 4	+2:	+ 1:	− 3	− 5
37202!	+ 4;	+ 4	+ 7	−1	+ 1	− 4	− 9
41117!	+ 4	+ 2;	+ 4;	−1	− 3	− 1:	− 3:
42379	− 1	+ 2;	+10;	−2:	− 3;	− 1	− 3;
43753*	+11:	− 1	−15:	+1	+ 3	+ 1	− 4
37041	− 3:	+ 5:	−10:	+6	+ 1:	− 3:	···

[a] The stars with exclamation mark (!) show appreciable wavelength dependence of the position angles. The stars marked with an asterisk (*) have low precision in position angle.

position angle. The same is true for HD 37202 in $1/\lambda=3.04$. For HD 22253, abnormally large values of percent polarization at $1/\lambda=2.79$ and 3.04 correspond to large differences in position angle. Improved precision may be necessary to substantiate these conclusions.

5. *Interpretations*

For a constant value of the refractive index we tend to see at shorter wavelengths the effects of clouds with smaller mean particle sizes and at longer wavelengths clouds with larger mean particle sizes. If the difference in the mean particle sizes for two clouds is sufficiently great, we may expect to see two maxima in the $P(\lambda)$ curve, indicating the superposition of two distinct $P(\lambda)$ curves, each characteristic of a given mean particle size (various characteristic curves are shown in Paper VI). If, in addition, the particle alignment in the two clouds is different, we should expect to find a dependence of the polarization position angle θ with wavelength λ, since the relative contribution to the polarization from each cloud will vary with wavelength.

Variations of position angle with wavelength might be explained by assuming that the starlight traverses two or more discrete clouds of interstellar particles in which the characteristics and the alignments of the particles differ. The illuminating star must be far away enough so that the light traverses at least two different particle clouds and at least two different orientations of the galactic magnetic field.

It is, however, not established observationally that the stars with rotation are always at great distances. For instance nearby σ Scorpionis may show some rotation. Another puzzle is in the systematic trends of rotation (Table IX), with one direction at longitudes smaller than 144° and the opposite direction at greater longitudes. Longitude 144° is probably the direction perpendicular to the local spiral arm. Some effect alike

TABLE X. Normalized polarizations.

HD	Normalized percentage polarization at $1/\lambda=$ 1.05	1.19	1.39	1.95	2.33	2.79	3.04
147165	70	75	99:	105	95	83	86
161056	72	···	105;	101	99;	74	76;
154445	74	···	106;	104	96;	81	73;
134335	57	90	85:	85	115	162	100
134320	101:	69	72	104	96:	84:	···
187929	74	90	104	95	105	···	···
183143	72;	···	102	103;	97	88:	73:
193443	87:	58:	113:	96	104:	97:	73:
198478	70	66;	88:	104	96	84	86
206936	36	47	66	97	103	···	···
207538	69:	73	88	97	103	97:	79:
207260	68	73	82	101	99	94:	69
217476	75:	84:	96:	102	98;	96	110:
218342	92:	87	103	106	94	101	104:
224014	77	86	100	105	95	82	86:
2905	76	76	94	104	96	85	90
6675	95	94	109	107	93	93	112
7927	68	74	89	100	100	87	87
12301	73	86	87	101	99	93	78
12953	57	78	86	101	99	94	85
14489	70	75	87	102	98	99	91:
18326	81	81	126:	98	102	94	100
21291	69	79	91	101	99	89:	80
21389	68	75	87	102:	98	92	86
30614	50:	63	80	102	98	94	84:
22253	83	83	91	103:	97	108	102
25291	72	76	82	101	99	102	95
24431	78	80	67	107	93	106:	95
24398	81	85	98	104	96	76:	58
31964	72	79	91	101	99	99	87:
36371	70;	78;	86:	102	98	83	81
37202	92	82	81	98	102	68	45
41117	69	80;	88;	101	99	86	87
42379	66	72;	92;	102:	98;	104	85;
43753	81:	98	105:	104	96	85	93
37041	126	130	126	120	80	54	46

TABLE XI. Ratio of polarization to total absorption, of visual to infrared, and of visual to ultraviolet polarizations. Approximate particle sizes.

HD	$\frac{p_{vis}}{RE_{B-V}}$	$\frac{P_{vis}}{P_{ir}}$	$\frac{P_{vis}}{P_{uv}}$	Particle diameters (μ)		
147165	0.024	1.38	1.18	...	0.3	0.2
	±.006	±.03	±.03		±.1	
161056	.041:	1.42:	1.35	...	.3	...
154445	.043:	1.39:	1.33	...	.3	...
134335	...	1.32:	0.74:	...	.2	.17
134320	...	1.05:	1.07:	...	.2	...
187929	.074:	1.24	...	...	.3	.2
183143	.027	1.40:	1.24	...	.3	...
193443	.015	1.41	1.20	...	.3	...
198478	.027	1.44	1.15	...	.2	...
206936	.016	2.13	...	...	...	...
207538	.016	1.35	1.09	...	.3	.2
207260	.015	1.34	1.16	...	.3	...
217476	.013	1.25	0.97	...	.3	.17
218342	.012	1.13	0.98	...	.3	.17
224014	.010:	1.23	1.19	...	.3	...
2905	.016	1.30	1.12	...	.3	.2
6675	.011	1.09	1.01	1.1	.3	.17
7927	.026	1.36	1.11	...	.3	.2
12301	.025	1.21	1.12	...	.3	.2
12953	.021	1.41	1.06	...	.3	.2
14489	.023	1.32	1.01	...	.3	.2
18326	.017	1.29	1.09	...	.3	.17
21291	.029	1.32	1.14	...	.3	...
21389	.023	1.32	1.06	...	.3	.2
30614	.018:	1.66	1.06	...	.2	.17
22253	.009	1.15	0.91	1.1?	.3	.17
25291	.024	1.28	0.95	...	.2	.17
24431	.009	1.12	0.89	...	.3	.17
24398	.012	1.20	1.48	...	.3	.2
31964	.020:	1.28	1.05	...	.2	...
36371	.017	1.32	1.18	...	.3	.2
37202	.101:	1.08	1.66	1.1	.3	...
41117	.022	1.31	1.13	...	.3	.2
42379	.018	1.41	1.03	...	.3	.17
43753	.017	1.13	1.14	...	.3	0.17
37041	0.017:	0.85	2.19	...	0.4	...

a Faraday rotation may play a role. Faraday rotation itself has been estimated by Greenstein (1960) to be completely negligible in optical measurements of interstellar polarization. Additional observations, with high precision in θ and distance, and a detailed study of the $\theta(\lambda)$ rotation appear in order.

Systematic trends of $P(\lambda)$ with galactic longitude are predicted by Greenberg and Shah (1966). For refractive index $m=1.33$ they studied the effects of aspect for fast spinning cylinders. When the spin is seen edge-on the computed polarization—wavelength dependence is steep. When the spin is seen nearly pole-on, the polarization-wavelength curve is considerably flattened, especially at shorter wavelengths.

Table XI lists the ratio of polarization versus total extinction p_{vis}/RE_{B-V} based on the values given in Table VI ($p_{vis}=P_{vis}/46$). Also listed are the ratios of visual versus infrared polarizations and visual versus ultraviolet polarizations. The infrared polarization P_{ir} is the straight mean of the percentage polarization (Table IV) at $1/\lambda=1.05$ and 1.19; the ultraviolet polarization, P_{uv}, at $1/\lambda=2.79$ and 3.04. The estimated probable errors are in the second line. Colons are used when a blank occurs in Table IV or when the ratio appears poorly established because of colons or large differences in Table IV.

The polarization versus total-extinction ratio may be an indicator of alignment because the polarization is maximum when the particle spin is seen edge-on, and zero when the spin is seen pole-on, both for about the same amount of extinction. There is no obvious correlation of either Table IX (residuals of position angles) or Table X (normalized polarizations) with the p_{vis}/RE_{B-V} values of Table XI. Stars which show a significant dependence of the polarization position angle on wavelength have both large and small values of p_{vis}/RE_{B-V}. Stars with values of $p_{vis}/RE_{B-V}\geq 0.020$ show characteristic polarization curves with one or two maxima. Stars with $p_{vis}/RE_{B-V}\leq 0.013$ also show characteristic polarization curves with one or two maxima.

As the flattening predicted by Greenberg and Shah (1966) is primarily in the ultraviolet, we should look primarily at the fourth column of Table XI. No correlation with galactic longitude or with p_{vis}/RE_{B-V} can be seen. Instead, the ratios vary in an irregular fashion from star to star, also in P_{vis}/P_{ir}. From star to star the ratios may change by more than three times their probable error.

A selection effect must be kept in mind as we have always chosen the most strongly polarized stars for the observing program. With a greater number of stars observed, it may be possible to find flattening superposed on the scatter. In the meantime, the scatter is explained by transverse of the starlight through various clouds having various particle sizes and field orientations.

In the last three columns of Table XI an estimate is made of the particle sizes that may predominate the polarization of various clouds. Five steps, (1)–(5), underlie this first approximation.

(1) While we realize that the interstellar particles may be composite and irregular in shape, it is assumed here that they are homogeneous and that all grains have the same index of refraction, $m=1.3-\epsilon i$, where ϵ is small. The shape is assumed to be that of long cylinders. Therefore, the only variables remaining are the size and size distribution.

(2) Each traversed interstellar cloud is assumed to have a *narrow* distribution of sizes about a mean diameter $2a$.

(3) Each mean diameter gives a characteristic shape of polarization versus $1/\lambda$, as follows: a well-defined maximum at $(1/\lambda)_0$, a steep decrease toward longer

wavelengths, and a gradual decline toward shorter wavelengths. The *characteristic curve* is seen in the calculations (Figs. 2–6 of Paper II; Paper VI) as well as in the observations (e.g. HD 21291 in Table X).

(4) Where there is an appreciable wavelength dependence in the position angles, the light apparently traverses at least *two* interstellar clouds having different particle size as well as different orientation of the magnetic field. For example, the wavelength dependence of HD 36371 would be interpreted with at least two particle sizes, even though our curve has only a single maximum. (With several narrow filters one could perhaps detect greater detail.)

(5) From the apparent maxima of each star in Table X, values of the above defined $(1/\lambda)_0$ are estimated. Particle diameters $2a$ are computed from

$$2\pi a(1/\lambda)_0(m-1)=C, \qquad (1)$$

where C is a constant (see Fig. 67 of van de Hulst 1957). From the figures of Paper II it is found that $C\simeq 0.4$. With the above assumption of refractive index m, expression (1) reduces to a simple relation between $(1/\lambda)_0$ and the diameter. For example, the light from HD 36371 may be traversing a cloud with $(1/\lambda)_0 \simeq 1.4\mu^{-1}$ and one with $2.0\mu^{-1}$, and the particle diameters are $2a\simeq 0.3\ \mu$ and $0.2\ \mu$, listed in Table XI.

A few stars show an excess of polarization at filters $1/\lambda=1.05$ and 1.19, for example HD 37202; others show an excess at $1/\lambda=2.79$ and 3.04, for example HD 217476. We need far-infrared and far-ultraviolet polarimetry to study these. In the meantime an estimate of $2a$ is made as follows. In visual light the polarization of HD 37202 shows a characteristic curve for $2a\simeq 0.3\ \mu$. But a rise—over and above that characteristic curve—becomes noticeable certainly for filter 1.05, and perhaps already for filter 1.19. The rise is explained as the short-wavelength "tail" of another characteristic curve but in the far-infrared, belonging to a large particle. The short-wavelength tail of the characteristic curve for $2a\simeq 0.3\ \mu$ would become noticeable at $1/\lambda\simeq 4.5$. The ratio 4.5/1.19, referring to expression (1), gives the ratio of $2a/0.3$; the $1.1\ \mu$ diameter for HD 37202 in Table XI is thus estimated.

Incidentally, μ Cephei shows an exceptionally steep shape of $P(\lambda)$. Furthermore, the amount of polarization appears to be variable with time (Sec. III), and the star should, therefore, not be considered in a general discussion of interstellar particles. It is also noted that μ Cephei shows rotation of the plane of polarization. This case certainly merits a special study.

If the difference of HD 134335 and 134320 is real, it would be amazing. These two stars in the north galactic spur are close together and yet their observed polarization dispersions differ appreciably. However, the amounts of polarization are small and the apparent difference may, therefore, be due to errors of observation.

The particle diameters in Table XI should not be taken too seriously. They are intended merely as an indication of how the variations in the $P(\lambda)$ curves for different stars may be interpreted in terms of the traverse of discrete clouds with different particle characteristics. It must be recalled that we have not taken into account the variation of shape nor of refractive index nor variations in the distribution of particle sizes for different clouds.

Greenberg and Shah (1966) compute for a distribution of particle sizes and orientations and for $m=1.33$ a $P(\lambda)$ curve that is similar to that for HD 21291. The maximum in their curve occurs near $2\pi a/\lambda=2.4$ while the observed maximum for HD 21291 occurs near $1/\lambda=1.7\ \mu^{-1}$, and the resulting grain size is $2a=0.45\ \mu$. Compared to our value of $2a=0.3$ in Table XI, it may be an indication of the effects of distributions that should be taken into account in closer approximations.

From the present first approximation, we draw the following conclusions:

(1) The wavelength dependence of the position angles, and the variations in the wavelength dependence of the percentage polarization from star to star, indicate that various interstellar clouds have various grain characteristics.

(2) The increase in polarization observed with our extreme infrared filters moreover indicates that some interstellar clouds have large particles. Incidentally, the Orion region is exceptional (HD 37041) with larger particles than usual, predominant even in the visual range.

(3) The increase in polarization observed with our ultraviolet filters indicates that some interstellar clouds have small particles.

The dispersion of interstellar polarization is nonuniform. This conclusion is similar to the one made in photometry where it has become clear (Johnson and Borgman 1963) that there is no uniform law of interstellar reddening.

REFERENCES

Behr, A. 1959, *Nachr. Akad. Wiss. Göttingen*, **II**. *Math.-Phys. Kl.*, No. 7, 185; *Veröff. Göttingen*, No. 126.

Blaauw, A. 1963, in *Basic Astronomical Data*, Vol. 3 of *Stars and Stellar Systems*, K. Aa. Strand, Ed. (University of Chicago Press, Chicago), p. 401.

Gehrels, T. 1960, *Astron. J.* **65**, 470 (Paper II).

——. 1966, *ibid.* **71**, 62 (Paper VI).

Gehrels, T., and Meltzer, A. S. 1966, *ibid.* **71**, 111 (Paper VII).

Gehrels, T., and Silvester, A. B. 1965, *ibid.* **70**, 579 (Paper V).

Gehrels, T., and Teska, T. M. 1960, *Publ. Astron. Soc. Pacific* **72**, 115.

Greenberg, J. M., Ed. 1966, *Proceedings of the IAU Colloquium on Interstellar Grains* (National Aeronautics and Space Administration, Washington, D. C.).

Greenberg, J. M., and Shah, G. 1966, *Astrophys. J.* (to be published).

Greenstein, J. L. 1960, *Lowell Obs. Bull.* **4**, 301.

Hall, J. S. 1958, *Publ. U. S. Naval Obs.* **17**, Part VI.

Hiltner, W. A. 1956, *Astrophys. J. Suppl.* **2**, 389.

Hoffleit, D. 1964, *Catalogue of Bright Stars* (Yale University Observatory, New Haven, Connecticut), 3rd rev. ed.

Hulst, H. C. van de 1957, *Light Scattering by Small Particles* (John Wiley & Sons, Inc., New York).

Johnson, H. L. 1966, in *Nebulae and Interstellar Matter*, Vol. 7 of

Stars and Stellar Systems, L. H. Aller and B. M. Middlehurst, Ed. (University of Chicago Press, Chicago).
Johnson, H. L., and Borgman, J. 1963, *Bull. Astron. Inst. Neth.* **17**, 115.
Kraft, R. P. 1963, in *Basic Astronomical Data*, Vol. 3 of *Stars and Stellar Systems*, K. Aa. Strand, Ed. (University of Chicago Press, Chicago), p. 433.
Kruszewski, A. 1962, *Acta Astron.* **12**, 234; also *Publ. Astron. Soc. Pacific* **74**, 519, 1962.
Martel, L., and Martel, M.-T. 1964, *Ann. Astrophys.* **27**, 203.
Serkowski, K. 1965a, *Acta Astronomica* **15**, 79.
——. 1965b, *Astrophys. J.* **141**, 1340.
——. 1966a, *Ann. Astrophys.* (to be published).
——. 1966b, *Lowell Obs. Bull.* (to be published).

Acknowledgments. This work is supported by the National Aeronautics and Space Administration (NsG-670 and NsG-733).

NO. 91 SOLID ORGANIC FILTERS FOR 2000 A TO 3000 A*

by S. F. PELLICORI, C. A. JOHNSON,† and F. T. KING†

ABSTRACT

Earlier work on the development of organic, narrow bandpass solution filters with transmittance maxima in the 2000–3000 Å range is extended to the fabrication of solid filters using a polymethyl siloxane resin as the host material. Three transmission filters are described having maxima at 2250 Å, 2265 Å, and 2840 Å, respectively, with bandwidths ≤ 225 Å. Transmittance and spectral response curves with CsTe photocathodes are given. Results of environmental tests show that these filters are well suited for balloon and space missions.

1. Introduction

Since the introduction[1] and development of liquid organic filters for the range 2000–3000 Å a program has been underway in cooperation with the Owens-Illinois Technical Center to develop solid organic filters with similar spectral characteristics. A new silicone, Glass Resin Type 650‡ developed by Owens-Illinois, Inc., is the host material which contains the organic filter components. Glass Resins are based on an alternating silicon-oxygen system and are classed generically as silicones. However, unlike conventional silicones, they can be cured to crystal-clear thermosetting materials without the use of fillers and modifiers. As a result, some of them contain better than 75% silicon and oxygen. This leads to physical and chemical properties different from those of commercial silicones. This glass-resin is transparent through the visible and middle uv regions; the external transmittance for a sample 1 mm thick is shown in Fig. 1. The resin does not change the locations of the selective absorption bands of the organic compounds compared with their absorptions in *n*-hexane solution.

2. Filters Produced

Figure 1 also shows the transmittances of three solid filter components containing as absorbers (the detailed composition of these filters is described in Sec. IV): Curve 3—2, 4-pentanedione; Curve 4—*p*-dimethylaminobenzaldehyde; and Curve 5—2-methylpyrazine plus *p*-dimethylaminobenzaldehyde. Curve 2 shows an interference filter (special Bausch & Lomb filter for 2250 Å) [*Note added in proof:* Recently, Thin Film Products, Inc., Cambridge, Massachusetts has produced interference filters at 2200 Å with better rejection above 3000 Å, thus reducing the leak for the combination to nearly one-tenth of the value shown in Fig. 2.] that is used as a component of one of the final filters to remove the longer wavelength transmission of 2, 4-pentanedione. Addition of Schott§ filter glasses and Dow Corning 200 Silicone Fluid[1] to prevent reflection losses results in the final filters (Fig. 2). Transmittance values <0.1% are extrapolated from the Cary 14 tracings. We suspect that the Cary values below 2000 Å are low by about 0.05 transmittance.

Combination with a CsTe (solar blind) photocathode produces the spectral response to equal energy at all wavelengths, shown in Fig. 3. The superiority to other types of filters in steepness of cutoff and off-band rejection is obvious. The CsTe cathode does not respond to the transmission of the organic compounds above 3500 Å. CuI or CsI photocathodes having no response above 2600 Å would permit the use of other organic compounds described in Ref. 1. We believe that inorganic compounds could also be added to the resin to absorb the visible.

3. Environmental Stability

The transmittance of the 2250-Å filter (curve 3 in Fig. 1) was investigated at temperatures ranging from +23°C to −23°C. No detectable change was observed over this range. Two filters each of the series shown in Fig. 2 were flown twice in a balloon-borne polarimeter, which is being developed for the Voyager space mission, to a 34.6-km altitude for a total of 18 h. The temperature inside the photometer was −18°C and the pressure as 3.5 mm Hg. Another of the filters (represented by curve 1′ of Fig. 2) was located outside the photometer and was exposed to an ambient temperature of −70°C for 10 min and to −44°C for a total of

*Reprinted with permission from *Applied Optics*, Dec. 1966, 5, 1966. Copyright 1966 by the Optical Society of America.

†Owens-Illinois Technical Center, Toledo, Ohio.

‡This is one member of a family of resins developed by Owens-Illinois, Inc., and so named because of their glass-like appearance.

§Jena Glaswerk Schott & Gen., Mainz.

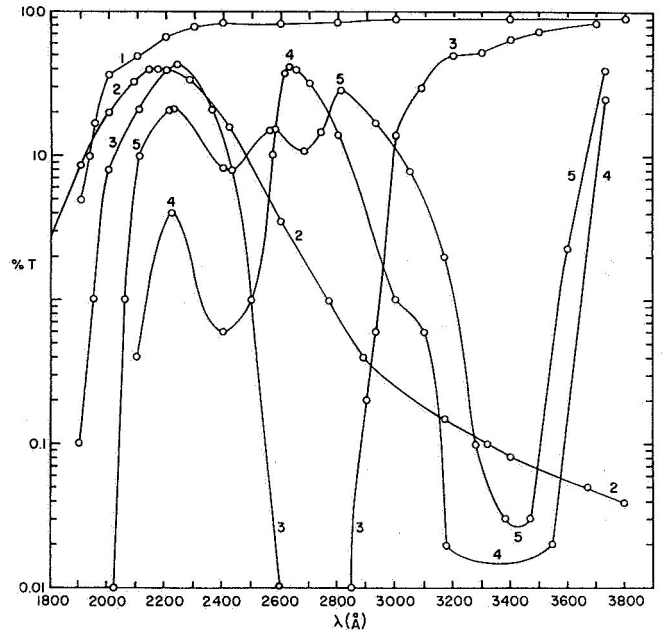

Fig. 1. External transmittance of organic compounds in Owens-Illinois Type 650 Glass Resin (curve 1, 1 mm thick) to make solid uv filter components. Curve 2 is of a special Bausch & Lomb interference filter for 2250 Å. The components of the filters represented by the remaining curves are given in Secs. II and IV.

18 h. No changes in the transmittances were detected in any of the filters after the flights.

Another set of these filters was flown in the Polariscope balloon system, and was used to obtain polarization measurements on a star and the daylight sky at a 36.1-km altitude on 27 May 1966.

A test was made to determine if the filters solarized to uv radiation. 1 h of irradiation at 23°C by 26 μW/cm^2 of the λ 2537-Å line produced no detrimental changes in the uv transmittance. Cast disks of the 650 resin (undyed) have been placed 20 cm from a 400-W uv lamp (Westinghouse H-33-1-CD), in air, and exposed for 1000 h. There was no change in the visible transmission of the castings.

A Glass Resin Type 650 casting among other materials was exposed to a simulated space radiation environment consisting of combined low energy protons (50 keV) and electromagnetic radiation, with wavelengths from 1216 Å in the extreme uv to 2 μ in the ir.[2] The casting was subjected to the equivalent of 340 h in space, during which solar flare conditions were simulated (10^{17} protons/cm^2 and 7.5 suns of solar EUV produced by hydrogen discharge). Following this radiation treatment, light transmittance dropped from 0.95 to 0.64 at 0.6 μ, a change of 0.31. Under these same conditions, fused silica (Corning No. 7940) showed a decrease of only 0.05 at 0.6 μ while all of the plastics tested degraded to near opacity. This information provides a good indication of the radiation resistance of Glass Resin Type 650 when compared with the other transparent plastics. The Glass Resin castings have been exposed to 10 Mrad of gamma radiation from a cobalt-60 source and 5 Mrad of thermal neutrons. No coloration resulted, and there was no loss of transparency. Under the same conditions, ordinary glass is discolored.

One disk containing *p*-dimethylaminobenzaldehyde to make curve 4 in Fig. 1, and one containing 2-methylpyrazine plus *p*-dimethylaminobenzaldehyde to make curve 4 in Fig. 1, were subjected to high vacua for extended periods. The test was to determine if the volatile organic absorbers would evaporate from the glass resin and degrade the filtering properties. The disks were 0.254 mm thick, and were fully exposed to the vacuum; i.e., they were not laminated with silicone fluid plus a colored glass. After one and one-half days at 1 x 10^{-8} mm Hg at about 0°C and four and three-fourths days at 1 $\times$ 10^{-6} mm Hg at +23°C, no changes in transmission could be detected. Two disks 1.27 mm thick containing 2,4-pentanedione to make curve 3 in Fig. 1 were kept at 1 $\times$ 10^{-6} mm at +23°C for four days. The transmission of one of the disks was unchanged, and the other decreased by 0.01 units. (It is uncertain whether this change was real because if some organic material evaporated, the transmission should have increased.) It is concluded that these filters are usable in the space environment for periods at least as long as above.

4. Preparation and Handling of Light Filters Using Glass Resin Type 650

The general procedure[3] used to prepare castings from glass resins was adapted to prepare the uv filters. Initially, glass resin 650 is a low molecular weight prepolymer dissolved in ethanol. First, a simple heat treatment, called a precure step, accomplishes two things: removal of the solvent, and starting the polymerization process to reduce time for postcuring.

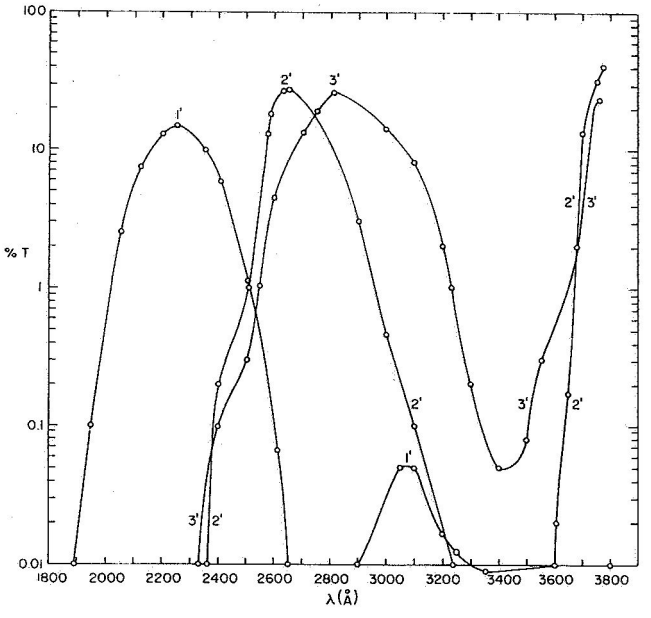

Fig. 2. External transmittances of Glass Resin filter components shown in Fig. 1 plus components to make the final filters that were used in three balloon flights: 1′ is curve 2 (Fig. 1) plus curve 3, 2′ is curve 4 plus 2 mm Schott UG-5, and 3′ is curve 5 plus 1 mm UG-11. 200 Silicone Fluid is used as a contacting agent.

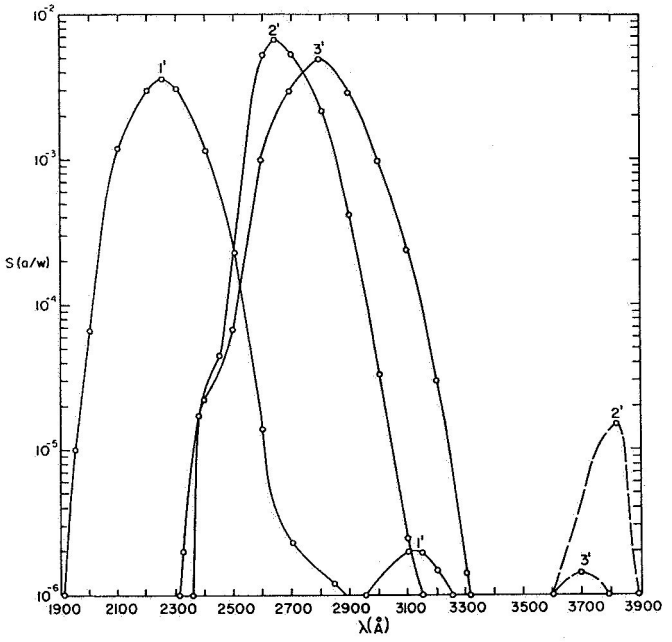

Fig. 3. Computed spectral response (cathode) to white light of filters of Fig. 2 combined with a CsTe photocathode.

Further heat treatment of the B-stage resins converts them to hard thermosetting materials. The length of time required for this final cure depends on the thickness of the casting.

The ethanol and water were boiled off from the glass resin (100 ml) as quickly as possible from a well-stirred solution in a 250-ml beaker. Within 15 min, the temperature of the low viscosity liquid (about 150 c/s) had reached 140°C. This rate of evaporation is critical for obtaining a proper precure and avoiding gellation of the resin. At this point the beaker was removed from the hot plate and the organic dye added with vigorous stirring. The solution was poured into 5.1-cm diam aluminum foil pans to make disks 3.2 mm thick; care was taken to entrap no more air bubbles than necessary. The disks, while still hot (>100°C), were placed directly into an oven maintained at 90°C. After 24 h, the disks were removed from the oven and allowed to cool to room temperature. The aluminum foil was stripped from the disks which were inverted and placed into a new foil aluminum pan. After six more days at 90°C, the disks were removed from the ovens. Then they were cut, ground, and polished to the thickness required to give the desired absorption after the light transmission of the original disk had been determined. The only precaution required during this operation was to avoid localized overheating which could cause cracking owing to thermal expansion. After the initial trial runs were finished, better estimates were made of the excess amount of volatile organic absorber that must be added at 130°C to leave the proper amount of dye in a polished disk of a convenient thickness. For example, since the boiling point of 2-methyl pyrazine was about 138°C, considerably more material was added to the glass resin being maintained at 130° C than one would add merely by calculation.

After several initial filters had been prepared in order to establish the proper technique, three types of filters were prepared as described below.

To prepare the 2250-Å filter, approximately 210 mg of 2,4-pentandione was added to 50 g of the glass resin at a temperature about 125°C to 130°C. The filter had a thickness of 1.270 ± 0.051 mm. The average deviation of the per cent transmittance at 2250-Å between the six filters was ±1%.

To prepare the 2665-Å filter, 100 g of *p*-dimethylaminobenzaldehyde was added to 50 g of the glass resin 650 at about 130°C. The filters had a thickness of 0.254 ± 0.025 mm. The average deviation of the per cent transmittance at 2665 Å between the six filters was ±2%.

To prepare the 2840-Å filter, about 200 g of 2-methylpyrazine and about 50 mg *p*-dimethylaminobenzaldehyde was added to 50 g of the glass resin 650 solution at about 130°C. The filters had a thickness of 0.254 ± 0.025 mm. The average deviation of transmittance at 2840 Å between the six filters was ±3%.

Six filters of each type were prepared for the balloon astronomical studies. The disks had uniform transmission over their area.

The glass resin is not as mar resistant as glass. Cleaning the filters must be done with soft tissue. The filters are insoluble in water. They can be soaked in pure *n*-hexane for up to 2 min with no harm. (Hexane dissolves the silicone fluid contacting agent.) Ethyl alcohol on a tissue can be used for cleaning the filters with light pressure. However, when dipped, the filters cannot survive in polar solvents because they crack.

The disks were cast by D. W. Gagnon and J. J. Tillman of the Owens-Illinois Technical Center. Appreciation is expressed to S. A. Hoenig of the Mechanical Engineering Department, University of Arizona for use of his high vacuum system. We are grateful to the Kitt Peak National Observatory for use of their Cary 14 recording spectrophotometer. This work was supported as part of the Polariscope program of the Atmospheric Sciences Section, National Science Foundation.

REFERENCES

1. S. F. Pellicori, Appl. Opt. **3**, 361 (1964).
2. C. A. Johnson and R. E. Martin, in *Proceedings of the Sixth Electrical Insulation Conference* (New York, 1965, p. 119).
3. *Combined Space Environment Effects on Typical Spacecraft Window Materials*, Final Report, Contract NAS9-2939 Avco Corporation, Tulsa Division, July, 1965.